รายงานวิจัยฉบับสมบูรณ์

เครื่องมือวัดกระแสไฟฟ้าโดยใช้เส้นใยแสง

Fiber Optic Current Sensors

โดย ผู้ช่วยศาสตราจารย์ ดร. ปริญญา ตันตสวัสดิ์

ธันวาคม 2544

สัญญาเลขที่ RSA/06/2541

รายงานวิจัยฉบับสมบูรณ์

เครื่องมือวัดกระแสไฟฟ้าโดยใช้เส้นใยแสง

Fiber Optic Current Sensors

ผู้ช่วยศาสตราจารย์ ดร. ปริญญา ตันตสวัสดิ์
สาขาวิชาวิศวกรรมไฟฟ้า สถาบันเทคโนโลยีนานาชาติสิรินธร
มหาวิทยาลัยธรรมศาสตร์

สนับสนุนโดย สำนักงานกองทุนสนับสนุนการวิจัย

บทคัดย่อ

รหัสโครงการ: RSA/06/2541

ชื่อโครงการ: เครื่องมือวัดกระแสไฟฟ้าโดยใช้เส้นใยแสง

ชื่อนักวิจัย: ผู้ช่วยศาสตราจารย์ ดร. ปริญญา ตันตสวัสดิ์

E-mail: prinya@siit.tu.ac.th

ระยะเวลาโครงการ: 3 ปี (1 มกราคม 2542 -31 ธันวาคม 2544)

วัตถุประสงค์:

วัตถุประสงค์หลักของงานวิจัยนี้มุ่งเน้นไปที่การศึกษาการลดผลตอบสนองของการวัดกระแสไฟฟ้าผิดพลาดของเครื่องมือวัดระแสไฟฟ้าโดยใช้เส้นใยแสงเนื่องจากอิทธิผลของ acoustic environmental perturbations เช่นการสั่นสะเทือนที่ส่วน sensing fiber โดยศึกษาทั้งจากการทดลองและทางทฤษฎีโดยการสร้างแบบจำลองทางคณิตศาสตร์

วิธีการทดลอง: สร้างเครื่องมือวัดกระแสไฟฟ้าแบบ unidirectional และ reciprocal polarimetric และทำการทดลองเพื่อตรวจสอบคุณสมบัติและผลตอบสนองของเครื่องมือวัดนี้ ทำทดลองผลตอบสนองของค่าความผิดพลาดของการวัดกระแสไฟฟ้าต่อขนาดของการสั่นสะเทือน และผลตอบสนองต่อความถี่ของการสั่นสะเทือน สร้างทฤษฎีแบบจำลองทางคณิตศาสตร์ของผลตอบสนองต่อการสั่นสะเทือนจากการเปลี่ยนแปลง linear birefringence วิเคราะห์และเปรียบเทียบผลตอบสนองจากการทดลองและจากทฤษฎีแบบจำลองที่สร้างขึ้น

ผลการทดลอง: ได้ผลทั้งทางทฤษฎีและการทดลองดังนี้

1. ผลการทดลองผลตอบสนองของค่าความผิดพลาดของการวัดกระแสไฟฟ้าแปรผันตามขนาดของการสั่นสะเทือนและขึ้นกับค่า bend-induced linear birefringence และได้ผลตอบสนองต่อความถี่ของการสั่นสะเทือนด้วย
2. ทฤษฎีแบบจำลองของผลการตอบต่อสนองต่อขนาดของการสั่นสะเทือนมีผลใกล้เคียงกับผลทดลอง

วิจารณ์ผลและสรุป: จากผลการทดลองและผลทางทฤษฎีแบบจำลองของผลตอบสนองเนื่องจากอิทธิผลของการสั่นสะเทือนที่ส่วน sensing fiber มีความสอดคล้องกัน ผลที่ได้จากการศึกษาชี้ให้เห็นว่าผลทางทฤษฎีนี้เหมาะสมสำหรับใช้ในการออกแบบเครื่องมือวัดโดยใช้เส้นใยแสงเพื่อลดผลกระทบจากการการสั่นสะเทือนได้ดีและอาจใช้สำหรับพัฒนา fiber optic devices ที่ใช้หลักการ acoustic modulation ได้

ข้อเสนอแนะ: ควรมีการศึกษาเกี่ยวกับค่าของการเปลี่ยนแปลง linear และ circular birefringences โดยใช้ optical modulator เพื่อเข้าใจปรากฏการณ์ที่เกิดจากการสั่นสะเทือนต่อ fiber optic sensor และปรับปรุงทฤษฎีแบบจำลองให้มีความถูกต้องแม่นยำขึ้น

คำหลัก: Fiber optic current sensor, current measurement, vibration, simulations and mathematical modeling, linear birefringence

Abstract

Project Code: RSA/06/2541

Project Title: Fiber Optic Current Sensors

Investigator: Assist. Prof. Dr. Prinya Tantaswadi

E-mail: prinya@siit.tu.ac.th

Project Period: 3 years (Jan. 1, 1999 – Dec. 31, 2001)

Objectives: The main objectives of this project are as follows:

1. To experimental study of the current measurement error due to effect of vibration to the sensing part of unidirectional and reciprocal polarimetric current sensors.
2. To implement mathematical modeling and to understand the mechanisms for this vibration sensitivity of these sensors. So this modeling can be helpful for optical current sensor design and may be used for fiber optic devices based on acoustic modulation.

Methodology: an optical polarimetric current sensor was built. Experimental study of vibration effects on current measurement error in the unidirectional polarimetric current sensor was performed. Mathematical modeling was formulated to predict the vibration sensitivity in the unidirectional and reciprocal polarimetric current sensors. Then, reciprocal current sensor was built and tested.

Results: Mathematical modeling of the vibration sensitivity was formulated and can show the relationships between current measurement error and vibration amplitude. Unidirectional and reciprocal polarimetric current sensors were built and tested. Current measurement error due to vibration effects on the unidirectional polarimetric sensor was studied. This error varies linearly with amplitude of vibrations. This confirms that our mathematical modeling is valid.

Discussions and Conclusions: The proposed mathematical modeling can be helpful in prediction of the unwanted current measurement error due to unavoidable mechanical vibrations for actual use. In practice, polarimetric current sensors have to be well packaged (from vibration under a certain limit that can be predicted from our modeling) to achieve the accuracy of 0.3%.

Suggestions: The physical mechanisms (*i.e.* birefringence changes) of vibration effects on the optical fiber sensors should be further investigated. A way to study the mechanisms is to measure actual values of both linear and circular birefringence changes in the fiber sensors under mechanical vibrations. This study is very helpful for optical fiber sensor design.

Keywords: Fiber optic current Sensor, current measurement, vibration, simulations and mathematical modeling, linear birefringence.

Final Report

Fiber Optic Current Sensors

By

Assist. Prof. Dr. Prinya Tantaswadi

December 2001

TABLE OF CONTENTS

LIST OF FIGURES

ACKNOWLEDGMENTS

Funding was provided by The Thailand Research Fund (TRF) under Grant No. TRF: RSA/06/2541. The author would like to thank Dr. James N. Blake of Nxtphase, USA, Prof. Alan J. Rogers of University of Surrey, UK, and Assoc. Prof. Dr. Pichet Limsuwan of King Mongkut's University of Technology, Thonburi for help and fruitful discussions. Also, the author would like to thank Mrs. Somna Maheshwari, Mr. Charoen Tangtrongbenchasil, and Mr. Saravuth Pothiya for their assistance in this study.

GLOSSARY OF SYMBOL

Symbol	*Parameter*
E	electric field intensity
$\bar{H}$	vector of magnetic field intensity
F	angle of Faraday rotation
I	current
V	Verdet constant
T	twist-induced circular birefringence
δ	bend-induced linear birefringence
α	total birefringence

GLOSSARY OF NOTATION

Symbol	*Meaning*
$\approx$	approximately equal to
$\propto$	be proportional to
$\alpha, \beta \gg T$;	
or	sequence of inequalities
$\alpha \gg T$ and $\beta \gg T$	
* (superscript)	complex conjugate
$\oint_C$	closed loop intergral
(a,b)	interval of the real line, $a < x < b$
A^T	matrix transpose
$A \cdot B$	matrix multiplication

Chapter 1

INTRODUCTION

In this report, we investigate the current measurement error due to acoustic environmental perturbations *i.e.* mechanical vibrations to the sensing part of unidirectional and reciprocal polarimetric current sensors. A novel mathematical modeling for prediction of this vibration effects on the current sensors is developed. It is based on the linear birefringence change in the sensing part. Although the basic theory of birefringence in optical fiber is well known, some interesting conclusions from this theory concerning the application to vibration sensitivity in fiber optic current sensors have not yet been drawn.

We demonstrate the experimental study and mathematical modeling of vibration sensitivity in a unidirectional and reciprocal polarimetric current sensors.

In this chapter, we provide the information about motivation and introduction of optical fiber current sensors and their undesirable current measurement errors due to the effects of environmental perturbations.

1.1 Motivation

Fiber-Optic current sensors, which rely on magneto-optic Faraday effect and Ampere's law, have received considerable attention for possible application in electric power industry as magneto-optic current transducers (MOCT) in the past few decades [1]-[6]. They all use optics

to isolate a high-voltage (HV) part of the system from a grounded part (see Fig. 1). Conventional current transformers (CTs) has been iron core copper wound transformers, ferromagnetic CTs, and *etc.* They typically use oil-paper or SF_6 insulation for safety in the HV environment. Their drawbacks are undesirable large size and weight, high cost, voltage and current isolation problems.

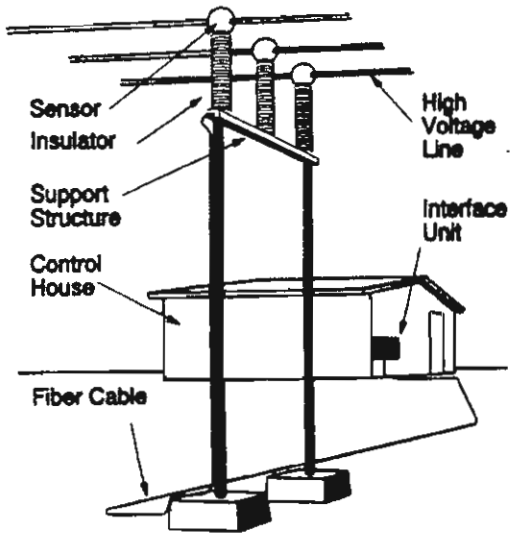

Fig. 1 Essential components of a MOCT system

MOCTs are optical and electronic or "optoelctronic" measurement systems. A fundamental way an MOCT differs from a conventional CT is in the signal power involved. In all the MOCTs considered here, the current being measured is represented, as it is transmitted from high potential to ground, as modulated light. In a conventional CT, the secondary signal has a power level of several watts. The power in the optical part of the MOCT is typically a few μW.

Diversity is present in all elements of the system shown in Fig. 1 [1]. The sensor itself may be optical or electronic, so the high-voltage part of the system may be active or passive. The insulator may be ceramic or polymer-it may be used to support the MOCT or it may be suspended from it. Typically, but not universally, it contains an optical fiber carrying the MOCT output signal. The way the current information is encoded in the fiber varies from system to system. This affects the design of the receiver at ground potential. An interface unit connects the MOCT system to the user device, which may be a relay or a meter or other equipment.

The MOCT has several advantages over a conventional device. One is light weight. The optical sensor may be much lighter than a conventional oil-filled CT of similar ratings. This lighter weight allows for savings during installation; the support structure is smaller, a smaller crane can be used, and installation time is shorter than for a conventional CT. Other advantages include noise immunity and safety: since the insulating part of an MOCT consists only of an optical fiber and a fairly standard insulator. The device is less likely to fail catastrophically than a conventional current transformer.

Furthermore, because of the ability to connect directly to the power line, the modularity, the promised increase in resolution, the lower costs and the compatibility to solid-state electronics, optical sensors will certainly be the means used to acquire data from the power system in future designs.

There are two important tasks in operating a power system: revenue metering and circuit protection. To best insure that optical sensors will

be at least as good as the technology they will replace. A summarized performance shown in Fig. 2 indicates approximate ranges for generalized current sensors [2].

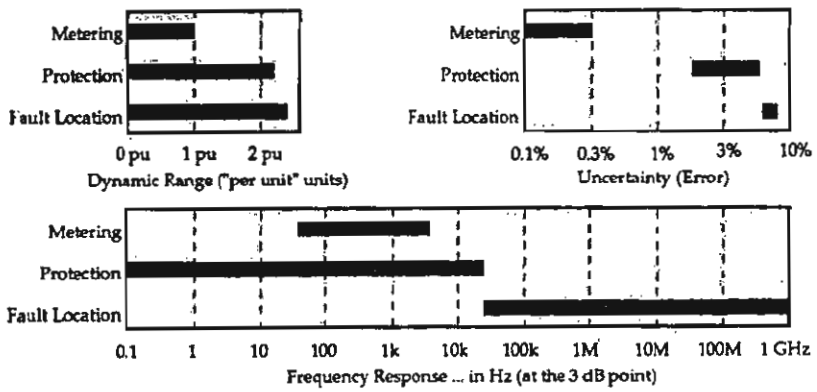

Fig. 2 Generalized sensor specification summary

The third task is Fault location. While not directly related to circuit protection, it is related to the time taking to bring a system back into operation after a system disturbance that would cause a temporary or permanent fault. Bonneville Power Administration (BPA)'s concept of timekeeping skills in order of microsecond level or "Microtime" allows for the use of synchronized counters or clocks and high frequency optical sensors to allow automatic and instant location of faults to within one tower on overhead lines and to within one meter in compressed gas networks. As Microtime was also developed as a means to allow for advanced phase angle telemetry (to a theoretical accuracy of 22 millidegrees), specialized salient features inherent with optical sensors (such as very fast response time) are important to the logical advancement in this area. In addition the use of technology in

this range allows for research equipment designs that are used for further system optimization studies.

The advantages of optical current sensors can be summarized as follows [1]-[5]:

Table 1 Ferromagnetic versus Optical CTs

Ferromagnetic CTs	Optical Sensors (MOCTs)
Narrower dynamic range	Broad dynamic range
Narrow frequency	Broad frequency response
Poor resolution	Low resolution
Hysteresis	No hysteresis
Large and bulky in size	Small size and small
Heavy	Light weight
Insulation problem	Inherently insulated
Less safe	More safe

Dynamic range: MOCTs have broad dynamic range of more than five orders of magnitude (*e.g.* 1 to 100,000 A). Assume nominal current to be 1,000 A. Current ranges for revenue metering and fault location are shown below:

- 10^{-3} x nominal current for low end accuracy (*e.g.* 1 A) and scale factor accuracy of 0.3%.

- 10^{2} x nominal for fault location (*e.g.* 100,000 A)

Frequency response: the conventional ferromagnetic CTs have low bandwidth (< 1 kHz), while the optical current sensors have a higher bandwidth (DC to about many MHz depending on configuration).

Several approaches of Faraday-based current sensors have been demonstrated. Although fiber-optic current sensors have several advantages over conventional current transformers (CTs), they have yet to overcome undesirable susceptibility to environmental perturbations and optical component stability to achieve the accuracy needed for certain applications such as revenue metering. One approach uses polarimetric techniques. This method of current sensing detects the intensity change due to polarization rotation from the induced magnetic field generated by current. The accuracy of this sensing method suffers from both linear and circular birefringence in the sensing fiber. To counter the birefringence errors, a reciprocal polarimetric type current sensor has been developed. The perturbations affect the birefringence property of the fiber in the sensing part. Unidirectional polarimetric current sensors suffer from environmental perturbations due to varying birefringence in the sensing part. This results in current measurement error or false current readings from environmental perturbations.

In this report, birefringence effects due to environmental perturbations on the current measurement error in the unidirectional and reciprocal fiber-optic polarimetric current sensors are investigated. A novel mathematical modeling of the vibration effects due to vibrations is formulated. From this study, the modeling can be helpful for the better design of current sensors with vibration immunity and may be useful for development of fiber-optic devices based on acoustic modulation.

1.2 Report Summary

In this report, chapter 1 provides the information about motivation and introduction of optical fiber current sensors and their unwanted current measurement error due to the effects of environmental perturbations.

In chapter 2, we describe backgrounds on two types of fiber-optic polarimetric current sensors: unidirectional and reciprocal current sensors. Their performance, component sensitivity, birefringence sensitivity, and $1/f$ noise problems associated with various designs are discussed.

In chapter 3, we describe the mathematical modeling of vibration sensitivity effects on the sensor. Preliminary results on the implementation of a reciprocal polarimetric current sensor are also presented.

In chapter 4, we describe the implementation of a unidirectional polarimetric current sensor. Experimental study of vibration sensitivity is also demonstrated. Furthermore, mathematical modeling of the vibration sensitivity effects on the sensor is formulated and shows good agreements with the experimental results.

In chapter 5, the summary of results of the preceding chapters and suggestions for future work is mentioned.

Chapter 2

LITERATURE REVIEWS

In this chapter, we present two approaches of Faraday rotation based fiber-optic current sensors. The fundamentals of the Faraday effect and undesirable birefringence effects in the sensing fiber are described. Jones calculus is introduced for analysis of optical current sensors. Then, two types of fiber optic polarimetric current sensors: unidirectional and reciprocal current sensors are reviewed in the following two sections. Theoretical analysis for understanding and predicting the characteristics and performances of these current sensors is also discussed.

2.1 Current Sensor Backgrounds

In this section, we describe the fundamentals of the Faraday effect and unwanted birefringence effects in the sensing fiber. Then, Jones calculus is introduced for analysis of optical current sensors.

2.1.1 Faraday effect in the sensing fiber

When light propagates in an optical fiber wound around a current carrying wire (see Fig. 1), the induced magnetic field causes a rotation of the linear polarization plane of lightwave by the magneto-optic Faraday effect. This angle of rotation, F, through which the plane of polarization rotates, is given by [7]-[9]

$$F = V \oint_C \vec{H} \cdot d\vec{l}\,, \tag{2.1}$$

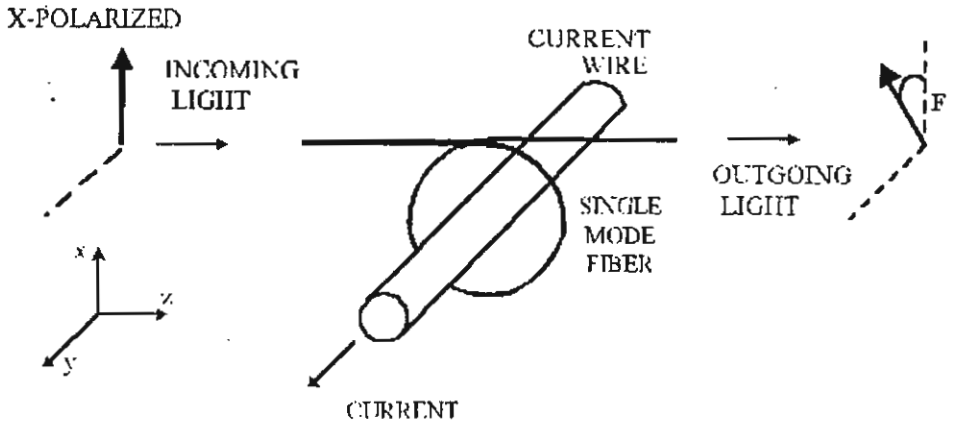

Fig. 3 Faraday effect in the single-mode fiber loop

where V is the Verdet constant of the optical fiber, $\vec{H}$ is the magnetic field intensity along the direction of light propagation, and l is the optical path along the fiber loop. From the Ampere's law, this closed loop integral of magnetic field around a wire is proportional the current, I, flowing through it, *i.e.*

$$I = \oint_C \vec{H} \cdot d\vec{l} \,. \tag{2.2}$$

Therefore, the angle of rotation, F, in the fiber loop configuration is given by

$$F = VNI \,, \tag{2.3}$$

where N is the integral number of turns of fiber wrapped around the current carrying wire. Note that the rotation of the plane of polarization depends only on the current being carried by the wire. This rotation neither depends on the location of the wire in the sensing loop nor the exact shape of the loop [10]. Also, this sensing loop is insensitive to all externally generated magnetic fields such as those

caused by currents carried in nearby wires. Because the sensing fiber makes a complete loop (or integral numbers of loops), the Faraday rotation produced in one part of the sensing loop by externally generated fields is exactly compensated by an inverse rotation in the part of the loop that is oppositely directed with respect to the magnetic field (see Fig. 4). Isolation of the current sensor from fields associated with nearby power lines is a critical performance parameter in electrical power systems applications.

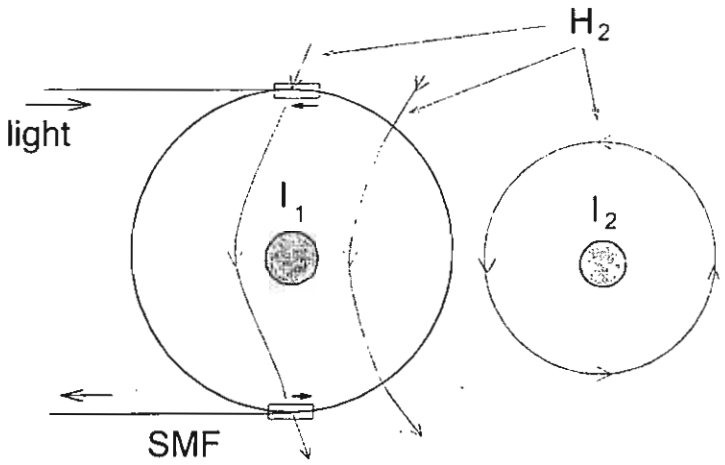

Fig. 4 Sensing fiber is insensitive to magnetic fields generated by a nearby wire $V\oint_C \vec{H}_2 \cdot d\vec{l}_1 = 0$, I_1 and I_2: current carrying in conductor 1 and 2, respectively; H_2: magnetic field generated by I_2; $\vec{l}_1$: optical path along the sensing loop.

The stability of Faraday rotation based current sensors, through the Verdet constant, depends on source wavelength and temperature. In addition, the Verdet constant is determined by the magnetic properties of material. For example, the operating wavelength λ is 633 nm and the Verdet constant V is 4.68 $\mu rad/A$. The Verdet constant in

diamagnetic materials, *e.g.* silica, is small and almost temperature independent, while in the paramagnetic materials, the Verdet constant is somewhat larger and temperature dependent. In practice, diamagnetic materials, such as glass, are used for the sensing fiber because of their temperature independence. The Verdet constant varies with λ^{-2}. Typical values for silica single-mode fiber are V = 4.0 μrad/ A at 820 nm and V = 4.68 μrad/A at 633 nm. Tang *et al.* [6] show that the temperature dependence in silica fiber $\frac{1}{V}\frac{\partial V}{\partial T}$ is 6.9x10^{-5}/K.

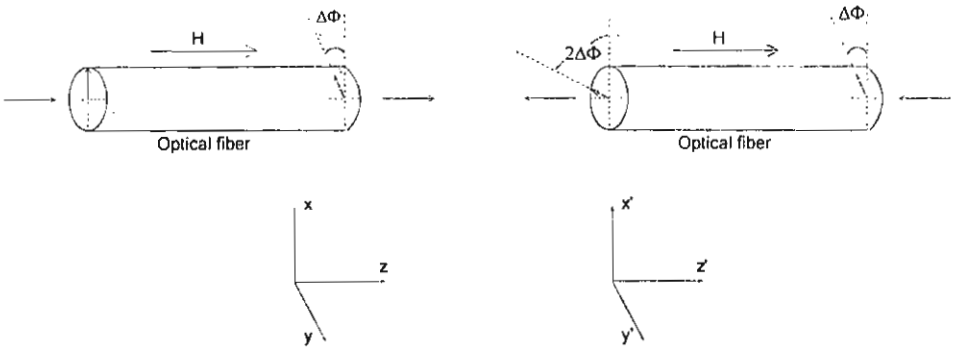

Fig. 5 Non-reciprocity in Faraday medium and its corresponding coordinates, $\Delta\Phi = VNI$.

Another property of Faraday rotation is non-reciprocity. When linearly polarized light propagates in one direction around a current-carrying wire, its plane of polarization undergones a rotation of $\Delta\Phi$ which is a function of the induced magnetic field (see Fig. 5). When the light propagates in the opposite direction, it also experiences the rotation, $\Delta\Phi$, with respect to the first direction of propagation [7]-[9]. This suggests that the Faraday induced rotation is only a function of the polarity of the magnetic field, and not the direction of propagation of

the lightwave. Such an effect is called non-reciprocal. This non-reciprocity comes about because the magnetic field, or equivalently, the magnetic polarization now points in the opposite direction relative to the reversed direction of propagation.

2.1.2 Jones Calculus of the sensing fiber

This section is devoted to the Jones calculus analysis of a sensing fiber. Such a fiber is typically single-mode and is susceptible to both the Faraday effect and undesirable birefringence effects.

a. Ideal sensing fiber

An ideal single-mode optical fiber for sensing exhibits only Faraday rotation and can be described by the Jones matrix as shown below [8], [9]

$$\bar{L} = \begin{bmatrix} A & -B \\ B & A^* \end{bmatrix}, \tag{2.5}$$

where

$$A = \cos F, \tag{2.6}$$

$$B = \sin F, \tag{2.7}$$

and F is the Faraday rotation.

b. Fiber with undesirable birefringences

In an actual sensing system, the sensing fiber exhibits, in addition to Faraday rotation, bend- and lateral stress-induced linear and twist-induced circular birefringence. Such effects corrupt the current sensor's

output signal, either by masking an actual current in the conductor or by yielding a false signal. Additionally, mechanical disturbances such as vibrations in the sensing fiber can yield a time-varying birefringence yielding a signal indistinguishable from a time-varying current.

b.1 Linear birefringence

Linear birefringence results from intrinsic geometric imperfections or applied stress [4]. Inherent linear birefringence can be minimized by certain manufacturing techniques. However, linear birefringence from bending the fiber into a sensing coil (*i.e.* bend-induced linear birefringence) is a major source of error in fiber-optic current sensors. This induced birefringence, δ_{DC}, can be predicted by [11]

$$\delta_{DC} = \pi n_0^3 (p_{11} - p_{12}) \frac{(1+\upsilon)}{\lambda} \frac{r^2}{R^2} = \frac{K}{\lambda} \frac{r^2}{R^2}, \tag{2.8}$$

where δ_{DC} is the retardation per unit length (degree/m), n_0 is the effective refractive index of the fundamental mode in the fiber without the perturbation, p_{ij} are the elements of the elasto-optic tensor, υ is the Poisson's ratio, λ is the wavelength, r is the fiber radius (including the core and cladding), and R is the bend radius. The parameters for fused silica fiber are $p_{11} - p_{12} = 0.15$ and $\upsilon = 0.17$. We obtain $K = 49.2$ (deg).

b.2 Circular birefringence

Another source of birefringence is twist-induced circular birefringence. For a linear state of polarization (SOP), the rotation of the polarization plane, Ω, is given by [12]

$$\Omega = \frac{g}{2}\tau , \tag{2.9}$$

where Ω is the rotation per unit length, τ is the twist per unit length, $g = \frac{1}{2} n_0^2 (p_{12} - p_{11})$. A typical value of g for silica fiber is 0.16 at 633 nm wavelength.

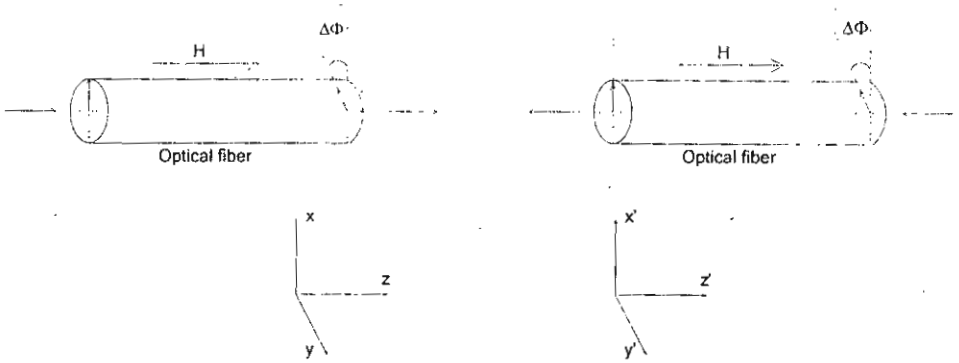

Fig. 6 Reciprocity and its corresponding coordinates

These birefringences affect the accuracy and stability of the sensor. However, since they exhibit reciprocal characteristics, they can be compensated. For a reciprocal optical effect (see Fig. 6), when linearly polarized light propagates in one direction, its plane of polarization undergones a rotation of, say, $\Delta\Phi$. When the light propagates in the opposite direction, it experiences the rotation, $-\Delta\Phi$, with respect to the first direction of propagation. The rotation cancels out after a round-trip. Many current sensor designs redirect light back through the fiber to cancel out such reciprocal birefringence effects.

The Jones matrix for an actual sensing fiber, which includes birefringence effects for both forward and backward propagation, can be described by

$$\vec{L} = \begin{bmatrix} A & -B \\ B & A^* \end{bmatrix}, \tag{2.10}$$

where

$$A = \cos\frac{\alpha}{2} + j\sin\frac{\alpha}{2}\cos(\chi) \tag{2.11}$$

$$B = \sin\frac{\alpha}{2}\sin(\chi) \tag{2.12}$$

$$\frac{\alpha}{2} = \sqrt{(VNI + T)^2 + (\frac{\delta}{2})^2} \tag{2.13}$$

$$\tan\chi = 2(VNI + T)/\delta, \tag{2.14}$$

Here δ is the total linear birefringence (assumed uniformly distributed) and T is total twist-induced circular birefringence (also assumed uniformly distributed).

For backward propagation, we can describe the sensing fiber by

$$\bar{L} = \begin{bmatrix} C & -D \\ D & C^* \end{bmatrix}, \tag{2.15}$$

When there is no Faraday effect (*i.e.* $F = 0$), reciprocity holds for the forward and backward propagation, *i.e.*

$$\bar{L} = \bar{L}^T, \tag{2.16}$$

In the backward direction, the twist-induced circular birefringence has the opposite sign by reciprocity. This circular birefringence becomes -T. Equation (2.16) requires that $A = C$ and $B = D$. This gives

$$C = \cos\frac{\beta}{2} + j\sin\frac{\beta}{2}\cos(\zeta), \tag{2.17}$$

$$D = \sin\frac{\beta}{2}\sin(\zeta), \tag{2.18}$$

$$\frac{\beta}{2} = \sqrt{(F-T)^2 + (\frac{\delta}{2})^2}, \tag{2.19}$$

$$\text{and } \tan\zeta = 2\ (F-T)/\delta, \tag{2.20}$$

Note that the linear birefringence, δ, does not change sign to satisfy the reciprocity condition.

To measure current I, with constant N and V, we can use polarimeter sensor to measure F. Two configurations of polarimetric current sensors can be used: unidirectional and reciprocal polarimetric current sensors.

2.2 Unidirectional Polarimetric Current Sensors

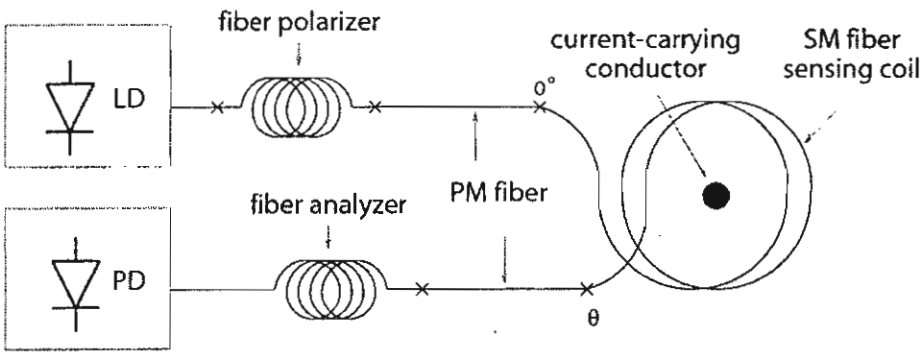

Fig. 7 Straightforward Polarimetric configuration, PM: polarization-maintaining fiber, SM: single-mode fiber, LD: laser diode, PD: photodetector.

This method of current sensing [1]-[5] detects the intensity change due to polarization rotation (see Fig. 7). Fiber polarizers are placed at the input and the output ends of the sensing fiber coil. Linearly polarized

light is launched into the sensing fiber. The plane of polarization of this light rotates by an amount proportional to the current in the wire. A polarization analyzer, aligned at 45° with respect to input polarizer, is placed in front of the detector. When no current in the wire, half of the light passes the analyzer and is detected (see Fig. 8). For positive current in the wire, the polarization state is rotated so as to increase its alignment with respect to the analyzer (point A), allowing less light to fall on the detector (point B). For a negative current, the polarization of the light rotates in opposite direction, allowing more light to fall on the detector. The rotation through which the polarization of the light is rotated is given by $F = VNI$, where V is the Verdet constant of the sensing coil, N is the integral numbers of fiber loops around the current carrying wire, and I is the current in the wire.

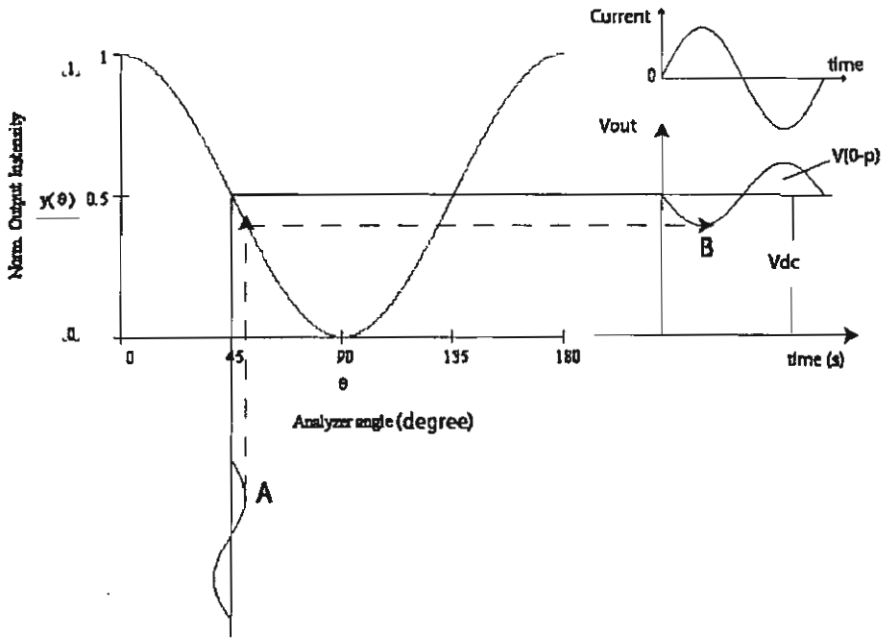

Fig. 8 The detected normalized intensity versus. the angular alignment between the analyzer and the input polarizer

Fig. 8 shows the detected normalized intensity as a function of the angular alignment between the analyzer and the polarization state of the light falling on the detector. Note that the detected intensity of this sensor follows a raised cosine function. The maximum scale factor and the maximum linear dynamic range is obtained when the analyzer is aligned at 45° to the input polarizer.

2.2.1 The effects of light source

We now consider the effect of the light source. The light source is preferably a broadband source (low coherence source). The use of this low coherence source avoids problems associated with coherent effects, *i.e.* unwanted interferences between waves having taken spurious paths through optical circuit. For example, the use of broadband source allows us to maintain accuracy with imperfect polarizers. Since all the wavelengths in the source are affected by the Faraday effect in a similar manner, the composite signal maintains its integrity. We also have the necessity of maintaining the wavelength spectrum of the source. The Verdet constant of the fiber glass varies with λ^{-2}. If the source wavelength drifts, or its spectrum changes shape, the scale factor of the sensor drifts. Since the center wavelength of a laser diode drifts by about 0.03% to 0.04% per °C, it is necessary to stabilize the temperature of the laser diode to within a few °C to maintain the 0.3% scale factor accuracy required for metering applications.

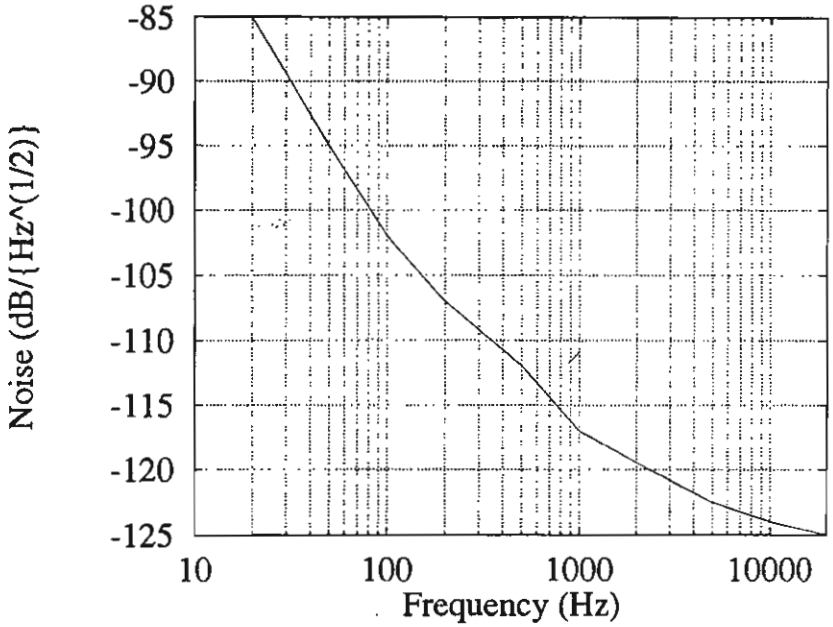

Fig. 9 Noise power spectrum on a typical 0.8 μm laser diode

The light source intensity noise can also be a severe problem, mainly because of the large 1/f intensity noise associated with laser diodes [13]-[15]. Since the current information is at low frequencies, the 1/f noise on the source becomes a problem. Fig. 9 shows a noise spectrum on a typical 0.8 μm laser diode [15]. The relative intensity noise (RIN) is about -125 dB/$\sqrt{}$Hz at frequency above 10 KHz but is only around -90 dB/$\sqrt{}$ Hz at the frequencies of most interest to electric power applications. This result agrees with the relative intensity noise of GaAlAs laser diodes reports by Dandridge *et al.* [14].

2.2.2 Dual polarization polarimetric current sensor

A solution to this problem is to implement the slightly more complicated optical circuit as shown in Fig. 10. In this configuration, the polarization analyzer of the previous optical circuit is replaced by a polarization beam splitter, and the optical powers in the orthogonal polarization states are detected. The signal processing of the two optical powers can be described by (see Fig. 10) [16],[17]

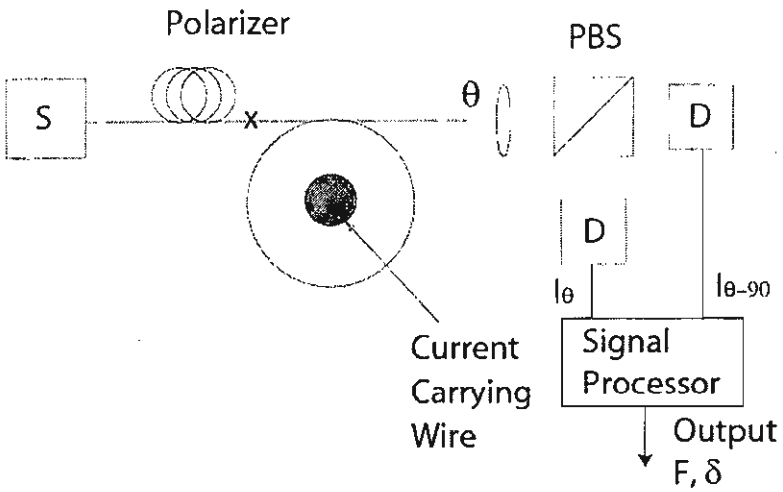

Fig. 10 Dual polarization polarimetric current sensor configuration, PBS: polarizing beam splitter, D: detector.

$$
\begin{aligned}
K &= \frac{I_\theta - I_{\theta-90}}{I_\theta + I_{\theta-90}} \\
&= 2\rho \frac{\sin\alpha}{\alpha} \sin 2(\theta-\eta) \\
&\quad + \left(\frac{2\rho}{\alpha}\right)^2 \cos\alpha \cdot \cos 2(\theta-\eta) \\
&\quad + \left(\frac{\delta}{\alpha}\right)^2 \left[\cos^2\left(\frac{\alpha}{2}\right) \cdot \cos 2(\theta-\eta) \right. \\
&\qquad \left. + \sin^2\left(\frac{\alpha}{2}\right) \cos 2(\theta+\eta) \right]
\end{aligned}
\tag{2.21}
$$

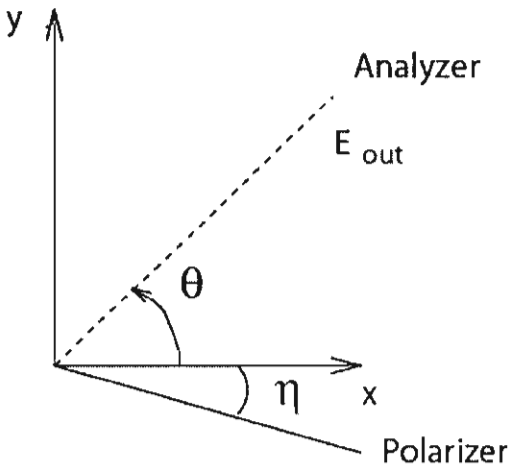

Fig. 11 Alignment of input polarizer and analyzer in the dual polarization polarimetric configuration

where

$$\rho = F + T, \tag{2.22}$$

I_θ and $I_{\theta 90}$ are sensor output intensity at azimuth angles of θ and θ-90°, respectively. η is the azimuth angle of the input polarizer. $\alpha/2$ is defined as $\sqrt{\rho^2 + (\alpha/2)^2}$. T corresponds to circular birefringence and δ represents linear birefringence in the sensing loop.

There are several advantages associated with using this signal processing scheme. First, by comparing these two sensor outputs, the polarization state of the light at the output of the sensor is recovered directly independent of the light source intensity or the source intensity noise. This approach of signal processing can be an alternative to AC/DC normalization scheme (see sect. 4.1.1). Another advantage of this method is that changes in fiber birefringence can be tracked since the

relative amounts of DC light falling on the two detectors is related to the static birefringence present in the sensing coil [16]. Thus a real time correction to the scale factor of the sensor can be computed. This property is interesting for sensor application with scale factor accuracy requirements of 0.3% or better over a very wide range of temperature, since it only takes a few degrees of uncharacterized birefringence to change scale factor more than this.

This method is adopted by Siemens bulk optical current sensor [17] to track the linear birefringence with temperature resulting in a temperature compensated current sensor. For simplicity, assume the circular birefringence, T, to be negligible (T=0). With the angular adjustment of $\sin 2(\theta-\eta)=1$, the signal processing output, K, when F=0 can be further simplified to

$$K=\sin^2\left(\frac{\delta}{2}\right)\cdot\cos 2(\theta+\eta) \tag{2.23}$$

The linear birefringence, δ, can be tracked this way. By adjusting $\sin 2(\theta-\eta)=1$ and assuming small current induced polarization state rotations, ($F \ll \delta$), the signal processing output, K, is given by

$$K\approx 2F\frac{\sin\delta}{\delta}+\sin^2\left(\frac{\delta}{2}\right)\cdot\cos 2(\theta+\eta) \tag{2.24}$$

The AC and DC part of the signal processing output, K, can be described by

$$K_{AC}\approx 2F\frac{\sin\delta}{\delta} \tag{2.25}$$

$$K_{DC}\approx \sin^2\left(\frac{\delta}{2}\right)\cdot\cos 2(\theta+\eta) \tag{2.26}$$

where the current on the line, I, is assumed to be AC. K_{AC} depends on the measured current, F, and linear birefringence, δ. K_{DC} depends only on the linear birefringence, δ. The AC part and DC part of the signal out, K, can be used to evaluate the drift of the operating point K_{DC} and thus the linear birefringence, δ. This information is then used to calibrate the F measurement.

2.3 Reciprocal Polarimetric Current Sensors

This type of fiber optic current sensors employs the same principle (to detect plane of polarization rotation) as that of the unidirectional polarimetric current sensors. The only difference is that this sensor interrogated in both directions. This optical circuit has the advantage of minimizing the birefringence induced offset problem associated with the unidirectional one.

Faraday mirror reciprocal fiber optic current sensor (see Fig. 12) uses a Faraday mirror at the end of the sensing fiber. The Faraday mirror consists of a Faraday rotator which rotates the polarization state of linearly polarized light by 45° followed by a mirror. Linearly polarized light entering the Faraday mirror will return in the orthogonal linear polarization (see Fig. 13). So if x polarized light goes in, y polarized light comes out. This orthogonal relation remains true for any orientation of the input linear polarization state.

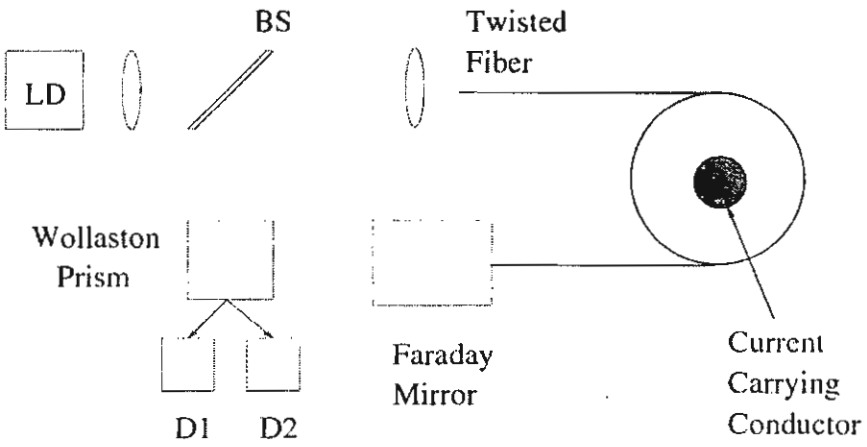

Fig. 12 Faraday mirror reciprocal fiber optic current sensor.

Fig. 12 shows the optical circuit [18]. Linearly polarized light enters the sensing fiber which in this case may be a twisted single-mode fiber. The twist in the single-mode fiber creates a circular birefringence that is sufficiently large to quench any residual linear birefringence which may have been present. The axis of the polarization state is rotated 90° by the Faraday mirror, and the polarization state of the light begins to unwind itself as it retraces its path through the twisted single-mode fiber. When the light reaches the original entry point of the sensing fiber, it comes back exactly orthogonal to its entry state except for the non-reciprocal rotation due to the Faraday effect which is doubled on the round trip. The final output state of the polarization thus depends only on current carried by the wire. This sensor output can be described by

$$E_{out} = \frac{1}{2}\vec{L}\cdot FM\cdot\vec{L}\cdot E_{in}, \tag{2.27}$$

where FM corresponds to Faraday mirror matrix. $\bar{L}$ and $\tilde{L}$ represent the sensing fiber matrix in the forward (from left-to-right) and backward direction [defined previously in (2.10) and (2.15)].

$$FM = \begin{bmatrix} 0 & -1 \\ 1 & 0 \end{bmatrix}, \tag{2.28}$$

Assume that the input light is linearly polarized in the x- axis, *i.e.*

$$E_{in} = \begin{bmatrix} E_x = 1 \\ E_y = 0 \end{bmatrix} = \begin{bmatrix} 1 \\ 0 \end{bmatrix}.$$

We obtain

$$E_{out} = \frac{1}{2}\begin{bmatrix} -(AD + BC) \\ BD - AC^* \end{bmatrix} \tag{2.29}$$

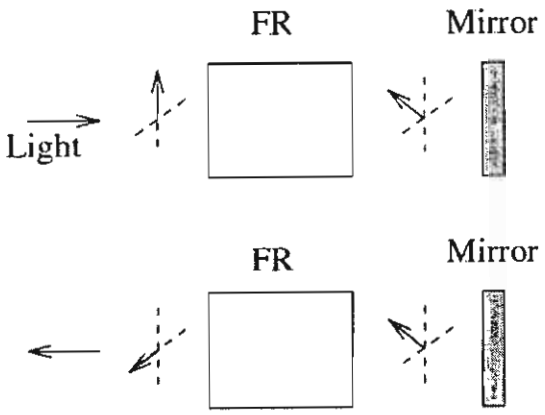

Fig. 13 Principles of Faraday mirror, FR: Faraday rotator

For highly twisted birefringence fiber ($T \gg \delta/2, F$), we obtain the simplified expression of the sensor output, E_{out}, as where A, B, C, and D retain their previous definitions

$$E_{out} \approx \frac{1}{2}\begin{bmatrix} -\sin F \\ \cos F \end{bmatrix}. \tag{2.30}$$

This sensor is immune to effect of vibration since any polarization rotation associated with the extra birefringence is undone during the return trip of the light through the sensor. This sensor configuration can be adapted well with the polarizing beam splitter, dual detection scheme, with all its advantages which were shown for the unidirectional polarimetric current sensor. When the polarizing beam splitter is used, this sensor may also more reliably sense DC currents - the ability to do this directly depends on the ideals operation of the Faraday mirror. Note that the successful operation of this sensor depends critically on the ideal operation of the Faraday mirror.

To complete this discussion, we summarize the comparison between the basic polarimetric and the reciprocal polarimetric fiber optic current sensing technique. The straightforward or uni-directional polarimetric current sensor is appropriate only for AC measurements, but the upper frequency limits is in the several MHz. The DC light is used for normalizing the AC measurement; birefringence gives erroneous result for DC current measurement. Vibrations, which impress a time varying birefringence onto the fiber show up as an apparent current. Birefringence also yields a scale factor degradation. Consequently, annealed fiber sensing coils with good vibration isolated packaging are required.

The vibration sensitivity of the straightforward polarimetric current sensor can be suppressed by using reciprocal, or bi-directional polarimetric current configuration. However, the scale factor of this type of sensor is still degraded by the presence of birefringence, so annealed fiber coils are still used. The Faraday mirror based current sensor, however, can use a highly twisted fiber instead of an annealed fiber, since it is insensitive to circular birefringence, and twist can be used to quench the effects of linear birefringence in the sensing loop. Finally, the reciprocal polarimetric current sensor has a better chance of measuring DC currents than the uni-directional polarimetric, but this measurement relies heavily on the quality of the optical components, such as the split ratios of the directional couplers or the exactness of the 45° in the Faraday mirror.

Furthermore, Faraday mirror is expensive due to the cost of Faraday rotator (about US$1,200). It is also difficult to fabricate into the fiber end. Therefore, we show a reciprocal configuration without a Faraday rotator, which makes sensor's cost to be cheaper. Its performance and the vibration sensitivity will be discussed in the next chapter.

Chapter 3

MATHEMATICAL MODELING OF RECIPROCAL FIBER-OPTIC POLARIMETRIC CURRENT SENSORS

In this chapter we discuss about reciprocal polarimetric current sensor. This configuration is similar to that of the Faraday mirror reciprocal sensor (mentioned in the sect. 2.3) but without a Faraday rotator, which is expensive and difficult to fabricate at the end of the sensing fiber.

First, we analyze the sensor's performance with Jones matrices and study about its state of polarization. Then, signal processed output or so called "normalized contrast ratio" and mathematical modeling of the vibration effects on current measurement error are described.

3.1 Overviews

Fiber-Optic current sensors, which rely on magneto-optic Faraday effect and Ampere's law, have been received considerable attention for possible application in electric power industry as magneto-optic current transformers (MOCT) in the past few decades [1]-[5]. These MOCTs inherently have several potential advantages over conventional ferromagnetic current transformers (CTs). These include flat bandwidth response (DC to several MHz), wide linear dynamic range (more than five orders of magnitude), no hysteresis, and by proper design insensitivity to electro-magnetic interference (EMI) and radio frequency interference (RFI) owing to their all-dielectric structure of fiber optics. Other advantages include smaller size, and consequently

lighter weight, making installation easier. Finally, they are completely immune from catastrophic explosive failures, where as iron-core CTs are not.

Several approaches of Faraday-based current sensors have been demonstrated. Although fiber-optic current sensors have several advantages over conventional CTs, they have yet to overcome undesirable susceptibility to environmental perturbations, *i.e.* temperature and acoustic perturbations, in the sensing part. One approach uses unidirectional polarimetric technique. This method of current sensing detects the intensity change due to polarization rotation from the induced magnetic field generated by current. The accuracy of this sensing method suffers from both linear and circular birefringence in the sensing fiber. To counter the birefringence errors, a reciprocal polarimetric type current sensor has been developed [18]-[21]. The perturbations affect the birefringence property of the fiber in the sensing part [21],[22]. Unidirectional polarimetric current sensors suffer from environmental perturbations due to varying birefringence in the sensing part [23]-[25]. This results in false current readings from environmental perturbations.

In this report, we analyze the performance of a reciprocal fiber optic current sensor including the output state of polarization, normalized contrast ratio, and effects of vibration on the sensor. The accuracy of the sensor is within 0.3% of the actual value and satisfies application in revenue metering. Two cases are considered for launched angles, η, with respect to the birefringence fast axis of the sensing fiber (see Fig. 14): η of 0 degree and 45 degrees.

3.2 Reciprocal Polarimetric Current Sensor with the Launched angle of 0 degree.

In this section, we show the mathematical modeling of sensor with η of 0°. The linear polarized light (E_{in}) is launched 0 degree to the fast axis of the fiber [19].

3.2.1 Mathematical descriptions of a reciprocal polarimetric current sensor

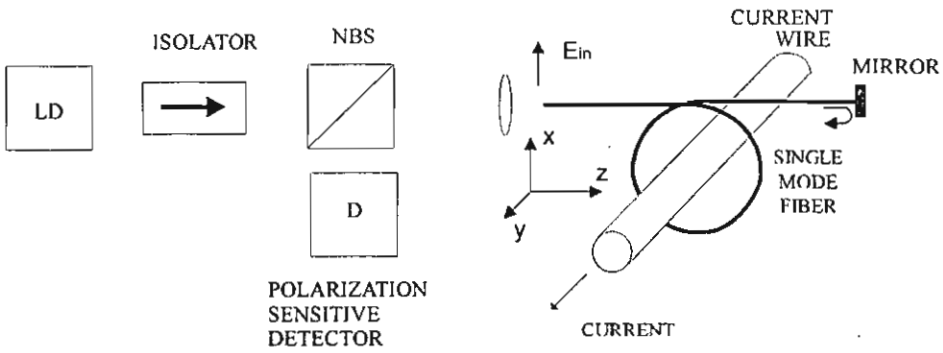

Fig. 14 Reciprocal fiber optic polarimetric current sensor, LD: laser diodes, NBS: non-polarizing beam splitter

The output electric field (E_{out}) of the sensor can be described by the Jones matrix [19]:

$$E_{out} = \frac{1}{2}\bar{L} \cdot M \cdot \vec{L} \cdot E_{in}, \tag{3.1}$$

where E_{in} represent input linearly polarized light in the x axis ($i.e.\ E_{in} = \begin{bmatrix} E_x = 1 \\ E_y = 0 \end{bmatrix} = \begin{bmatrix} 1 \\ 0 \end{bmatrix}$).

$\vec{L}$ represents a sensing fiber matrix when light propagating forward (from left-to-right in Fig. 14).

$\overleftarrow{L}$ represents a sensing fiber matrix when light propagating backward (from right-to-left), and M is the Jones matrix of the mirror.

$$\overleftarrow{L} = \begin{bmatrix} A & -B \\ B & A^{*} \end{bmatrix}, \tag{3.2}$$

where

$$A = \cos\frac{\alpha}{2} + j\sin\frac{\alpha}{2}\cos(\chi), \tag{3.3}$$

$$B = \sin\frac{\alpha}{2}\sin(\chi), \tag{3.4}$$

$$\frac{\alpha}{2} = \sqrt{(VNI + T)^2 + (\frac{\delta}{2})^2} \tag{3.5}$$

and $\tan\chi = 2(VNI + T)/\delta$. (3.6)

The VNI is the Faraday rotation induced by current and T is the circular birefringence. δ represents total linear birefringence. α represents the total birefringence. Assume both the total linear and circular birefringence to be uniformly distributed along the single-mode fiber optic sensing part.

$$\vec{L} = \begin{bmatrix} C & -D \\ D & C^{*} \end{bmatrix}, \tag{3.7}$$

where

$$C = \cos\frac{\beta}{2} + j\sin\frac{\beta}{2}\cos(\zeta), \tag{3.8}$$

$$D = \sin\frac{\beta}{2}\sin(\zeta), \tag{3.9}$$

$$\frac{\beta}{2} = \sqrt{(VNI - T)^2 + (\frac{\delta}{2})^2}, \tag{3.10}$$

$$\text{and } \tan\zeta = 2(VNI - T)/\delta, \tag{3.11}$$

$$M = \begin{bmatrix} 1 & 0 \\ 0 & 1 \end{bmatrix}. \tag{3.12}$$

3.2.2 State of polarization

To analyze the performance of the sensor, we first look at the sensor's output state of polarization. With linearly polarized input at the birefringence axis of sensing fiber, the normalized output electric field using (3.1), (3.2), (3.7), and (3.12) can be described by

$$E_x = AC - BD = a_1 \exp(j\delta_x), \tag{3.13}$$

$$E_y = AD + BC^* = a_2 \exp(j\delta_y), \tag{3.14}$$

where a_1, δ_x, a_2, and δ_y are the amplitude and phase of the electric field in the x- and y- axis, respectively.

The output state of polarization can be expressed on the Poincaré sphere (S_1, S_2, S_3) [26],[27]

$$S_1 = a_1^2 - a_2^2, \tag{3.15}$$

$$S_2 = 2a_1 a_2 \cos(\delta_x - \delta_y), \tag{3.16}$$

$$\text{and } S_3 = 2a_1 a_2 \sin(\delta_x - \delta_y). \tag{3.17}$$

In this Poincaré sphere, the state of polarization can be plotted on the surface of a sphere (see Fig. 15). Right circular polarization is on the North Pole, left circular on the South Pole, linear polarization on the

equator, and elliptical polarization in between. With input light aligned to birefringence axis of the sensing fiber, in an ideal fiber ($\delta, T \approx 0$), we would expect only Faraday rotation to occur. In this sensor, the rotation angle is $2VNI$. This is due to the fact that Faraday rotation is VNI in the forward direction down the fiber and, by nonreciprocal effect of Faraday effect, additional Faraday rotation is VNI in the backward direction down the same fiber. Thus, the total Faraday rotation of $2VNI$ occurs in the sensor. Assume that the input light is linearly polarized in the x-axis or vertical direction. It is (1,0,0) on Poincaré sphere or a dot shown in Fig. 15. In Fig. 15(a), the Faraday rotation angle of $2VNI$ will be equivalent to $4VNI$ along the equator (angle on the sphere is twice as much as the angular rotation and output is still linearly polarized). For example, the VNI of 0.01 π radians produces 0.04 π radians of rotation along the equator [see Fig. 21(a)]. The characteristic curve of a practical case (δ = 2 π and T = 120 π radians or $\delta/2T = 0.83\%$) is shown in Fig. 15(b). It is similar to the ideal case but with a very small deviation from the equator. The deviation from the ideal case produces some small susceptibility to varying birefringence and will be demonstrated in the next section. Fig. 15(c) with thin line for $\delta = \pi/6$ and $T = 0$ and thick line: $\delta = \pi/2$ and $T = \pi$ ($\delta/2T = 25\%$) shows that the sensor is not practical for current sensing when T does not dominate δ or $\delta/2T$ is not small. Fig. 15(b) shows that the desired response, which is close to that of the ideal one in Fig. 15(a), can be obtained by large T or $\delta/2T \ll 1$. The characteristic curve evolves around the equator (see Fig. 15(a) and (b)).

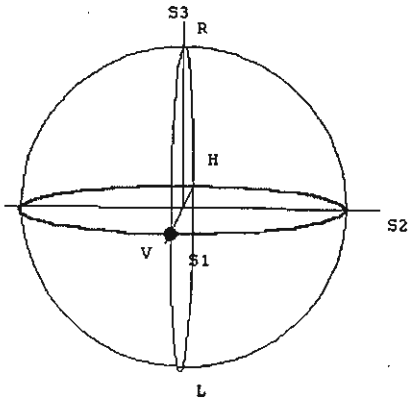

(a)

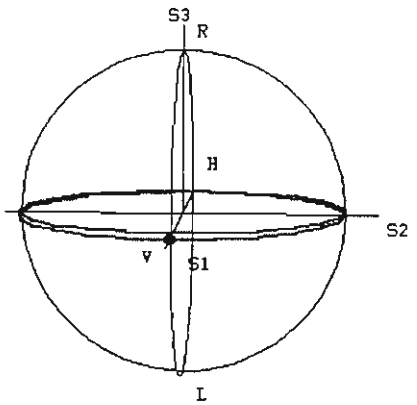

(b)

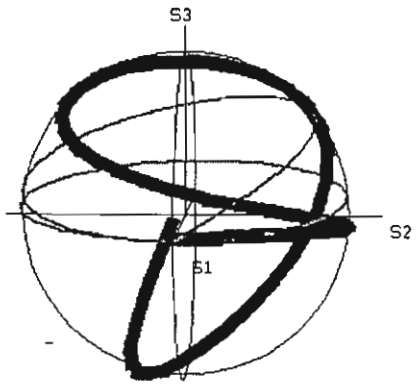

(c)

Fig. 15 Characteristic curves of the output polarization on the Poincaré sphere for $VNI = 0$ to π radians for (a) ideal case: $\delta = 0$ and $T = 0$ (b) $\delta = 2\pi$ and $T = 120\pi$ radians (c) the thin line: $\delta = \pi/6$ and $T = 0$ and the thick line: $\delta = \pi/2$ and $T = \pi$ radians.

3.2.3 Analysis of the normalized contrast ratio

The Wollaston prism is aligned 45° and –45 ° to the birefringence axis of the output end of the sensing fiber. The contrast ratio (K) is defined by [19]

$$K = \frac{I_{xo} - I_{yo}}{I_{xo} + I_{yo}}, \tag{3.18}$$

where I_{xo} and I_{yo} are the intensity at 45° and –45 ° with respect to the birefringence . fast axis of the output end of the sensing fiber, respectively. We can derive (3.19) using (3.1) to (3.12). Then, the contrast ratio (K) is given by

$$K = Sin(\alpha)Cos(\beta)Sin(\chi) + \frac{Sin\beta}{2}[Sin(2\chi - \zeta)(Cos\alpha - 1) + Sin\zeta(Cos\alpha + 1)] \quad (3.19)$$

Ideal case, T and δ are very small and negligible (such that $T, \delta \approx 0$). Equation (3.19) becomes

$$K = K_{ideal} = Sin(4VNI) \quad (3.20)$$

K provides the measurement of current and is linear ($K = Sin(4VNI) \approx 4VNI$) up to few tenths of a radian, or about 10^5 Amperes for a one-turn sensing coil. K is independent of the circular and linear birefringence in the sensing fiber. However, in practice, the use of high circular birefringence T or "spun" fiber ($VNI, \delta << T$) can overcome the intrinsic linear birefringence. To understand the performance of the sensor, we show the characteristic plot of the deviation of K, which is defined by

$$\Delta K(\%) = \frac{(K - K_{ideal})}{K_{ideal}} \times 100\% \quad (3.21)$$

as a function of linear birefringence (δ) and twist-induced circular birefringence (T) (see Fig. 16). The VNI is assumed to be 0.01π and the expected value of K_{ideal} from (3.20) is 0.125333. Fig. 16 shows the case when T is large and $\frac{\delta}{2T} \ll 1$. This sensor [19] shows reduced sensitivity to vibration significantly compared to that of the one-way "unidirectional" polarimetric sensor [22],[24],[25].

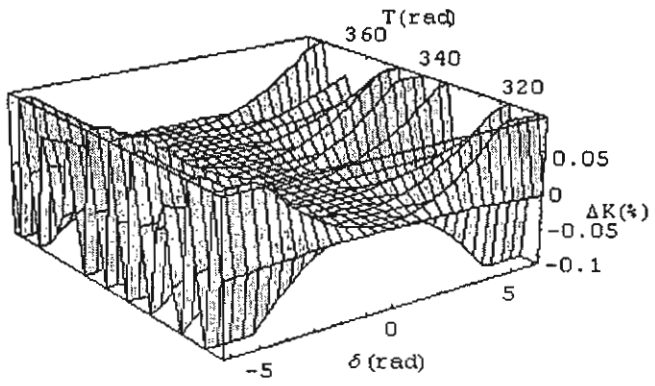

Fig. 16 The deviation of K (ΔK) as a function of linear birefringence (δ) and twisted circular birefringence (T)

The required intrinsic circular birefringence may be obtained by spun high birefringence fiber, twisted low birefringence fiber or winding low birefringence fiber in a toroidal geometry (see Fig. 17) [21],[23]. In the toroidal configuration, which we use in our simulation, T is about 120 π and δ is about a few π radians.

a. Linear birefringence versus vibration

There are two sources of linear birefringence in the sensing fiber: bending-induced linear birefringence (δ) and vibration-induced linear birefringence caused by transverse strain or vibration (δ_v), which can be described by [23]

$$\delta_v = 2\pi/\lambda \, \Delta n \, l, \tag{3.22}$$

where Δn is the refractive index change induced by stress in the medium (silica in this case), l is the effective length (under perturbation) of fiber, and λ is the center wavelength of the source. The refractive index change is given by

$$\Delta n = -n^3/2\, p\sigma = 0.311\sigma, \tag{3.23}$$

where n is the (unperturbed) refractive index of medium, σ is the strain, and p is the photoelastic constant of fiber (p = 0.2 in silica). The value of the Faraday rotation (VNI) depends on the Verdet constant (V). Typical value of V is 4.68 $\mu rad/$ A or 0.268°/(kA). In our case, we wrap the sensing fiber around an acrylic torus (see Fig. 17) so that the bend-induced linear birefringence is about a few π radians and a large twist-induced birefringence is about 120 π radians. As a result, the conditions of $\delta/2T \ll 1$ and $VNI \ll \delta \ll T$ are satisfied. Because the vibration affects linear birefringence, to induce a π-radian birefringence change $\Delta n = \lambda/2 = 3.165\times10^{-7}$ for a fiber length of 1 m. We can find the strain of 1.019x10^{-6} using (3.23). Reference [24] shows that δ_v in unidirectional polarimetric current sensor of 0.2 *rad* results in an apparent current of several hundred Amperes. In the following sections we will assume that δ_v changes by 0.2 π *rad* (a few times larger than 0.2 *rad*) between –0.1 π and 0.1 π from the static bend-induced linear birefringence δ (assumed to be 1.9 π radians).

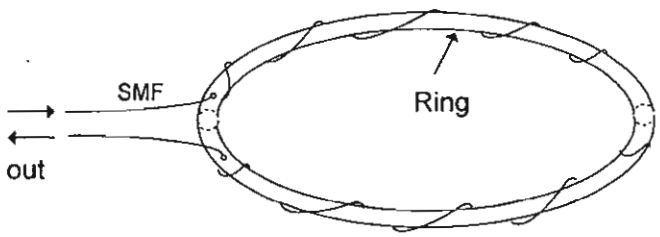

Fig. 17 The schematic of winding sensing fiber around a torus (with outside diameter of 45 cm) in order to add a large amount of circular birefringence, SMF: single-mode fiber. The torus has a cross section diameter of about 2 cm

In this sensor, Fig. 18 shows that the deviation of K is within 0.10% of the ideal case $(T, \delta \approx 0)$ when the range of values of the linear birefringence and circular birefringence are (1.8 π, 2.0 π) and (119.5 π, 120.5 π) radians, respectively.

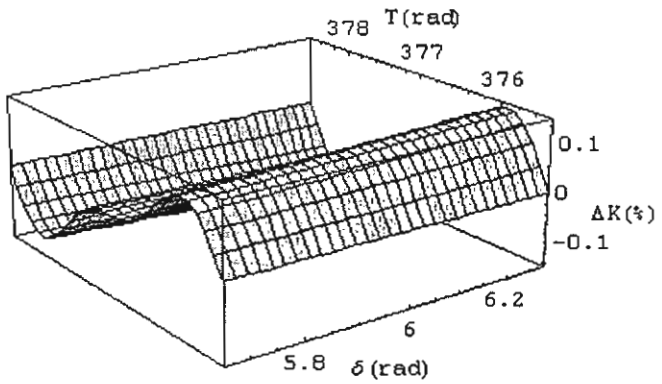

Fig. 18 In case of birefringence changes due to vibration, the deviation of K (ΔK) when VNI = 0.01 π radians as a function of linear birefringence (δ is between 1.8 π and 2.0 π radians) and circular birefringence (T is between 119.5 π and 120.5 π radians).

b. Deviation of ΔK versus linear birefringence

This sensor exhibits small dependence on linear birefringence. Fig. 19 shows that the absolute value of the deviation of K is below 0.007% when δ is less than 2 π radians when $VNI = 0.01\pi$ and T = 120 π radians. In this case, the approximation of K is

$$Sin(4VNI)[1-1.750\text{x}10^{-6}\delta^2] = 0.125333[1-1.750\text{x}10^{-6}\delta^2].$$

Using (3.19) and (3.21), $\Delta K(\%)$ is given by

$$\Delta K(\%) = -1.750\text{x}10^{-4}\delta^2. \qquad (3.24)$$

Maximum δ to achieve the accuracy of 0.3% for revenue metering application from (3.24) is 13.18 π *rad.*

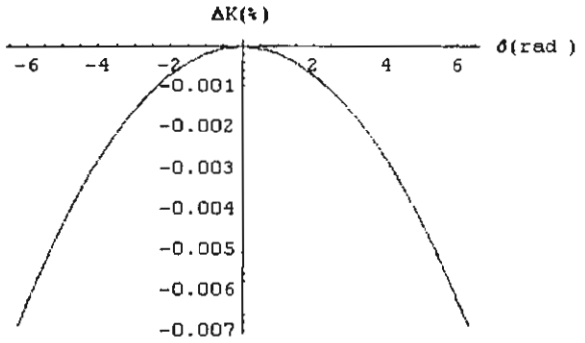

Fig. 19 Simulated deviation of K in percent varies with linear birefringence ($VNI = 0.01\pi$, $T = 120\pi$)

c. Apparent current versus linear birefringence

Environmental acoustic perturbations and mechanical vibration on the sensing fiber can cause angular rotation of lightwave polarization and may affect birefringence property of the sensing fiber [22],[24]. The result could be misread as actual current. Reference [22] shows that mechanical vibrations with a magnitude of 3.0 $g_{p\text{-}p}$ (1 g = 9.8 m/s^2) applied to a sensing fiber of unidirectional polarimetric sensor can cause an apparent current of 400 $A_{p\text{-}p}$. Simulated apparent current (T = 120 π, $\delta_v = 0.1\pi \sin(2\pi f_v t)$, and the total linear birefringence is assumed to vary between 1.8π and 2.0π radians) for this sensor is shown in Fig. 20. The frequency of vibration (f_v) and varying linear birefringence (δ_v) is chosen to be 50 Hz, which is common to electric power systems [22]. Very small apparent currents of less than 2.0x10^{-5} Amperes for 633 nm

wavelength when the total linear birefringence δ is (1.8π, 2.0π) radians and the δ_v is shown in Fig. 20(a).

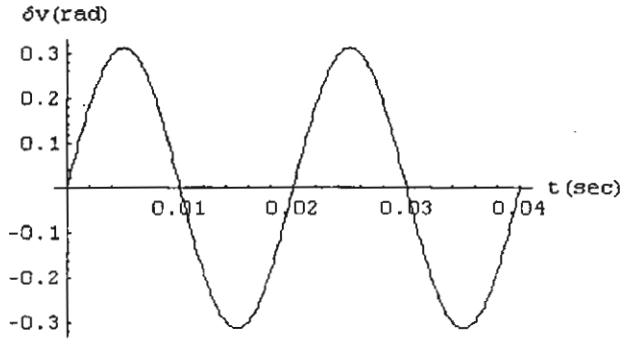

(a)

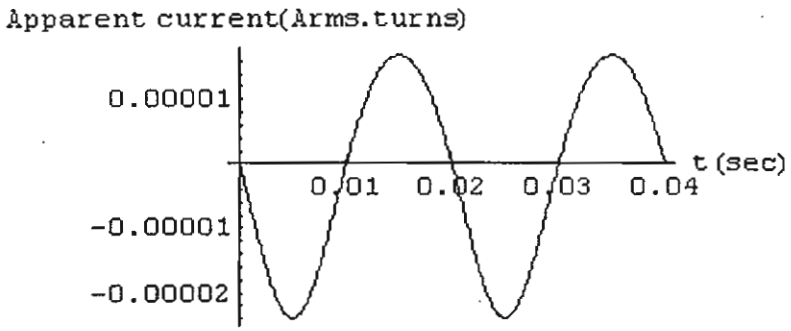

(b)

Fig. 20 Simulated apparent current (b) in Amperes.turns versus birefringence change (a) (VNI = 0 and T = 120π)

3.2.4 Mathematical model and state of polarization

Reference [24] shows that the linear birefringence change due to vibration of 0.2 radians can induce a large apparent current (equivalent to several hundred $A_{p\text{-}p}$) in unidirectional polarimetric current sensor. However, Fig. 18 indicates that when both δ and T change as much as 0.2 π (many times larger than 0.2 radians) and 1 π radians, respectively, the ΔK or accuracy of the sensor is

within 0.1% (0.3% is required for revenue metering). Fig. 21 shows the two cases when δ and T change due to vibration and the current is applied (VNI = 0.01 π) to the sensor. The dot and the small line in Fig. 21 represent the SOP under vibration when δ and T change, respectively.

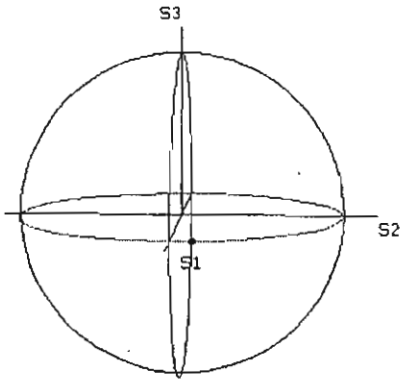

(a)

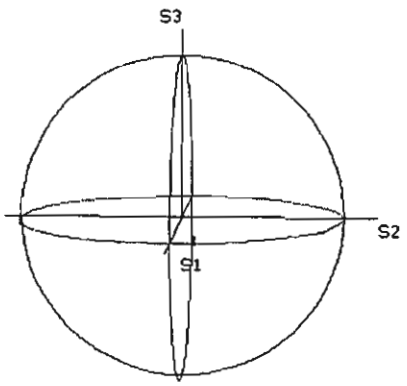

(b)

Fig. 21 State of polarization of the output of sensor with vibration on the Poincaré sphere VNI= 0.01 π (a) linear birefringence (δ is between 1.8 π and 2.0 π radians) T = 120 π (b) twisted circular birefringence (T is between 119.5 π and 120.5 π radians) δ = 2 π radians.

3.3 Analysis of the Sensor with the Launched Angle $\eta = 45^o$

In this section, we discuss about the performance of a reciprocal fiber optic current sensor with $\eta = 45^o$ [28] (see Fig. 14) including the output state of polarization, normalized contrast ratio, and effects of vibration on the sensor. This configuration show a better performance than that with $\eta = 0^o$.

3.3.1 State of polarization

When the linear polarized light (E_{in}) is launched 45° to the fast axis of the fiber, the output electric field of the sensor is given by (3.1). However, the input electric field can be described by

$$E_{in} = \begin{bmatrix} E_x = \cos(45^o) \\ E_y = \sin(45^o) \end{bmatrix} = \frac{1}{\sqrt{2}} \begin{bmatrix} 1 \\ 1 \end{bmatrix}, \tag{3.24}$$

where $\vec{L}$, $\bar{L}$, and M are defined earlier in section 3.2.

3.3.2 The normalized contrast ratio (K)

Using (3.1) to (3.12) and (3.25), we obtain

$$K = -\cos(\alpha)\cos(\beta) + \cos(\zeta - \chi)\sin(\alpha)\sin(\beta) \tag{3.26}$$

For ideal case, T and $\delta \approx 0$ are negligible, so (3.26) becomes

$$K_{ideal} = -\cos(4VNI) \tag{3.27}$$

However, in practice, the use of high circular birefringence T or "spun" fiber ($VNI, \delta << T$, e.g. $\delta = 1.9\pi, T = 120\pi$) can overcome the intrinsic

linear birefringence. This K is called K_{dc} and can be described by (see Appendix 3A)

$$K_{dc} = -\cos(4VNI) + \frac{\delta^2}{\alpha\beta}\sin(\alpha)\sin(\beta) \tag{3.28}$$

To understand the performance of this sensor, we show the characteristic plot of the deviation of K (ΔK), which is

$$\Delta K(\%) = \frac{K - K_{dc}}{K_{dc}} \times 100\% \tag{3.29}$$

In this sensor, Fig. 22 shows that the absolute value of the deviation of K is within 0.01% of that of an ideal case (T, $\delta \approx 0$) when the range of values of the linear and circular birefringences are (1.8π, 2.0π) and (119.5π, 120.5π) radians, respectively.

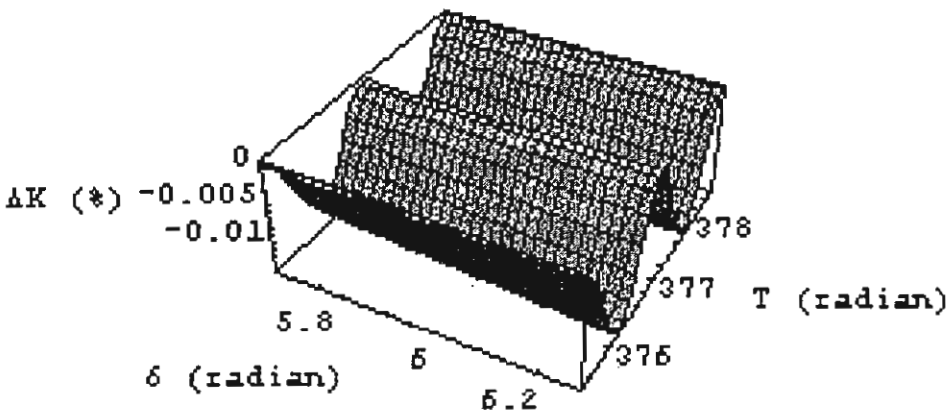

Fig. 22 The deviation of K (ΔK) when VNI = 0.01 π radians as a function of δ is between 1.8 π and 2.0 π radians T is between 119.5 π and120.5 π radians.

3.3.3 Deviation of ΔK versus linear birefringence

This sensor exhibits small dependence on linear birefringence. Fig. 23 shows that the absolute value of the deviation of K is below 1×10^{-4}% when δ is between -2 π and 2 π radians with VNI = 0.01 π and T = 120 π radians. Using (3.26),(3.28), and (3.29), $\Delta K(\%)$ is given by

$$\Delta K(\%) = 2.59616\times10^{-6}\delta^2 - 9.24994\times10^{-5}. \qquad (3.29)$$

In Fig. 23, maximum value of $|\delta|$ to achieve the accuracy of 9.24994×10^{-5}% is 8.38 radians. Zero vibration sensitivity occurs ($\Delta K = 0$) when $|\delta|$ is about 6.0 radians

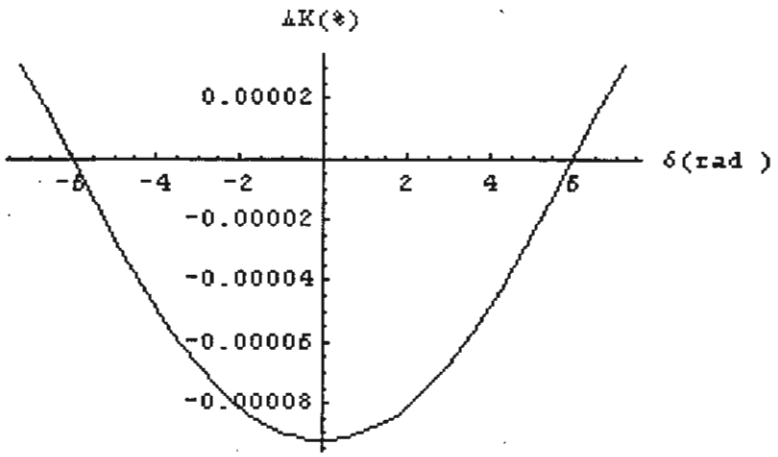

Fig. 23 Simulated deviation of K in percent varies with linear birefringence ($VNI = 0.01\pi$, $T = 120\pi$)

3.3.4 Apparent current versus linear birefringence

Acoustic vibration on the sensing fiber can cause angular rotation of light wave polarization and may affect birefringence property of the sensing fiber. The result could be misread as an actual current.

Mechanical vibrations with a magnitude of 3.0 $g_{p\text{-}p}$ (1g = 9.8 m/s^2) applied to a sensing fiber of unidirectional polarimetric sensor can cause an apparent current of 400 $A_{p\text{-}p}$. Simulated apparent current (T = 120 π, δ_v = 0.3 sin(2π f_v t), and the total linear birefringence is assumed to vary between 1.8π and 2.0π radians) for this sensor is shown in Fig. 24. The frequency of vibration (f_v) and varying linear birefringence (δ_v) are chosen to be 50 Hz, which is common to electric power systems [22]. Very small apparent currents of less than $2.5x10^{-8}$ Amperes for 633 nm wavelength when the total linear birefringence δ is (1.8π, 2.0π) radians and the δ_v is shown in Fig. 4(a).

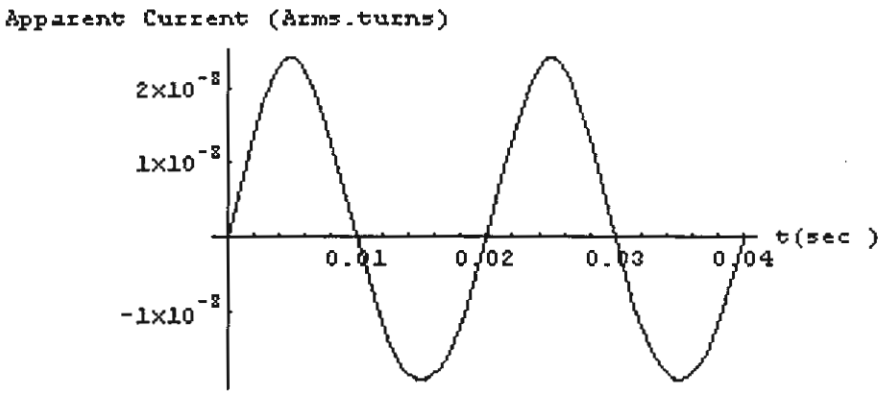

(a)

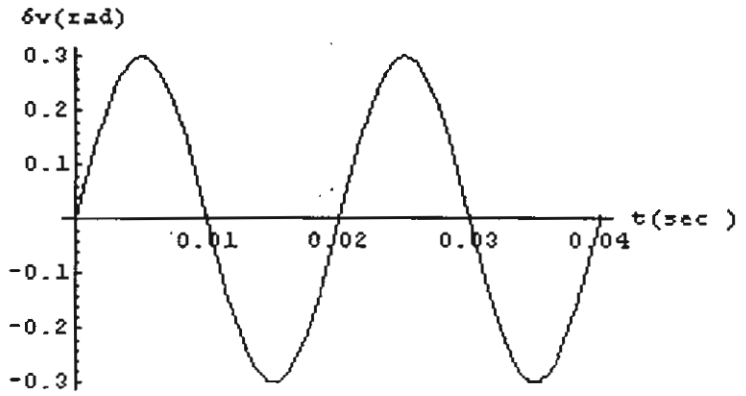

(b)

Fig. 24 Simulated apparent current (b) in Amperes.turns versus birefringence (a) (VNI= 0 and T= 120π)

3.4 Discussions and conclusions

The mathematical model of reciprocal fiber-optic current sensor is demonstrated. The performance of the current sensor is similar to that of the ideal case ($\delta, T \approx 0$). This can be shown by the state of polarization of the sensor output when $\delta/2T$ is small (T dominates δ and VNI). To satisfy the conditions of $\delta/2T \ll 1$ and $VNI \ll \delta \ll T$ helical winding on an acrylic torus is used (see Fig. 17). We can find the normalized contrast ratio K being affected by unwanted changes in linear birefringence δ caused by acoustic perturbations and mechanical vibrations and circular birefringence T. For large T, deviation of K (%) is a quadratic function of δ but the contribution of perturbations and vibrations is small and within 0.1% (0.3% of the actual value required for applications in revenue metering). The apparent current shows that the susceptibility of sensor to varying linear birefringence is small and

negligible. Two cases of the launched angles (0 and 45 degrees) are considered. Configuration with the launched angle of 45 degrees has a better performance and much lower vibration sensitivity.

Appendix 3A

To verify K_{dc}, from (3.26)

$$K = -\cos(\alpha)\cos(\beta) + \cos(\zeta - \chi)\sin(\alpha)\sin(\beta)$$

K_{dc} is occurred in practical when $\delta = 1.9\pi$ and $T = 120\pi$, and $T \gg VNI$

$$\left(\frac{\delta}{2(T+VNI)}\right)^2 \approx \left(\frac{\delta}{2(T-VNI)}\right)^2 \ll 1.$$

So $$\alpha \approx 2(T+VNI)\sqrt{1+\left(\frac{\delta}{2(T+VNI)}\right)^2}$$

$$\approx 2(T+VNI)\left(1+\frac{1}{2}\left(\frac{\delta}{2(T+VNI)}\right)^2\right)$$

$$\approx 2(T+VNI)$$

where , $\sqrt{1+x} \approx 1+\frac{x}{2}$, $x \ll 1$,

$$\beta \approx 2(T-VNI)\sqrt{1+\left(\frac{\delta}{2\cdot(T-VNI)}\right)^2}$$

$$\approx 2(T-VNI)\left(1+\frac{1}{2}\left(\frac{\delta}{2(T-VNI)}\right)^2\right),$$

$$\approx 2(T-VNI),$$

where $\sqrt{1-x} \approx 1-\frac{x}{2}$, $x \ll 1$ then, $\alpha - \beta = 4VNI$, the first term on the right-hand side of (3.26) becomes

$$-\cos(\alpha)\cos(\beta) = -\cos(\alpha - \beta)$$

$$= -\cos(4VNI)$$

and $\cos(\zeta - \chi) = \cos(\zeta)\cos(\chi) + \sin(\zeta)\sin(\chi)$, using (3.6) and (3.11) to obtain

$$\cos(\zeta - \chi) = \frac{\delta^2}{\alpha\beta} + \frac{4}{\alpha\beta}(T^2 - VNI^2)$$

when VNI is very small and $2T \approx \alpha \approx \beta$, then $\cos(\zeta - \chi)$ become

$$\cos(\zeta - \chi) = \frac{\delta^2}{\alpha\beta} - 1$$

Substitute into (3.26), to get

$$K_{dc} = -\cos(\alpha)\cos(\beta) - \sin(\alpha)\sin(\beta) + \frac{\delta^2}{\alpha\beta}\sin(\alpha)\sin(\beta)$$

$$= -\cos(\alpha - \beta) + \frac{\delta^2}{\alpha\beta}\sin(\alpha)\sin(\beta)$$

$$= -\cos(4VNI) + \frac{\delta^2}{\alpha\beta}\sin(\alpha)\sin(\beta)$$

Chapter 4

EXPERIMENTAL STUDY OF VIBRATION SENSITIVITY IN UNIDIRECTIONAL POLARIMETRIC CURRENT SENSORS

In this chapter, we describe the implementation of a unidirectional polarimetric current sensor. Experimental study of vibration sensitivity is also demonstrated. Furthermore, mathematical modeling of the vibration sensitivity effects on the sensor is formulated and shows good agreements with the experimental results.

4.1 Mathematical Descriptions of Unidirectional Polarimetric Current Sensors

In this section, we discuss about the mathematical modeling of unidirectional polarimetric current sensors [24],[25]. Two cases of analyzer angle with respect to the input polarizer are described. The modeling provides information about birefringence sensitivity and vibration sensitivity for the current measurement error.

Fig. 25 shows a simplified configuration of unidirectional polarimetric current sensors. Linear polarized light from HeNe laser is coupled to the single-mode fiber. Polarization controller in front of the sensing fiber is to launch the linear polarized into the fast axis of fiber loop forming a sensing part. Light passes through a polarizer (we usually call an "analyzer") at the fiber output. θ is the angle between the analyzer and fast birefringence axis at the end of sensing fiber loop. A simplified configuration consists of input linear polarized electric field (E_{in})

entering the sensing fiber loop, an analyzer aligned θ degrees with respect to the birefringence fast axis of the fiber loop, and a detector. The analyzer angle θ of 45° provides maximum sensitivity and linear dynamic range. In this configuration, we can simulate a large current by using magnetic field generating coil with *e.g.* N=1,000 turns. By the Ampere's law (2.1) and (2.2), if the input current is 1 A, the equivalent magnetic field will be similar to the field generated by wrapping one turn of fiber around a current conductor with 1,000 A in it.

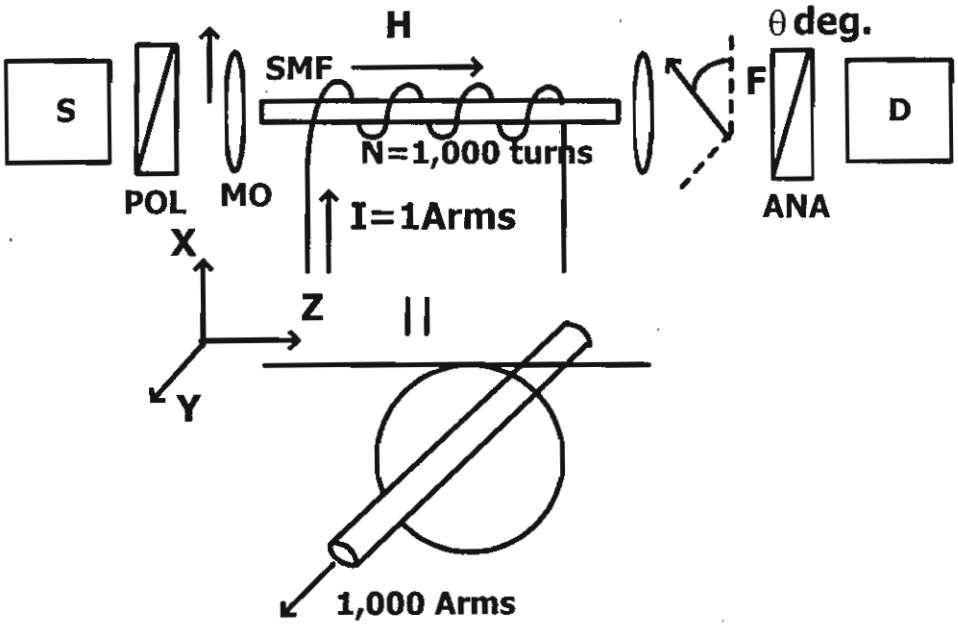

Fig. 25 Unidirectional polarimetric current sensor

The output electric field (E_{out}) of the sensor impinging on the detector can be described by Jones Calculus

$$E_{out} = P \cdot R(\theta) \cdot \vec{L} \cdot E_{in}, \tag{4.1}$$

where E_{in}, $\vec{L}$, $R(\theta)$, and P represent input linearly polarized light in the x- axis, sensing fiber matrix, coordinate rotation matrix with the angle difference between the output analyzer and the birefringence fast axis at the fiber end (θ), and P is the analyzer matrix ($P=\begin{bmatrix}1 & 0\\ 0 & \varepsilon\end{bmatrix}$), respectively. Extinction ratio ε of a good quality polarizer is very small (ε is better than –50 dB or $\varepsilon \leq 7\text{x}10^{-3}$) and can be assumed negligible in our analysis.

$$\vec{L}=\begin{bmatrix}A & -B\\ B & A^{*}\end{bmatrix}, \tag{4.2}$$

where

$$A=\cos\frac{\alpha}{2}+j\sin\frac{\alpha}{2}\cos(\chi) \tag{4.3}$$

$$B=\sin\frac{\alpha}{2}\sin(\chi) \tag{4.4}$$

$$\frac{\alpha}{2}=\sqrt{(VNI+T)^2+(\frac{\delta}{2})^2} \tag{4.5}$$

$$\tan\chi=2(VNI+T)/\delta \tag{4.6}$$

where δ, F, T, and α are the linear birefringence, Faraday rotation, twisted-induced circular birefringence, and total birefringence in radians. Coordination rotation matrix $R(\theta)$ is given by

$$R(\theta)=\begin{bmatrix}cos\theta & sin\theta\\ -sin\theta & cos\theta\end{bmatrix} \tag{4.7}$$

There are two cases for angle, θ, between the input polarizer and analyzer.

a. Angle θ of 45 degrees

We analyze the effect of birefringence in the sensing loop on this current sensor. There are two types of birefringence in the sensing coil: linear and circular birefringence. Using (4.1) to (4.7), a normalized output intensity ($Intensity \propto |E_{out}|^2$) on the detector is given by (see Appendix 4A)

$$I_{45^\circ}/I_0 = \frac{1}{2}\left[1 + 2(F+T)\cdot\frac{\sin\alpha}{\alpha}\right], \tag{4.8}$$

where I_0 is the maximum intensity at the detector. Equation (4.8) shows that the sensor output intensity is distorted by both the linear and circular birefringences.

When the circular birefringence is the dominate source of birefringence in the sensing coil ($T \gg \delta/2$ and thus $F+T \gg \delta/2$), the sensor output intensity can be described by

$$I_{45^\circ}/I_0 = \frac{1}{2}[1 + \sin 2(F+T)] \tag{4.9}$$

Circular birefringence, usually associated with a twist in the fiber, causes the plane of linear polarization to rotate. When this birefringence is the dominate source in the fiber sensing coil, this effect of plane of linear polarization rotation is indistinguishable from that produced by a DC current. Thus this birefringence causes an apparent offset in current reading. Equation (4.9) confirms this circular birefringence effect. If the circular birefringence is sufficiently large, it also causes a change in the scale factor since it effectively changes the angle of the output analyzer. However, when the output analyzer is set to an angle of 45°, we have zero sensitivity in the scale factor to a slight angular

misalignment of the output analyzer, or alternatively we can tolerate small changes in any circular birefringence (ΔT) that may exist in the sensing coil. This is due to the fact that the sensor scale factor is reduced by factor of $\cos(\Delta T)$.

Linear birefringence in the sensing loop gives rise to preferred axes within the sensing loop. This results in a reduced sensitivity to current by factor of $\frac{\sin\delta}{\delta}$. Linear birefringence also causes the linear polarization state of the light to assume a slightly elliptical polarization state, with its major axis slightly rotated. Thus, it also can yield an apparent DC current.

In this case, when the linear birefringence is the dominate source of birefringence in the sensing coil ($\delta/2 \gg F+T$), the sensor output intensity is given by

$$I_{45^\circ}/I_0 = \frac{1}{2}\left[1+2(F+T)\cdot\frac{\sin\delta}{\delta}\right]. \qquad (4.10)$$

Note that Equation (4.10) confirms the reduction of the scale factor by the factor $\frac{\sin\delta}{\delta}$.

In addition, this birefringence causes non-uniform sensitivity to induced magnetic field along the loop, because birefringence causes the light polarization state to evolve away from linearly polarized state as it propagates along the loop. As the sensitivity is non-uniform along the sensor, the sensing coil does not perform the closed line integral of $\vec{H}\cdot d\vec{l}$. Thus the sensor will exhibit some dependence on where the

conductor is within the sensor and will also exhibit some sensitivity to externally generated magnetic field [10].

Bend-induced linear birefringence in the sensing coil affects this type of current sensor significantly. For example, with a sensing coil made from 125 μm diameter single-mode fiber forming a single turn 6 cm diameter coil for 0.82 μm wavelength exhibits bend-induced linear birefringence of 166°, using (2.8). The sensor scale factor is reduced by 10.9 dB (from the output without linear birefringence). Compared to a sensing coil made from the same diameter single-mode fiber forming a single turn 30 cm diameter coil for 1.3 μm wavelength exhibits bend-induced linear birefringence of only 5.91°. The sensor scale factor is reduced by only 0.02 dB (from the output without linear birefringence).

To avoid problems associated with linear birefringence inherent in this type of current sensor, annealed fiber is used [4],[5]. Sensing coils with less than one degree of linear birefringence per turn can be achieved. One drawback of this approach is that annealed fibers are brittle and must be handled and packaged very carefully. Even when annealed fiber coils are used, the total birefringence can still yield a rotation in the polarization state equivalent to that produced by hundreds of Ampere of DC currents. For example, the total linear birefringence of 45° in a fiber sensing coil yields an DC current offset of about 261 A (4.68 μrad/A at 633 nm). The total output also directly depends on the light source intensity, which can be normalized through a directional coupler, but directional coupler has uncertain split ratio.

In practice, the AC output optical signals can be divided by DC output to yield the AC current [5]. The signal-processed output is then described by

$$I_{AC}/I_{DC} = 2(F+T)\frac{\sin(\sqrt{4(F+T)^2+\delta^2})}{\sqrt{4(F+T)^2+\delta^2}}. \quad (4.11)$$

This signal processing output eliminates both coupler uncertainties and light source intensity uncertainties. Only the DC current information is lost, the AC current can be measured with a bandwidth down to a few Hz up to many MHz.

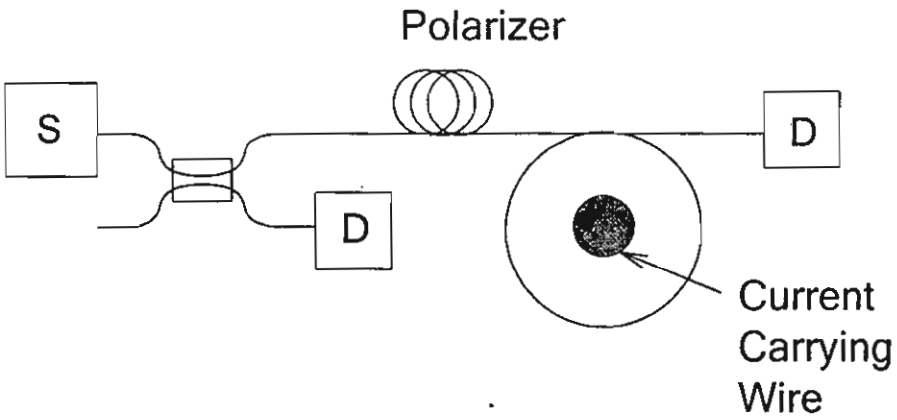

Fig. 26 Normalized unidirectional polarimetric current sensor

b. In our experimental study, θ of 60 degrees is used

In our experiment, we align the analyzer with θ of 60°, where the output signal-to-noise ratio (SNR) is better than that of θ of 45°, where the sensitivity of the sensor is maximum. Using (4.1) to (4.7), a normalized output intensity ($Intensity \propto |E_{out}|^2$) on the detector is given by

$$I_{60^\circ}/I_0 = \frac{1}{4} + \frac{\sqrt{3}}{2}\frac{\sin\alpha}{\alpha}\cdot(F+T) + 2\left[\frac{\sin(\alpha/2)}{\alpha}\cdot(F+T)\right]^2, \tag{4.12}$$

where I_0 is the maximum intensity at the detector. Substituting (4.5) into (4.12), we obtain

$$I_{60^\circ}/I_0 = \frac{1}{4} + \frac{\sqrt{3}}{2}\frac{\sin(\sqrt{4(F+T)^2+\delta^2})}{\sqrt{4(F+T)^2+\delta^2}}\cdot(F+T) + \left[1-\cos(\sqrt{4(F+T)^2+\delta^2})\right]\cdot\frac{(F+T)^2}{4(F+T)^2+\delta^2} \tag{4.13}$$

4.1.1 Current measurement

Equation (4.13) shows that the normalized output intensity is a function of F, δ, and T. With the input light aligned to birefringence fast axis of the sensing fiber, in an ideal fiber ($\delta, T \approx 0$), we would expect only Faraday rotation ($F=VNI$) to occur. Equation (4.13) becomes

$$I_{60^\circ}/I_0 = \frac{1}{2}\left[1+\sin(2F-30^\circ)\right] \tag{4.14}$$

Equation (4.14) indicates that the normalized output intensity is constant when there is no applied current (F = 0). When AC current ($I(t) = D\sin\omega t$) is applied (where D is zero-to-peak (0-p) amplitude in Ampere), F can be described by

$$F(t) = VNI(t) = (VND)\sin\omega t = F_0\sin\omega t, \tag{4.15}$$

where $\omega = 2\pi f$ and f is frequency of the applied current. V is the Verdet constant and a function of wavelength (4.68 μrad/A for wavelength of 633 nm). Then, $F_0 = VND$ is constant and depends on the current amplitude, the number of turns, and wavelength of operation. Substituting (4.15) into (4.14), we obtain the phase

modulation signal. Detector's output voltage (v_D) is proportional to the impinged output intensity ($v_D \propto I_{60^o}$) and is given by

$$v_D = \frac{K}{2}\left[1+\sin(2F_0 \sin\omega t - 30^o)\right], \tag{4.16}$$

where K is the maximum output voltage at the detector.

When F_0 is small, the output voltage at the detector of (4.16) can be approximated by (see Appendix 4B)

$$v_D(t) = v_{DC} + v_{AC}(t) \approx v_{DC} + v_{(0-p)}\sin(\omega t) \approx \frac{K}{2}\left[1+2\sqrt{3}F_0 \sin(\omega t)\right], \tag{4.17}$$

when F_0 is small and less than 0.04 radian, the output zero-to-peak (0-p) detector voltage $v_{(0-p)}$ is linear proportional to the applied current amplitude (D) as given by $V_{(0-p)} \propto 2\sqrt{3}F_0$.

4.1.2 Signal modulation

Current measurement can be found by a ratio of $v_{(0-p)}$ and v_{DC}, which is known as "signal modulation." Thus, signal modulation using (4.17) is given by

$$v_{(0-p)}/v_{DC} = 2\sqrt{3}F_0 = 2\sqrt{3}VND \tag{4.18}$$

The sensor output is linear up to 0.04 *rad* ($\sin(x) \approx x$) or about 8,500 A ($0.04 rad/V = 4.68\text{x}10^{-6}$ for wavelength of 633 nm). If the applied current is 1,000 A, the signal modulation using (4.18) will be $1.62\text{x}10^{-2}$. In practice, δ is not negligible but T is *e.g.* $\delta = 0.660$ and T = 0.05 radians. When the applied current is 1,000 A, the signal modulation using (4.13) is $1.378\text{x}10^{-2}$. Scale factor of the sensor is defined by

$SF = \frac{\text{signal modulation (in practice)}}{\text{signal modulation of the ideal case}}$. In this case, the scale factor SF is 0.85.

4.2 Experimental Setup and Results on Vibration Effects

In this section, we discuss about previous works and our research sponsored by TRF on vibration effects on unidirectional polarimetric current sensors. Vibrations induce an AC birefringence into the sensing coil. Since birefringence creates an effective offset current, an AC birefringence creates an apparent AC current, which is in the bandwidth of the sensor output.

4.2.1 Previous Works

This section is devoted to discussion of acoustic vibration effects on a unidirectional polarimetric current sensor (see Fig. 27). Shayne *et al.* [22] have shown the effects of acoustic vibrations on various components in this polarimetric current sensor.

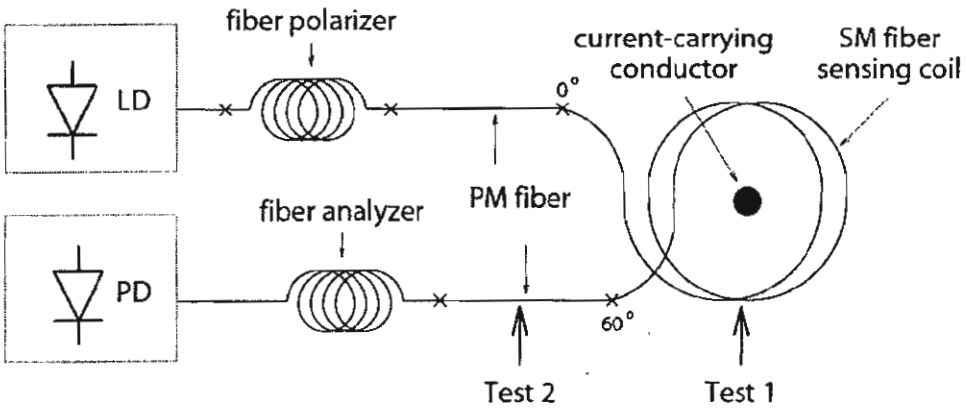

Fig. 27 Experimental setup for studying of mechanical vibration effects in unidirectional polarimetric current sensors

Fig. 27 illustrates the experimental set-up for studying these effects. The sensor is the unidirectional polarimetric sensor with input polarizer and analyzer to measure the rotation of the plane of polarization induced by the current carrying wire. The authors generated acoustic vibrations by using a small DC motor driving an unbalanced load. This motor was attached to a plate, which was used to couple the vibrations from the motor to various optical fiber components. For each test, a few inches of optical fiber was perturbed. A piezo-electric accelerometer attached to the optical fiber vibration plate was used to quantify the vibrations to the fiber. The fundamental frequency component of the applied acoustic waves was 200 Hz. Frequencies in this bandwidth are of great concern for electric power systems. Second and third harmonic (120 and 180 Hz) acoustic vibrations are prevalent in electric power systems.

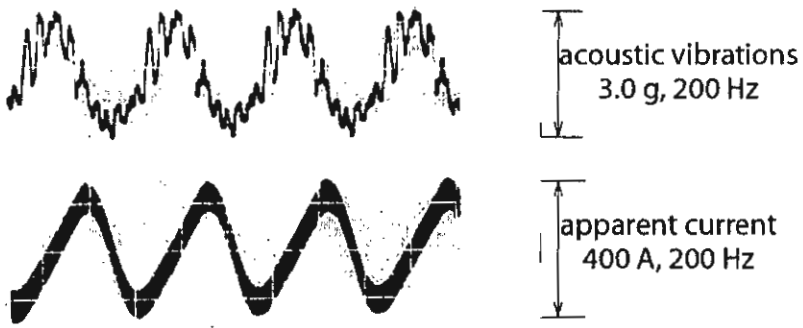

Fig. 28 (Test 1) response to the vibrations at the sensing coil.

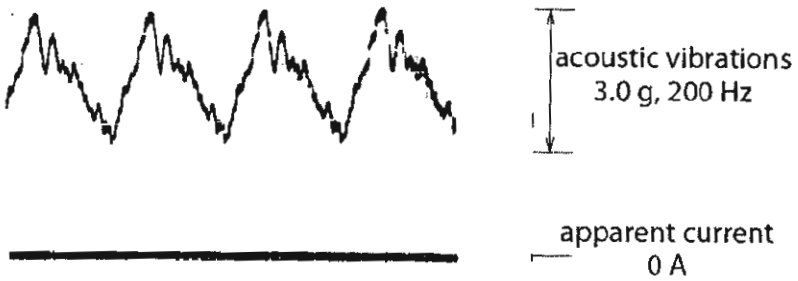

Fig. 29 (Test 2) response to the vibrations at the PM fiber lead

Fig. 28 and Fig. 29 show the influence of the acoustic vibrations on the sensing coil and the PM fiber lead, respectively. In Fig. 28, the acoustic perturbations with a magnitude of 3.0 *g* were applied to the Faraday sensing coil. As can be seen, this magnitude of vibration causes an apparent current of about 400 Amperes. It is noticeable that the higher frequency components in the vibration signal do not show up in the current output; apparently they were effectively damped by the fiber jacket, or the tape, which affixed the fiber to the vibration plate. These vibrations sufficiently modulate the angular rotation of the lightwave polarization azimuth to create what appears as an actual current in the conductor. Note that this polarimetric current sensor is highly susceptible to acoustic vibrations applied to the sensing coil. In this configuration, the sensing coil must be encased in a vibration insensitive package to avoid erroneous detection of a current signal. In Fig. 29, acoustic vibrations with a magnitude of 3.0 *g* coupled to the PM fiber leads yield no noticeable apparent current. This results from the

fact that the PM fiber leads are built with such high internal stress that they allow virtually no cross coupling from one linearly polarized mode to the other under the mechanical stress induced by the acoustic waves.

From this work, there are several frequency components of vibration and the authors did not study about false current versus vibration amplitude. In our research, we demonstrate the experimental study of this vibration effects on the current sensors. Vibration of a selected frequency and vibration of different amplitudes can be applied in the experimental study.

4.2.2 Actual current measurement

The following two sections are devoted to our techniques for experimental study of vibration sensitivity effects on current measurement error [24],[25]. The sensor depicted in Fig. 30 was built. A wire coil was used as the current carrying conductor. It was wrapped around one turn of sensing fiber and had a 1,000 turns to simulate large value of current. The optical source was a HeNe laser with 20 mW of output optical power. The operating wavelength is 633 nm. 3M single-mode fiber was employed. Fiber polarization controller (PC) was used prior to the single-mode fiber loop (with a radius of 30 cm to simulate the sensing part) in order to launch the linearly polarization into the linear birefringence (fast) axis of the sensing fiber. The state of polarization of the output was linearly polarized. The analyzer was aligned 60° to the angle with maximum output intensity (fast axis of the fiber end).

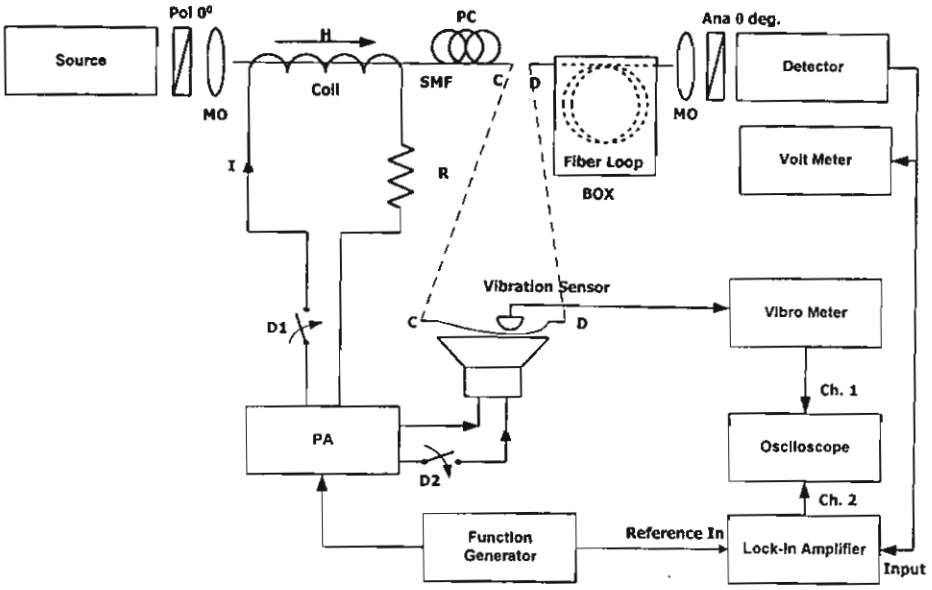

Fig. 30 Unidirectional polarimetric current sensor and its experimental set-up, MO: microscope objective lens, SMF: single-mode fiber, PC: polarization controller, Ana: analyzer, PA: power amplifier

We can find characteristics of the fiber sensor by applying current to the coil and then measuring signal modulation. The coil generates magnetic field and induces Faraday rotation in the sensor. Applied current of 1 A to the coil of 1,000 turns is equivalent to the current of 1,000 A to sensing fiber of 1 turn or 1,000 A.turn (see details on page 52). The power amplifier supplies the current to the sensing coil in Fig. 30 (switch D1 is closed and D2 is opened). The sensor's output voltage consists of two parts: a DC part (v_{DC}) corresponding to the average output intensity at analyzer angle θ of 60° and an AC part (v_{AC}) corresponding to actual current measurement. Its rms value can be measured by a lock-in amplifier. In an ideal case or annealed fiber being used (δ_{DC} is about 1 to 2 degrees/ turns), we get signal modulation of 1.62×10^{-2}. From our experiment, signal modulation is

1.29×10^{-2}. This agrees well with our analysis that δ_{DC} and T are 0.660 and 0.05 radians, respectively.

4.2.3 Relationships between vibration and false current

In Fig. 30, mechanical vibration was applied just in front of the single-mode fiber loop. A speaker was kept in a closed box and about 7 cm of fiber was attached to the top of the box. This box was made from acoustic absorbing material in order to isolate acoustic perturbations from disturbing alignment of the photodetector and the other optic components in the system. Thus, only vibration sensitivity can be measured. A power amplifier supplies signal of 400 Hz to the speaker (switch D2 is closed and D1 is opened). This produces vibration of 400 Hz to the fiber. A piezo-electric accelerometer was attached to the top of the box closed to the fiber to quantify the magnitude and frequency contents of mechanical vibration. The vibration sensor is NP-3110s manufactured by Ono Sokki and its signal conditioner is IMV TrendVibro Z model VM 4105. The output voltage of the detector was given to a Stanford Research lock-in amplifier model SR 530 to read the rms value of the AC part ($v_{(0\text{-}p)}$). DC value (v_{DC}) is measured by a DC voltmeter. Fig. 31 shows the effect of vibration on the sensor when no applied current to the sensing coil. The vibration amplitude is 6.63 (0-p) m/s^2 at the frequency of 400 Hz. Fig. 32 shows

signal modulation versus amplitude of vibration from the accelerometer in $m_{(0\text{-}p)}$ /s^2. The output of the IMV vibrometer and the lock-in amplifier were given to an oscilloscope (see Fig. 31).

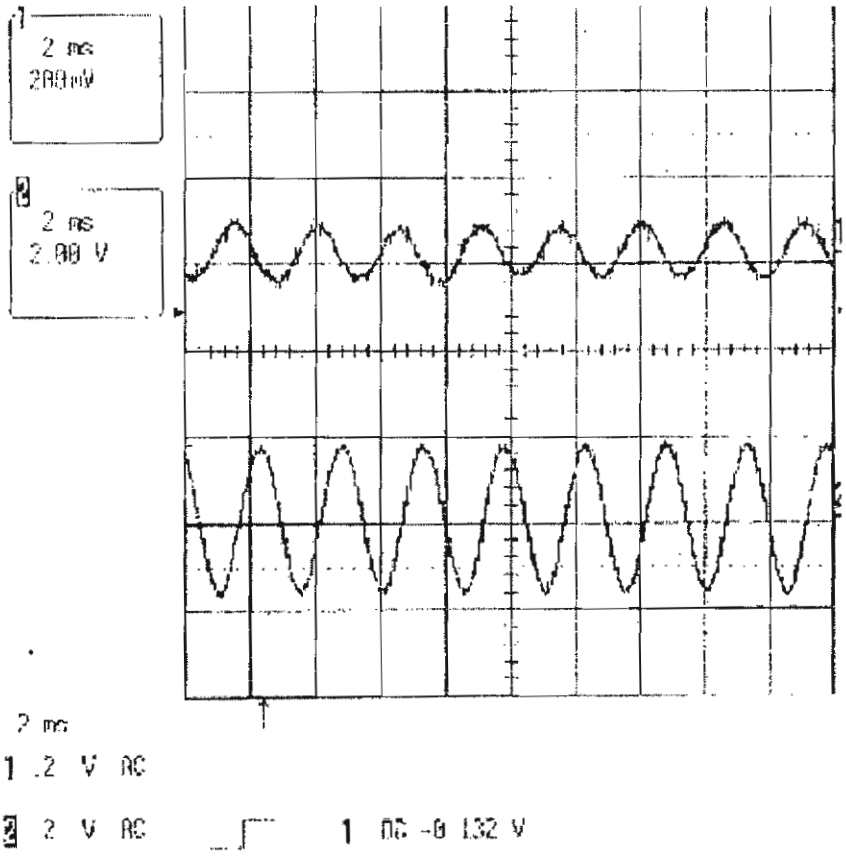

Fig. 31 Vibration of 6.63 m/s^2 at the frequency of 400 Hz (top trace) and corresponding sensor's output (bottom trace)

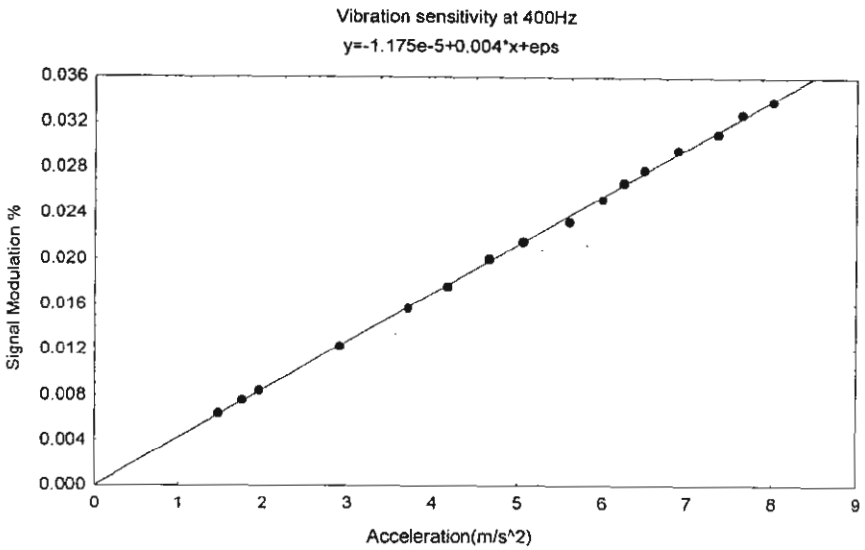

Fig. 32 Signal modulation versus vibration amplitude $m_{(0\text{-}p)}/s^2$. The frequency of vibration is 400 Hz

4.3 Mathematical Modeling of the Vibration Sensitivity

We model the linear birefringence in the sensing fiber being composed of bending-induced linear birefringence (δ_{DC}) and vibration-induced linear birefringence caused by transverse strain or vibration (δ_v), which can be described by [23]

$$\delta_v = {}^{2\pi}/_{\lambda}\,\Delta n\, l, \tag{4.19}$$

where Δn is the refractive index change induced by stress in the medium (silica in this case), l is the effective length (under perturbation) of fiber, and λ is the center wavelength of the source. The refractive index change is given by

$$\Delta n = -n^3/2\, p\sigma = 0.311\sigma, \tag{4.20}$$

where n is the (unperturbed) refractive index of medium, σ is the strain and p is the photoelastic constant of fiber (p = 0.2 in silica). The value of the Faraday rotation (VNI) depends on the Verdet constant (V). Typical value of V is 4.68 $\mu rad/A$ or 0.268°/(kA). Because the vibration affects linear birefringence, to induce a π-radian birefringence change $\Delta n = \lambda/2 = 3.165\times10^{-7}$ for a fiber length of 1 m. We can find the strain of 1.019x10^{-6} using (4.20).

The bending-induced birefringence (δ_{DC}) of a fiber loop with radius R under no tension can be described by

$$\delta_{DC} = K\left(r/R\right)^2 \ °/\text{m}, \tag{4.21}$$

where K = 7.7x10^7 °/m (for silica fiber) and r is the radius of fiber (r = 62.5 μm)

Thus, the (static) bending-induced linear birefringence per turn is

$$\delta_{DC} = 2\pi K r^2/R \simeq 0.6\pi/R \ °/\text{turn} \tag{4.22}$$

In our case, R of 0.3 m results in δ_{DC} of 6.3 °/turn. Six turns of fiber loop result in δ_{DC} of 37.8°.

Assume that (total) linear birefringence (δ) in single-mode sensing part is the algebraic sum of the (static) bending-induced linear birefringence

(δ_{DC} due to loop radius) and vibration-induced linear birefringence (δ_V). Then, the (total) linear birefringence can be expressed by

$$\delta = \delta_{DC} + \delta_v \sin(\omega_v t), \tag{4.23}$$

where $\omega_v = 2\pi f_v$ and f_v is the frequency of the vibration δ_v and T is much smaller than δ_{DC} in our configuration.

4.3.1 False current versus vibration amplitude

In this section we formulate a mathematical model of the vibration sensitivity or measurement error due to vibration. In (4.13), even when no current and no vibration are applied (F = 0 and further assume that the δ_{DC} and T to be constant), the output will be constant. However, the presence of vibration perturbs the linear birefringence and modulates the angular rotation, which cannot be distinguishable from that of the Faraday rotation (F). This results in signal modulation even no applied current. It is named apparent current or false current. Substituting (4.23) into (4.13), we obtain a phase modulation signal. Assume the change of δ_{DC} and T (from vibrations) to be small and negligible. In this case, we formulate a mathematical model for vibration sensitivity when there is only vibration on the sensing fiber (F = 0) to be given by

$$\begin{aligned} I_{60^\circ}/I_0 = \frac{1}{4} + \frac{\sqrt{3}}{2}\frac{\sin\left(\sqrt{4T^2 + (\delta_{DC} + \delta_v \sin\omega_v t)^2}\right)}{\sqrt{4T^2 + (\delta_{DC} + \delta_v \sin\omega_v t)^2}} \cdot T \\ + \left[1 - \cos\left(\sqrt{4T^2 + (\delta_{DC} + \delta_v \sin\omega_v t)^2}\right)\right] \cdot \frac{T^2}{4T^2 + (\delta_{DC} + \delta_v \sin\omega_v t)^2} \end{aligned} \tag{4.24}$$

Using Lock-in amplifier or the spectrum analyzer, we can examine the frequency components of the DC, first-harmonic, second-harmonic, and higher harmonic components. Assume the values of the δ_{DC} and T to be 0.660 (37.8°) and 0.05 radians, respectively. The value of δ_v is assumed to vary linearly with the mechanical vibration to the sensing fiber and, thus, signal modulation varies with the same frequency. When δ_v is small and the applied vibration is of single-frequency, the signal modulation due to vibration can be approximated by (when $2T, \delta_v \ll \delta_{DC}$)

$$I_{60^\circ}/I_0 = \frac{1}{4} + \frac{\sqrt{3}}{2}\frac{\sin(\delta_{DC} + \delta_v \sin\omega_v t)}{\delta_{DC} + \delta_v \sin\omega_v t}\cdot T + [1-\cos(\delta_{DC} + \delta_v \sin\omega_v t)]\cdot\frac{T^2}{(\delta_{DC} + \delta_v \sin\omega_v t)^2}. \quad (4.25)$$

We can expand (4.25) using Bessel function as given by (see Appendix 4B)

$$\left.\frac{I_{60^\circ}}{I_0}\right|_{1f} = \frac{1}{4} + \frac{\sqrt{3}}{2}B_1\left[J_0(\delta_v)\sin(\delta_{DC}) + 2J_1(\delta_v)\cos(\delta_{DC})\sin(\omega_v t)\right] + B_2\left[1 - J_0(\delta_v)\cos(\delta_{DC}) + 2J_1(\delta_v)\sin(\delta_{DC})\sin(\omega_v t)\right], \quad (4.26)$$

where

$$B_1 = \frac{T}{\sqrt{4T^2+\delta^2}} = \frac{T}{\sqrt{4T^2 + (\delta_{DC} + \delta_v \sin(\omega_v t))^2}}, \quad (4.27)$$

$$B_2 = \frac{T^2}{4T^2+\delta^2} = \frac{T^2}{4T^2 + (\delta_{DC} + \delta_v \sin(\omega_v t))^2}, \quad (4.28)$$

$J_n(x)$ is the Bessel function of the first kind of order n of a variable x.

4.3.2 Simulated false current due to vibrations

Using (4.25) and (4.26), Fig. 33 shows that when the vibration is small and is of single-frequency, the signal modulation varies linearly with δ_v and has the same frequency as that of the vibration. The other higher harmonics are negligible. The relation between vibration-induced linear birefringence δ_v and signal modulation is given by

$$\text{signal modulation} = 3.1652 \times \delta_v \tag{4.27}$$

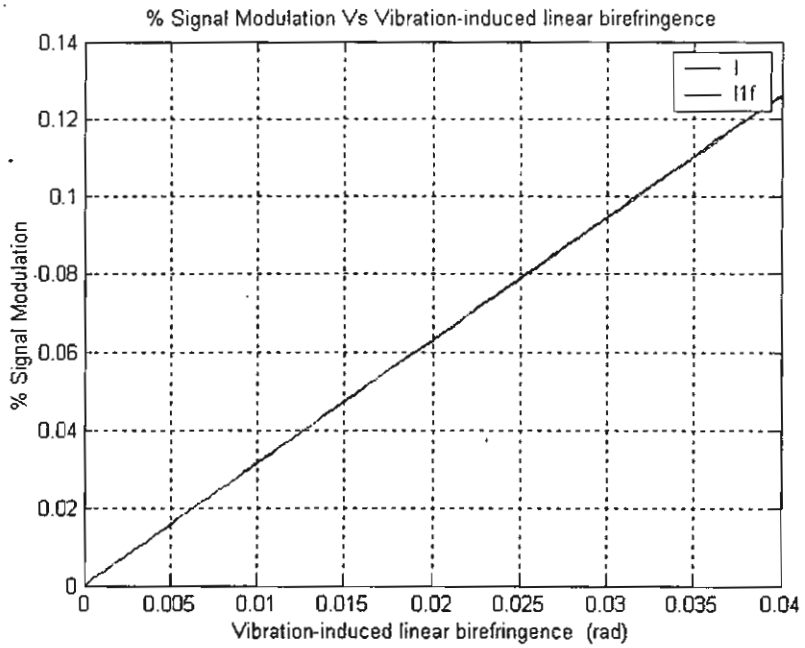

Fig. 33 Signal modulation versus vibration-induced linear birefringence δ_v *(rad):* I and I_{1f} are from (4.25) and (4.26), respectively

Fig. 33 shows that the signal modulation (in percent) varies linearly with δ_v. Then, slope of the signal modulation (%) versus δ_v can be calculated for different values of the number of fiber turns (see Fig. 34).

However, the slope does not change linearly with number of turns. This is due to the fact that slope of the signal modulation (see Fig. 35) is a function of the static bend-induced linear birefringence (δ_{DC}). The maximum of the slope or sensitivity to the vibrations occurs at δ_{DC} of 129°. The minimum sensitivity are at 0° and 258°. However, scale factor of the sensor ($\frac{\sin \delta_{DC}}{\delta_{DC}}$) has to be taken into considerations in the sensor design as well.

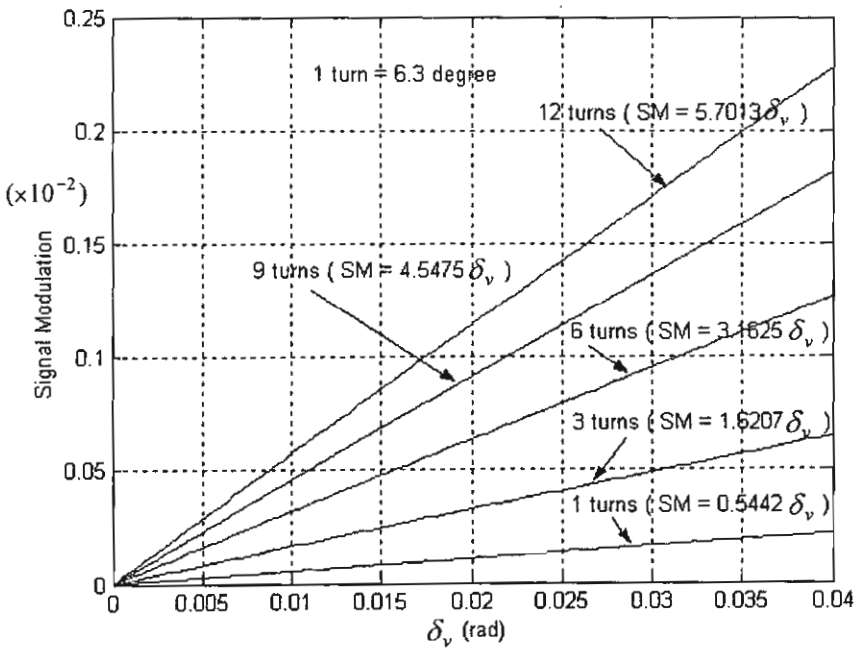

Fig. 34 Signal modulation versus δ_v of 1, 3, 6, 9, and 12 turns, SM: signal modulation

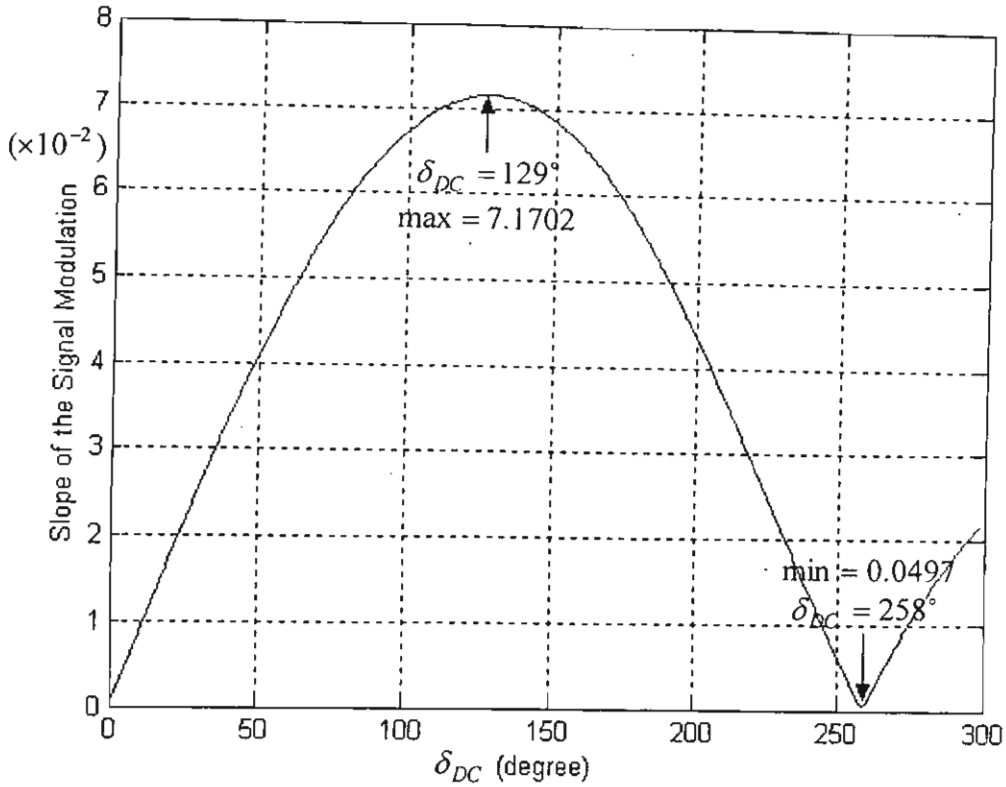

Fig. 35 Slope of the signal modulation (%) versus δ_{DC}

4.4 Discussions

In actual current measurement, under no vibration $\delta_V = 0$ only δ_{DC} and T are constant and the applied current of 1,000 A.turn, the signal modulation is 1.378×10^{-2} (1.29×10^{-2} in our experiment) using (4.13). This is due to the efficiency of magnetic producing coil is only 93.6%. The signal modulation (or false current) varies linearly with vibration amplitude. Also, simulation of our model shows that signal modulation varies linearly with $\delta_{I'}$. Thus, $\delta_{I'}$ varies linearly with vibration amplitude (see Fig. 36). Furthermore, we can find a relationship between false

current and vibration amplitude using (4.27). As a result, 1 g (9.8 m/s^2) of vibration produces around 46 A.turns of the false current. With good packaging and the annealed sensing fiber (δ_{DC} is about 1 to 2 degrees/ turns) being used, the effect will be a few orders of magnitude smaller. In our system vibration lower than 0.6 m/s^2 (due to noise floor limit) does not result into false current. Further reduction of the vibration sensitivity could be done by a damped packaging of the sensing fiber. It can be placed in a highly elastic silicone gel so no inert forces will be allowed and the fiber will be protected from deformation. Also, we can protect the fiber leads to the sensing fiber by using PM fiber leads which may be strewn virtually anywhere throughout the power systems with no concern of false signal detection due to vibrations. The noise equivalent current is about $0.33 A_{rms} \cdot turn / \sqrt{Hz}$.

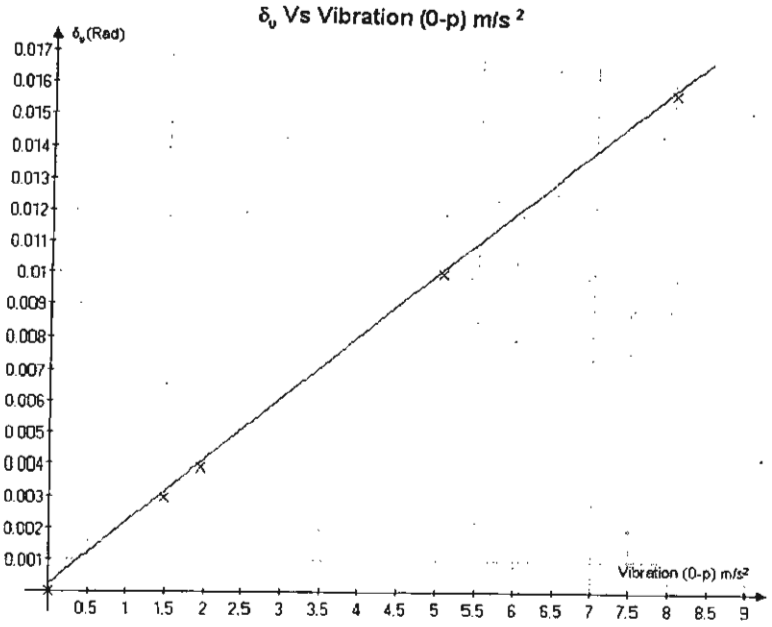

Fig. 36 Linear birefringence change Versus Vibration amplitude (0-p) in m/s^2

4.5 Conclusions

We have demonstrated a novel mathematical model for vibration sensitivity in the unidirectional polarimetric current sensor (UDPS). Experimental study shows that the linear birefringence $\delta_{l'}$ due to mechanical vibration (to our understanding, no experimental studies were reported for vibration sensitivity with a single frequency of vibration and no effect of acoustic perturbations to the other optic components) changes linearly with vibration amplitude. This sensor's residual sensitivities to environmental disturbances can be further reduced by a damped packing such as putting sensing fiber part in a gel-filled tube together with employing two polarization scheme, where the two sensor's output at the $+45^o$ and -45^o to the output fiber axes. Also, 'spun' low birefringence or annealed fiber can be used to reduce the value of (static) linear birefringence δ_{DC}. Further investigation of

the magnitude of linear birefringence change under the influence of vibration should be done experimentally with the help of optical modulator.

Appendix 4A

Given that θ is 45°. Substituting (4.2) and (4.7) into (4.1), we obtain

$$\begin{bmatrix} E_{+45^\circ} \\ 0 \end{bmatrix} = \frac{1}{\sqrt{2}} \begin{bmatrix} 1 & 1 \\ 0 & 0 \end{bmatrix} \begin{bmatrix} A & -B \\ B & A^* \end{bmatrix} \begin{bmatrix} 1 \\ 0 \end{bmatrix}$$

$$\begin{bmatrix} E_{+45^\circ} \\ 0 \end{bmatrix} = \frac{1}{\sqrt{2}} \begin{bmatrix} A+B \\ 0 \end{bmatrix}$$

Substituting (4.3) and (4.4), we obtain

$$E_{+45^\circ} = \frac{1}{\sqrt{2}} (\cos\frac{\alpha}{2} + j \sin\frac{\alpha}{2} \cos\chi + \sin\frac{\alpha}{2} \sin\chi)$$

$I_{+45} \propto |E_{+45}|^2$. Then,

$$I_{+45^\circ} = \frac{I_0}{2} (\cos^2\frac{\alpha}{2} + \sin^2\frac{\alpha}{2} \sin^2\chi + 2\cos\frac{\alpha}{2} \sin\frac{\alpha}{2} \sin\chi + \sin^2\frac{\alpha}{2} \cos^2\chi),$$

where I_o is the maximum intensity at the detector.

$$I_{+45^\circ} / I_0 = \frac{1}{2} (1 + \sin\alpha \sin\chi)$$

From (4.6), we obtain

$$\sin\chi = 2(F+T)/\alpha$$

Thus, $I_{45^\circ} / I_0 = \frac{1}{2} \left[1 + 2(F+T) \cdot \frac{\sin\alpha}{\alpha} \right]$.

Appendix 4B

4B.1

This section shows derivation of (4.17). Using (4.16) and assume $2F_0 << 1$. Approximation of $\sin(2F_0 \sin \omega t - 30^\circ)$ is given by

$$\sin(2F_0 \sin \omega t - 30^o) = \sin(2F_0 \sin \omega t)\cos(30^o) - \cos(2F_0 \sin \omega t)\sin(30^o),$$

where expansion of

$$\sin(2F_0 \sin \omega t) = 2[J_1(2F_0)\sin \omega t + J_3(2F_0)\sin 3\omega t + ..],$$

$$\cos(2F_0 \sin \omega t) = J_0(2F_0) + 2[J_2(2F_0)\sin 2\omega t + J_4(2F_0)\sin 4\omega t + ..],$$

when $x << 1$, the approximation of

$J_0(x) \approx 1$,

$J_1(x) \approx 0.5x$. Therefore, $J_1(2F_0) \approx F_0$,

$J_2(x), J_3(x), J_4(x) << 1$

Thus,

$$1 + \sin(2F_0 \sin \omega t - 30^o) \approx \frac{1}{2} + \sqrt{3}[J_1(2F_0)\sin \omega t + J_3(2F_0)\sin 3\omega t + ..] - [J_2(2F_0)\sin 2\omega t + J_4(2F_0)\sin 4\omega t + ..],$$

$$\approx \frac{1}{2} + \sqrt{3}J_1(2F_0)\sin \omega t,$$

$$\approx \frac{1}{2} + \sqrt{3}F_0 \sin \omega t$$

4B.2

We can expand and approximated equation (4.25) using Bessel function. In equation (4.25), First we define that

$$B_1 = \frac{T}{\sqrt{4T^2 + \delta^2}} = \frac{T}{\sqrt{4T^2 + (\delta_{DC} + \delta_v \sin(\omega_v t))^2}}$$

$$B_2 = \frac{T^2}{4T^2 + \delta^2} = \frac{T^2}{4T^2 + (\delta_{DC} + \delta_v \sin(\omega_v t))^2}$$

where

$$\sin(\delta_v \sin(\omega_v t)) = 2\sum_{k=0}^{\infty} J_{2k+1}(\delta_v)\sin((2k+1)\omega_v t)$$

$$\cos(\delta_v \sin(\omega_v t)) = J_0(\delta_v) + 2\sum_{k=1}^{\infty} J_{2k}(\delta_v)\cos(2k\omega_v t)$$

$$\left.\frac{I_{60^\circ}}{I_0}\right|_{1f} = \frac{1}{4} + \frac{\sqrt{3}}{2} B_1\left[J_0(\delta_v)\sin(\delta_{DC}) + 2J_1(\delta_v)\cos(\delta_{DC})\sin(\omega_v t)\right]$$
$$+ B_2\left[1 - J_0(\delta_v)\cos(\delta_{DC}) + 2J_1(\delta_v)\sin(\delta_{DC})\sin(\omega_v t)\right]$$

When $\delta_v << 1$ the approximated of

$J_0(\delta_v) \approx 1$ and $J_1(\delta_v) \approx 0.5\delta_v$.

Chapter 5

CONCLUSION

In this chapter, we discuss about summary of results for both unidirectional and reciprocal polarimetric current sensors in the first section and then interested topics for future research work.

5.1 Summary of Results

From our research project, we have investigated the preliminary results and made a mathematical modeling for current measurement error due to vibrations, which is one of the environmental perturbations to current sensors. The vibration affects the accuracy of the current measurement. We propose a mathematical modeling that can be helpful in prediction of the unwanted current measurement error due to unavoidable mechanical vibrations from environmental perturbations. In practice, polarimetric current sensors have to be well packaged (from vibration under a certain limit that can be predicted from our modeling) to achieve the accuracy of 0.3% for application in power systems.

From the study in this research project, we obtain the following results for

5.1.1 Unidirectional polarimetric current sensor

a. In chapter 4, experimental study of vibration sensitivity of the sensing part of the sensor and characterization of current measurement error or (apparent) false current versus vibration amplitude are demonstrated.

b. Mathematical modeling of the vibration sensitivity based on linear birefringence changes are shown. This modeling agrees well with our experimental study.

c. The sensor's performances *e.g.* noise floor and sensitivity of the sensor are investigated.

5.1.2 Reciprocal current sensor

a. In chapter 3, vibration sensitivity of a reciprocal current sensor was investigated. Two launched angles of 0 and 45 degrees to the fast birefringence axes were compared. Configuration with launched angle of 45 degrees has a better performance and much lower vibration sensitivity.

b. Experimental study of the current measurement with reciprocal sensor is demonstrated. The output response varies linearly with the input current amplitude.

c. From the mathematical modeling, the vibration sensitivity of a reciprocal configuration is much lower than that of a unidirectional one.

From the results listed above, we can conclude that the objectives of this research to study vibration sensitivity effect on polarimetric current sensors and mathematical modeling of vibration sensitivity has been fulfilled. It will be useful in aiding the design of optical current sensor configuration and provides a good modeling for better vibration isolation design of the optical fiber current sensors.

5.2 Future Work

The physical mechanisms (*i.e.* birefringence changes) of vibration effects on the optical fiber sensors should be further investigated. A way to study the mechanisms is to measure actual values of both linear and circular birefringence changes in the fiber sensors under mechanical vibrations. This study is very helpful for optical fiber sensor design.

The following research topics can be considered as the future work.

1. Optical modulator should be used to measure actual linear birefringence change corresponding to vibration amplitude. Also, the frequency response of the birefringence change versus vibration should be further investigated.

2. Improved mathematical modeling of the vibration sensitivity of the reciprocal polarimetric current sensor with vibration at a part of the sensing fiber. In the present modeling, we assume the vibration to be uniformly distributed on the sensing part. In actual, vibration may not be uniformly distributed or be exposed to a short potion on the sensing part. We should verify our mathematical modeling with experimental result of the system.

3. A two-detector scheme for reducing the effect of intensity fluctuation of the light source should be implemented.

REFERENCES

1. D.C. Erickson, "A primer on optical current and voltage sensors and an update on activity," in *the* 1992 *IEEE Eng. Symp. Bonneville Power Administration,* Portland, OR, Mar. 31 to Apr. 1, 1992.

2. For a review of the large literature volume, see "Optical current transducers for power systems: a review," IEEE Power Systems Instrumentation & Measurement Committee, presented at *the* 1994 *IEEE PES Winter Meeting,* New York, NY, 94-WM 241-0 PWRD.

3. T. W. Cease, S. J. Weikel, and J. G. Driggans, "Optical voltage and current sensor used in revenue metering system," *IEEE Trans. on Power Deliv.,* vol. 6, no. 4, pp. 1374-1379, Oct. 1991.

4. G. W. Day and A. H. Rose, "Faraday effect sensors: the state of the art," *Proc. SPIE,* vol. 985, pp. 138-150, 1988.

5. T. W. MacDougall, D. R. Lutz, and R. A. Wandmacher, "Development of a fiber optic current sensor for power systems," *IEEE Trans. on Power Deliv.,* vol. 7, no. 2, pp. 848-852, Apr. 1992.

6. D. Tang, A. H. Rose, G. W. Day, and S. M. Etzel, "Annealing of linear birefringence in single-mode fiber coils: application to optical fiber current sensors," *J. Lightwave Technol.,* vol. 9, no. 8, pp. 1031-1037, Aug. 1991.

7. A. Yariv and P. Yeh, *Optical Waves in Crystals,* New York: John Wiley & Sons, pp. 94-147,1984.

8. W. Tabor, *et al.,* "Electromagnetic propagation through materials possesing both Faraday rotation and birefringence: experiments with Ytterrbium Orthoferrite," *J. Appl. Phys.*, vol. 40, no. 7, pp. 2760.

9. A. Smith, "Polarization and magnetooptic properties of single-mode optical fibre," *Appl. Opt.*, vol. 17, no. 52, 1978.

10. E. Shafir, N. Shaked, A. Ben-kish, and M. Tur, "The response of Faraday-effect fiber-optic current sensors to noncentered currents," in *the 9th Int. Conf. on Optical Fiber Sensors*, Firenze, Italy, pp. 435-442, May 1993.

11. R. Ulrich, S. C. Rashleigh, and W. Eickloff, "Bending-induced birefringence in single-mode fibers," *Opt. Lett.*, vol. 5, no. 60, pp. 273-275, Jun. 1980.

12. R. Ulrich and A. Simon, "Polarization optics of twisted single mode fibers," *Appl. Opt.*, vol. 18, no. 13, pp. 2241-2251, Jul. 1979.

13. A. Dandridge, *et al.*, "Laser noise in fiber-optic interferometer systems," *Appl. Phys. Lett.*, vol. 37, pp. 526-528, Sept. 1980.

14. A. Dandridge and H. F. Taylor, "Correlation of low-frequency intensity and frequency fluctuations in GaAlAs-lasers," *IEEE J. Quant. Electron.*, vol. QE-18, pp. 1738-1750, Oct. 1982.

15. S. X. Short, "An optical fiber Faraday effect current sensor for power system applications," Master of Science Thesis, Texas A&M University, May 1995.

16. Z. Ren, *et al.*, "Discrimination between linear birefringence and Faraday rotation in optical fiber current sensors by polarization multiplexing," *Fiber Optic and Laser Sensors VII*, vol. 1169, pp. 226-232, 1989.

17. P. Menke and T. Bosselmann, "Temperature compensation in magnetooptic AC current sensors using an intelligent AC-DC signal evaluation," *IEEE J. Lightwave Technol.*, vol. 13, no. 7, pp. 1362-70, 1995.

18. C. Pistoni and M. Martinelli, "Vibration-insensitive fiber-optic current sensor," *Opt. Lett.*, vol. 18, no. 4, pp. 314-316, Feb. 1993.

19. P. Tantaswadi, S. Maheshwari, and C. Tangtrongbenchasil "Study of current measurement error due to vibration in reciprocal fiber-optic polarimetric current sensor," *IEEE-PEDS 2001*, Bali, Indonesia, pp. 699-704, Oct. 2001.

20. A. J. Rogers, J. Xu, and J. Yao, "Vibration immunity for optical-fiber current measurement," *J. Lightwave Technol.*, vol. 13, no. 7, pp. 1371-1377, Jul. 1995.

21. S. Short, *et al.*, "Elimination of birefringence induced scale factor errors in the in-line Sagnac interferometer current sensor," *IEEE J. Lightwave Technol.*, vol. 16, no. 10, pp. 1844-1850, October 1998.

22. S. Short, P. Tantaswadi, *et al.*, "Environmental sensitivity comparison of in-line Sagnac and polarimetric type current sensor," *IEEE Trans. Power Delivery*, vol. 11, no. 4, pp. 1702-1706, 1996.

23. A. Rogers, Optical Fiber Current Measurement In: *Optical Fiber Sensor Technology*, Grattan K and Meggit B, Eds., Vol. I, Chapman & Hall, pp. 432-438, 1995.

24. P. Tantaswadi, S. Maheshwari, and C. Tangtrongbenchasil, "Experimental study of vibration sensitivity in unidirectional polarimetric current sensors," *Int. Symp. on Opt. and Quantum Technol. (ISOQT)*, KMITL, Bangkok, pp. 94-99, Dec. 2001

25. S. Pothiya, P. Tantaswadi, and S. Maheshwari, "Mathematical modeling of vibration sensitivity in unidirectional polarimetric current sensors," *Int. Symp. on Opt. and Quantum Technol. (ISOQT)*, KMITL, Bangkok, pp. 113-118, Dec 2001.

26. M. Born and E. Wolf, *Principles of optics*, Oxford: Pergamon, 6th ed., 1980.

27. S. Carrara, State of Polarization In: *Drift reduction in optical fiber gyroscopes*, Ph.D. dissertation, Stanford U., 1988.

28. P. Tantaswadi and C. Tangtrongbenchasil "Simulation of uniformly distributed vibration effects on a reciprocal fiber-optic polarimetric current sensor," *Int. Symp. on Opt. and Quantum Technol. (ISOQT)*, KMITL, Bangkok, pp. 119-122, Dec. 2001

OUTPUTS

The result of this research project has been submitted in the following international journal papers.

1. P. Tantaswadi, S. Maheshwari, and C. Tangtrongbenchasil, "Numerical investigation of vibration sensitivity in a reciprocal fiber-optic polarimetric current sensor," *J. ScienceAsia,* submitted for publication.

2. P. Tantaswadi, S. Maheshwari, and C. Tangtrongbenchasil, "Vibration sensitivity in unidirectional polarimetric current sensor," *J. ScienceAsia,* submitted for publication.

3. S. Pothiya, P. Tantaswadi, and S. Maheshwari, "Experimental study and mathematical modeling for current measurement error due to vibrations in straightforward fiber-optic polarimetric current sensors" to be submitted to *Optical Rev.,* Opt. Soc. of Japan.

4. P. Tantaswadi and C. Tangtrongbenchasil, "Mathematical modeling of vibration upon a small section of sensing fiber in reciprocal polarimetric current sensors," to be submitted to *Comp. & Elect. Engr.,* Elsevier.

In addition, the results of this related work to this project are published in international conferences as follows:

1. P. Tantaswadi, " Simulation of birefringence effects in reciprocal fiber-optic polarimetric current sensor," *Int. Conf. on Meas. of Light,*

LIGHTMETRY 2000, Proc. SPIE, Pultusk, Poland, June 2000, pp. 158-164.

2. A. Andreev and P. Tantaswadi, " Mathematical model for calculation of the optical rotation and the contrast of the image," *Int. Conf. on Meas. of Light, LIGHTMETRY 2000*, Proc. SPIE, Pultusk, Poland, June 2000, pp. 206-210.

3. P. Tantaswadi, S. Mahcshwari, and C. Tangtrongbenchasil "Study of current measurement error due to vibration in reciprocal fiber-optic polarimetric current sensor," *IEEE-PEDS 2001*, Oct. 2001, Bali, Indonesia, pp. 699-704.

4. P. Tantaswadi, S. Maheshwari, and C. Tangtrongbenchasil "Experimental study of vibration sensitivity in unidirectional polarimetric current sensors," *Int. Symp. on Opt. and Quantum Tech.* (ISOQT), Dec. 2001, KMITL, Bangkok, pp. 94-99.

5. S. Pothiya, P. Tantaswadi, and S. Maheshwari "Mathematical modeling of vibration sensitivity in unidirectional polarimetric current sensors," *Int. Symp. on Opt. and Quantum Tech.* (ISOQT), Dec. 2001, KMITL, Bangkok, pp. 113-118.

6. P. Tantaswadi and C. Tangtrongbenchasil "Simulation of uniformly distributed vibration effects on a reciprocal fiber-optic polarimetric current sensor," *Int. Symp. on Opt. and Quantum Tech.* (ISOQT), Dec. 2001, KMITL, Bangkok, pp. 119-122.

The above papers are attached in the Appendix of this report.

Furthermore, this research project has been used for main parts of Theses of the following graduate students:

1. Mrs. Somna Maheshwari, M.S.E.E. (exp. Mar. 2002)

2. Mr. Charoen Tangtrongbenchasil, researh assistant for this project (June 2000 - present) and currently a Master's student.

3. Mr. Saravuth Pothiya, Ph. D. student

In addition, it has provided many research topics in Senior Project courses (since 1999) for more than 20 Undergraduate students in Electrical Engineering to do fiber optic experiments and simulations.

Appendices

Appendix A

The following sections contain manuscripts of

A.1 P. Tantaswadi, S. Maheshwari, and C. Tangtrongbenchasil, "Numerical investigation of vibration sensitivity in a reciprocal fiber-optic polarimetric current sensor," *J. ScienceAsia,* submitted for publication.

A.2 P. Tantaswadi, S. Maheshwari, and C. Tangtrongbenchasil, "Vibration sensitivity in unidirectional polarimetric current sensor," *J. ScienceAsia,* submitted for publication.

A.3 Letters of acceptance of the manuscripts A.1 and A.2

Appendix A.1

Manuscript of

P. Tantaswadi, S. Maheshwari, and C. Tangtrongbenchasil, "Numerical investigation of vibration sensitivity in a reciprocal fiber-optic polarimetric current sensor," *J. ScienceAsia,* submitted for publication.

Numerical Investigation of Vibration Sensitivity in a Reciprocal Fiber-optic Polarimetric Current Sensor

P. Tantaswadi, S. Maheshwari, and C. Tangtrongbenchasil
Sirindhorn International Institute of Technology, Thammasat University,
Electrical Engineering Program,
PO Box 22, Thammasat Rangsit Post Office, Pathumthani 12121, Thailand,
Tel. (662) 986-9009 ext. 1805, Fax (662) 986-9113, E-mail: prinya@siit.tu.ac.th

Abstract

There have been several ongoing researches in the area of fiber optic current sensors for application in electric power industry in the past few decades. These optical current sensors inherently have several advantages over conventional ferromagnetic current transformers. These include higher bandwidth (DC to many MHz), broad linear dynamic range (more than five orders of magnitude), and by proper design, insensitivity to electro-magnetic interference (EMI) and radio frequency interference (RFI). However, the optical current sensors exhibit sensitivity to environmental perturbations such as temperature and acoustic vibration.

The basic theory of birefringence and Faraday rotation in optical fiber is well known, but some very interesting conclusions from this theory concerning the application to vibration sensitivity in fiber optic current sensors have not been drawn yet.

In this paper we present a general mathematical model of a current sensor for calculating vibration sensitivity due to birefringence effect at the sensing part in a reciprocal polarimetric current sensor. Acoustic vibration, which is prevalent in electric power systems, causes error in current measurement or an apparent (false) current. The model will aid in designing a sensor's configuration with immunity to acoustic vibrations, which perturb linear birefringence in the sensing fiber.

Numerical investigation of the sensor with high circular birefringence in the sensing part is given. Also, the state of the polarization at the output and a normalized contrast ratio of the sensor are discussed. Accuracy of the sensor is within 0.3% of the actual value and satisfies applications in revenue metering.

Keywords: fiber optic sensor, current measurement, acoustic perturbations and mechanical vibrations, polarimetric current sensor, birefringence.

Introduction

There have been several ongoing researches in the area of fiber optic current sensors in the past few decades [1-5]. Current measurement is performed in the electric power industry for revenue metering, relay/protection and control. Several potential advantages over conventional ferromagnetic current transformers (CTs) include broad linear dynamic range (more than five orders of magnitude), broad bandwidth (DC to many MHz), no hysteresis, and by proper design, insensitivity to electro-magnetic interference (EMI) and radio-frequency interference (RFI). Other advantages include smaller size, and consequently lighter weight, making installation easier. Finally, they are completely immune from catastrophic explosive failures, whereas iron-core CTs are not.

Several approaches of Faraday-based current sensors have been demonstrated. Although fiber-optic current sensors have several advantages over conventional CTs, they have yet to overcome undesirable susceptibility to environmental perturbations, *i.e.* temperature and acoustic perturbations, in the sensing part [6-7]. One approach uses unidirectional polarimetric technique. This method of current sensing detects the intensity change due to polarization rotation from the induced magnetic field generated by current. The accuracy of this sensing method suffers from both linear and circular birefringence in the sensing fiber. To counter the birefringence errors, a reciprocal polarimetric type current sensor has been developed. The perturbations affect the birefringence property of the fiber in the sensing part. Unidirectional polarimetric current sensors suffer from environmental perturbations due to varying birefringence in the sensing part [7]. This results in false current readings from environmental perturbations.

In this paper, we analyze the performance of a reciprocal fiber optic current sensor including the output state of polarization, normalized contrast ratio, and effects of vibration on the sensor. The accuracy of the sensor is within 0.3% of the actual value and satisfies application in revenue metering.

Principles

When light propagates in an optical fiber wound around a current carrying wire (see Fig. 1), the induced magnetic field causes a rotation of the linear polarization plane of lightwave by the magneto-optic Faraday effect. This angle of rotation, $\Delta\phi$, through which the plane of polarization rotates, is given by

$$\Delta\phi = V \oint_C \vec{H} \cdot d\vec{l} \,, \tag{1}$$

where V is the Verdet constant of the optical fiber, $\vec{H}$ is the magnetic field intensity along the direction of light propagation, and l is the optical path along the fiber loop. From Ampere's law, this closed loop integral of magnetic field around a wire is proportional the current, I, flowing through it, *i.e.*

$$I = \oint_C \vec{H} \cdot d\vec{l} \,. \tag{2}$$

Therefore, the angle of rotation, $\Delta\phi$, in the fiber loop configuration is given by

$$\Delta\phi = VNI \,, \tag{3}$$

where N is the integral number of turns of fiber wrapped around the current carrying wire. The stability of Faraday rotation based current sensors, through the Verdet constant, depends on source wavelength and temperature. For example, the operating wavelength λ is 633 nm and the Verdet constant V is 4.68 *μrad/* A.

To measure current I, with constant N and V, we can use a polarimetric sensor to measure $\Delta\phi$. In conventional unidirectional polarimetric current sensors, a linearly polarized light is launched into a single-mode sensing fiber and the output polarization is analyzed by a Wollaston prism for evaluation of the current and static linear birefringence [3-4]. In practice, the propagation of light through the fiber loop exhibiting additional linear birefringence due to bending and twist-induced circular birefringence can be described by Jones calculus (see next section). These birefringences affect the accuracy and

sensitivity to environmental perturbations *i.e.* temperature and vibrations of the sensor. Reciprocal fiber-optic current sensors (see Fig. 1) interrogate the light in both directions. Since linear and twist-induced birefringences exhibit reciprocal characteristics, the reciprocal rotation of these birefringences cancels when light propagates along and is back-reflected down a fiber. The Faraday magneto-optic effect exhibits nonreciprocal characteristics, the Faraday rotation doubles when light propagates along and is back-reflected down a fiber. Thus, this optical circuit has the advantage of minimizing the birefringence induced offset problems associated with the unidirectional polarimetric current sensor.

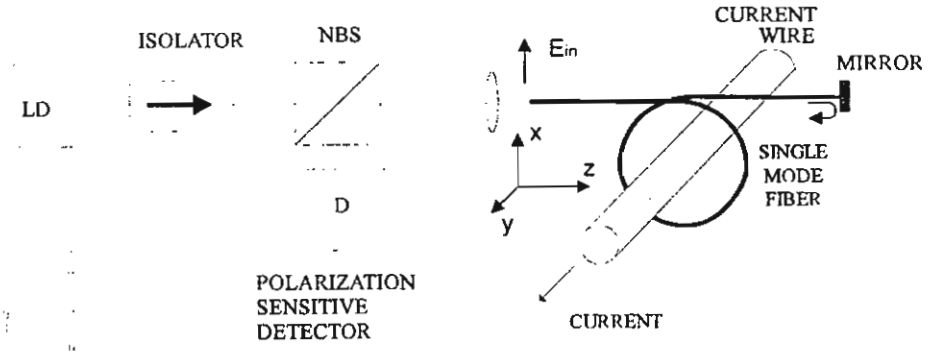

Fig. 1 Reciprocal fiber optic polarimetric current sensor, LD: laser diode, NBS: non-polarizing beam splitter

State of Polarization (SOP)

To analyze the performance of the sensor, we first look at the sensor's output state of polarization. The output electric field (E_{out}) of the sensor can be described by the Jones matrix [1-2]:

$$E_{out} = \frac{1}{2}\bar{L} \cdot M \cdot \bar{L} \cdot E_{in}, \tag{4}$$

where E_{in} represent input linearly polarized light in the x axis (*i.e.* $E_{in} = \begin{bmatrix} E_x = 1 \\ E_y = 0 \end{bmatrix} = \begin{bmatrix} 1 \\ 0 \end{bmatrix}$),

$\bar{L}$ represents a sensing fiber matrix when light propagating forward (from left-to-right in Fig. 1),

$\bar{L}$ represents a sensing fiber matrix when light propagating backward (from right-to-left),

and M is the Jones matrix of the mirror.

$$\bar{L} = \begin{bmatrix} A & -B \\ B & A^* \end{bmatrix}, \tag{5}$$

where

$$A = \cos\frac{\alpha}{2} + j\sin\frac{\alpha}{2}\cos(\chi) \tag{6}$$

$$B = \sin\frac{\alpha}{2}\sin(\chi) \tag{7}$$

$$\frac{\alpha}{2} = \sqrt{(VNI + T)^2 + (\frac{\delta}{2})^2} \tag{8}$$

$$\tan\chi = 2(VNI + T)/\delta. \tag{9}$$

The VNI is the Faraday rotation induced by current and T is the circular birefringence. δ represents total linear birefringence. α represents the total birefringence. Assume both the total linear and circular birefringence to be uniformly distributed along the single-mode fiber optic sensing part.

$$\bar{L} = \begin{bmatrix} C & -D \\ D & C^* \end{bmatrix}, \tag{10}$$

where

$$C = \cos\frac{\beta}{2} + j\sin\frac{\beta}{2}\cos(\zeta), \tag{11}$$

$$D = \sin\frac{\beta}{2}\sin(\zeta), \tag{12}$$

$$\frac{\beta}{2} = \sqrt{(VNI - T)^2 + (\frac{\delta}{2})^2}\,, \tag{13}$$

$$\tan\zeta = 2(VNI - T)/\delta\,, \tag{14}$$

$$M = \begin{bmatrix} 1 & 0 \\ 0 & 1 \end{bmatrix}. \tag{15}$$

With linearly polarized input at the birefringence axis of sensing fiber, the normalized output electric field using Eq (4), (5), (10), and (15) can be described by

$$E_x = AC - BD = a_1 \exp(j\delta_x)\,, \tag{16}$$

$$E_y = AD + BC^* = a_2 \exp(j\delta_y)\,, \tag{17}$$

where a_1, δ_x, a_2, and δ_y are the amplitude and phase of the electric field in the x- and y- axis, respectively.

The output state of polarization can be expressed on the Poincaré sphere (S_1, S_2, S_3) [8,9]

$$S_1 = a_1^2 - a_2^2,\ S_2 = 2a_1 a_2 \cos(\delta_x - \delta_y),\ \text{and}\ S_3 = 2a_1 a_2 \sin(\delta_x - \delta_y) \tag{18}$$

In this Poincaré sphere, the state of polarization can be plotted on the surface of a sphere. Right circular polarization is on the North Pole, left circular on the South Pole, linear polarization on the equator, and elliptical polarization in between [8,9]. With input light aligned to birefringence axis of the sensing fiber, in an ideal fiber ($\delta, T \approx 0$), we would expect only Faraday rotation to occur. In this sensor, the rotation angle is $2VNI$. This is due to the fact that Faraday rotation is VNI in the forward direction down the fiber and, by nonreciprocal effect of Faraday effect, additional Faraday rotation is VNI in the backward direction down the same fiber. Thus, the total Faraday rotation of $2VNI$ occurs in the sensor. Assume that the input light is linearly polarized in the x-axis or vertical direction. It is (1,0,0) on Poincaré sphere or a dot shown in Fig. 2. In Fig. 2 (a), the Faraday rotation angle of $2VNI$ will be

equivalent to $4VNI$ along the equator (angle on the sphere is twice as much as the angular rotation and output is still linearly polarized). For example, the VNI of 0.01 π radians produces 0.04 π radians of rotation along the equator [see Fig. 8(a)]. The characteristic curve of a practical case ($\delta = 2\pi$ and $T =$ 120 π radians or $\delta/2T = 0.83\%$) is shown in Fig. 2 (b). It is similar to the ideal case but with a very small deviation from the equator. The deviation from the ideal case produces some small susceptibility to varying birefringence and will be demonstrated in the next section. Fig. 2 (c) with thin line for $\delta =$ $\pi/6$ and $T = 0$ and thick line: $\delta = \pi/2$ and $T = \pi$ ($\delta/2T = 25\%$) shows that the sensor is not practical for current sensing when T does not dominate δ or $\delta/2T$ is not small. Fig. 2 (b) shows that the desired response, which is close to that of the ideal one in Fig. 2(a), can be obtained by large T or $\delta/2T \ll 1$. The characteristic curve evolves around the equator (see Fig. 2 (a) and (b)).

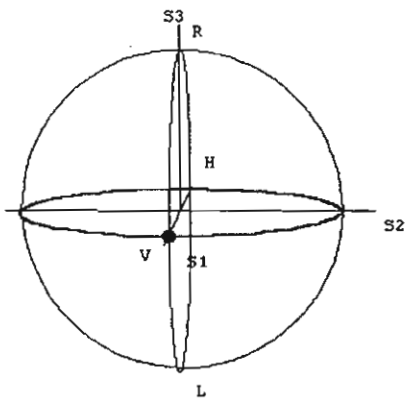

(a)

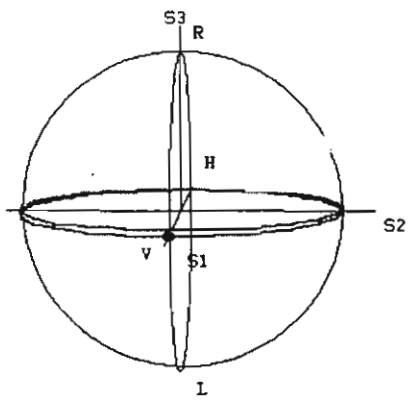

(b)

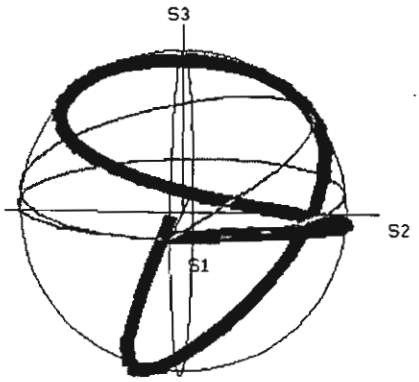

(c)

Fig.2 Characteristic curves of the output polarization on the Poincare sphere for $VNI = 0$ to π radians for (a) ideal case: $\delta = 0$ and $T = 0$ (b) $\delta = 2\pi$ and $T = 120\pi$ radians (c) the thin line: $\delta = \pi/6$ and $T = 0$ and the thick line: $\delta = \pi/2$ and $T = \pi$ radians.

Analytical Descriptions of the Normalized Contrast Ratio (K)

The Wollaston prism is aligned 45° and –45 ° to the birefringence axis of the output end of the sensing fiber. The contrast ratio (K) is defined by

$$K = \frac{I_{xo} - I_{yo}}{I_{xo} + I_{yo}}, \tag{19}$$

where I_{xo} and I_{yo} are the intensity at 45° and –45 ° on the birefringence axis of the output end of the sensing fiber, respectively. We can derive Eq (19) using Eq (4) to (15). Then, the contrast ratio (K) is given by

$$K = Sin(\alpha)Cos(\beta)Sin(\chi) + \frac{Sin\beta}{2}[Sin(2\chi - \zeta)(Cos\alpha - 1) + Sin\zeta(Cos\alpha + 1)] \tag{20}$$

Ideal case, T and δ are very small and negligible (such that $T, \delta \approx 0$) Eq (20) becomes

$$K = K_{ideal} = Sin(4VNI) \tag{21}$$

K provides the measurement of current and is linear ($K = Sin(4VNI) \approx 4VNI$) up to few tenths of a radian, or about 10^5 Amperes for a one-turn sensing coil. K is independent of the circular and linear birefringence in the sensing fiber. However, in practice, the use of high circular birefringence T or "spun" fiber ($VNI, \delta << T$) can overcome the intrinsic linear birefringence. To understand the performance of the sensor, we show the characteristic plot of the deviation of K, which is defined by,

$$\Delta K(\%) = \frac{(K - K_{ideal})}{K_{ideal}} \times 100\% \tag{22}$$

as a function of linear birefringence (δ) and twist-induced circular birefringence (T) (see Fig. 3). The VNI is assumed to be 0.01π and the expected value of K_{ideal} from Eq (21) is 0.125333. Fig. 3 shows the case when T is large and $\frac{\delta}{2T} \ll 1$. The sensor shows reduced sensitivity to vibration significantly compared to that of the one-way "unidirectional" polarimetric sensor [10].

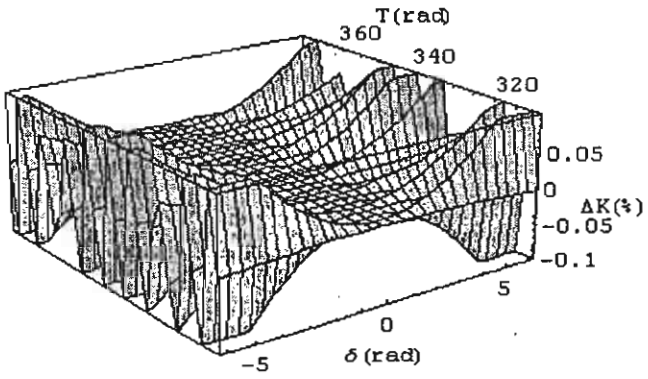

Fig. 3 The deviation of K (ΔK) as a function of linear birefringence (δ) and twisted circular birefringence (T)

The required intrinsic circular birefringence may be obtained by spun high birefringence fiber, twisted low birefringence fiber or winding low birefringence fiber in a toroidal geometry (see Fig. 4) [5,6]. In the toroidal configuration, which we use in our simulation, T is about 120 π and δ is about a few π radians.

a. Mathematical Descriptions of Linear Birefringence Vs Vibration

There are two sources of linear birefringence in the sensing fiber: bending-induced linear birefringence (δ) and vibration-induced linear birefringence caused by transverse strain or vibration (δ_v), which can be described by [11]

$$\delta_v = 2\pi/\lambda \, \Delta n \, l \,. \tag{23}$$

where Δn is the refractive index change induced by stress in the medium (silica in this case), l is the effective length (under perturbation) of fiber, and λ is the center wavelength of the source. The refractive index change is given by $\Delta n = -n^3/2 \, p\sigma = 0.311\sigma$. (24)

where n is the (unperturbed) refractive index of medium, σ is the strain and p is the photoelastic constant of fiber (p = 0.2 in silica). Value of the Faraday rotation (VNI) depends on the Verdet constant (V). Typical value of V is 4.68 $\mu rad/$ A or 0.268°/(kA). In our case, we wrap the sensing fiber around an acrylic torus (see Fig. 4) so that the bend-induced linear birefringence is about a few π radians and a large twist-induced birefringence is about 120 π radians. As a result, the conditions of $\delta/2T \ll 1$ and $VNI \ll \delta \ll T$ are satisfied [5,6]. Because the vibration affects linear birefringence, to induce a π-radian birefringence change $\Delta n = \lambda/2 = 3.165\times10^{-7}$ for a fiber length of 1 m. We can find the strain of 1.019×10^{-6} using Eq (24). Ref. 10 shows that δ_v in unidirectional polarimetric current sensor of 0.2

rad results in an apparent current of several hundred Amperes. In the following sections we will assume that δ_v changes by 0.2 π *rad* (a few times larger than 0.2 *rad*) between – 0.1 π and 0.1 π from the static bend-induced linear birefringence δ (assumed to be 1.9 π radians).

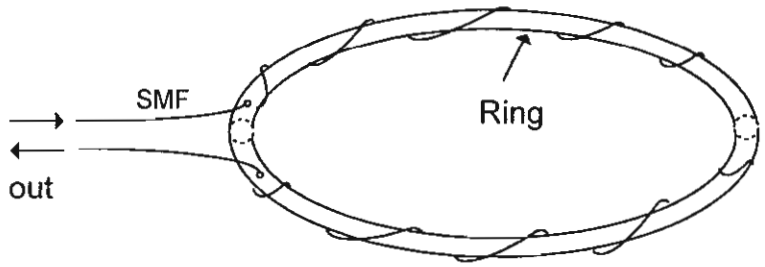

Fig. 4 The schematic of winding sensing fiber around a torus (with outside diameter of 45 cm) in order to add a large amount of circular birefringence, SMF: single-mode fiber. The torus has a cross section diameter of about 2 cm.

In this sensor, Fig. 5 shows that the deviation of K in percent is within 0.10% of the ideal case ($T, \delta \approx 0$) when the range of the linear birefringence and circular birefringence are (1.8 π, 2.0 π) and (119.5 π, 120.5 π) radians, respectively.

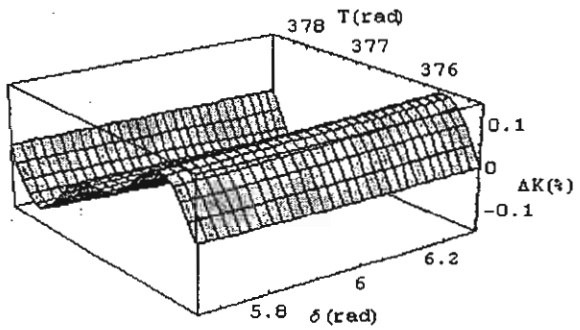

Fig. 5 In case of birefringence changes due to vibration, the deviation of K (ΔK) when VNI = 0.01 π radians as a function of linear birefringence (δ is between 1.8 π and 2.0 π radians) and circular birefringence (T is between 119.5 π and 120.5 π radians).

b. Deviation of K (ΔK) Vs linear birefringence

This sensor exhibits small dependence on linear birefringence. Fig. 6 shows that the absolute value of the deviation of K in percent is below 0.007% when δ is less than 2 π radians when $VNI = 0.01\pi$ and T = 120 π radians. In this case, the approximation of K is

$Sin(4VNI)[1-1.750\text{x}10^{-6}\delta^2] = 0.125333[1-1.750\text{x}10^{-6}\delta^2]$. Using Eq (22), $\Delta K(\%)$ is given by

$$\Delta K(\%) = -1.750\text{x}10^{-4}\delta^2 . \qquad (25)$$

Maximum δ to achieve the accuracy of 0.3 % for revenue metering application from Eq (25) is 13.18 π *rad.*

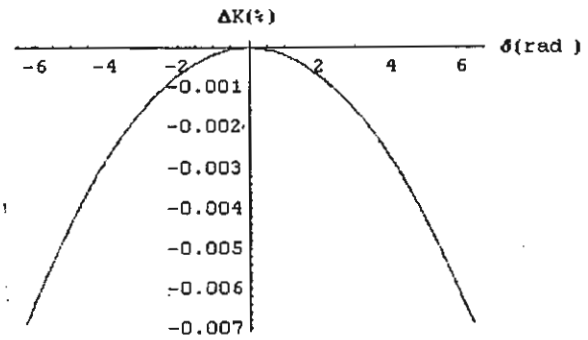

Fig.6 Simulated deviation of K in percent varies with linear birefringence ($VNI = 0.01\pi$, $T = 120\pi$)

c. Apparent current Vs linear birefringence

Environmental acoustic perturbations and mechanical vibration on the sensing fiber can cause angular rotation of lightwave polarization and may affect birefringence property of the sensing fiber [11]. The result could be misread as actual current. Ref. 7 shows that mechanical vibrations with a magnitude of 3.0 $g_{p\text{-}p}$ (1g = 9.8m/s^2) applied to a sensing fiber of unidirectional polarimetric sensor can cause an

apparent current of 400 $A_{p\text{-}p}$. Simulated apparent current ($T = 120\ \pi, \delta_v = 0.1\pi \sin(2\pi f_v t)$, and the total linear birefringence is assumed to vary between 1.8π and 2.0π radians) for this sensor is shown in Fig. 7. The frequency of vibration or varying linear birefringence (f_v) is chosen to be 50 Hz, which is common to electric power systems [6]. Very small apparent currents of less than 2.0×10^{-5} Amperes for 633 nm wavelength when the total linear birefringence δ is (1.8π, 2.0π) radians and the δ_v is shown in Fig. 7(a).

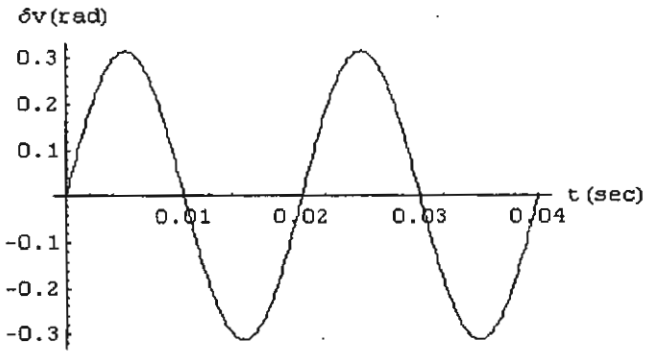

(a)

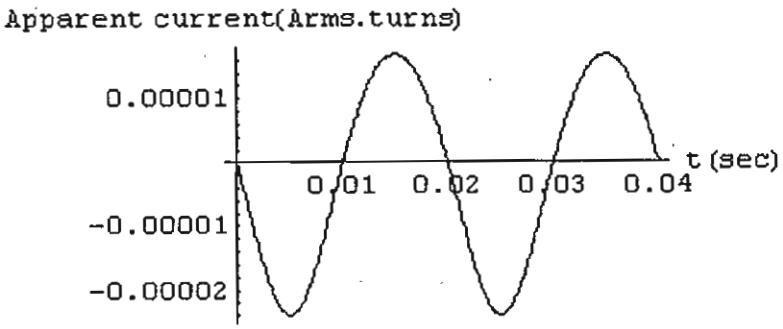

(b)

Fig.7 Simulated apparent current (b) in Amperes.turns Vs birefringence (a) ($VNI = 0$ and $T = 120\pi$)

Mathematical Model and State of Polarization under Vibration

Ref. 10 shows that the linear birefringence change due to vibration of 0.2 radians can induce a large apparent current (equivalent to several-hundred A_{p-p}) in unidirectional polarimetric current sensor [10]. However, Fig. 5 indicates that when both δ and T change as much as 0.2 π (many times larger than 0.2 radians) and 1 π radians, respectively, the ΔK or accuracy of the sensor is within 0.1% (0.3% is required for revenue metering). Fig. 8 shows the two cases when δ and T change due to vibration and the current is applied ($VNI = 0.01\ \pi$) to the sensor. The dot and small line in Fig. 8 represent the SOP under vibration when δ and T change, respectively.

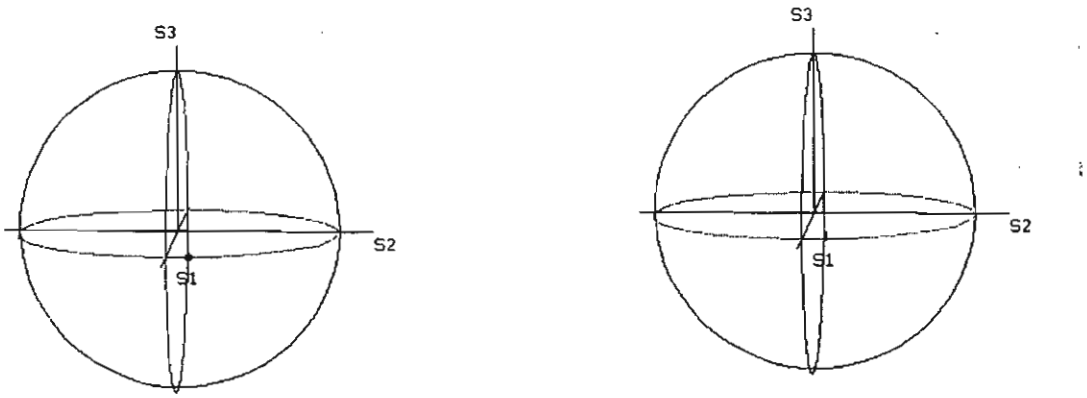

(a) (b)

Fig. 8 State of polarization of the output of sensor with vibration on the Poincare sphere $VNI = 0.01\ \pi$ (a) linear birefringence (δ is between 1.8 π and 2.0 π radians) $T = 120\ \pi$ (b) twisted circular birefringence (T is between 119.5 π and 120.5 π radians) $\delta = 2\ \pi$ radians.

Discussion and Conclusion

The mathematical model of reciprocal fiber-optic current sensor is demonstrated. The performance of the current sensor is similar to that of the ideal case ($\delta, T \approx 0$). This can be shown by the state of polarization of the sensor output when $\delta/2T$ is small (T dominates δ and VNI). To satisfy the conditions of $\delta/_{2T} \ll 1$ and $VNI \ll \delta \ll T$ helical winding on a acrylic torus is used. We can find the normalized contrast ratio K being affected by unwanted changes in linear birefringence δ caused by acoustic perturbations and mechanical vibrations and circular birefringence T. For large T, deviation of K (%) is a quadratic function of δ but the contribution of perturbations and vibrations is small and within 0.1% (0.3% of the actual value required for applications in revenue metering). The apparent current shows that the susceptibility of sensor to varying linear birefringence is small and negligible.

Acknowledgement

Funding was provided by The Thailand Research Fund (TRF). The authors would like to thank Dr. James N. Blake of Nxtphase, USA, Prof. Alan J. Rogers of University of Surrey, UK, and Assoc. Prof. Dr. Pichet Limsuwan of King Mongkut's University of Technology, Thonburi for help and fruitful discussions. Also, the authors would like to thank Mr. Parvich Tokakuna, Ms. Phanraphee Bunphalamlert, and Mr. Yodtao Yodying for their assistance in "Mathematica" programming

References

1. Tabor, *et. al* Electromagnetic propagation through materials possesing both Faraday rotation and birefringence: experiments with Ytterrbium Orthoferrite. *J. Appl. Phys.***40(7)**, 2760.
2. Smith A (1978) Polarization and magnetooptic properties of single-mode optical fibre. *Appl. Opt.* **17(52)**.

3. Ren Z, *et al* (1989) Discrimination between linear birefringence and Faraday rotation in optical fiber current sensors by polarization multiplexing. *Fiber Optic and Laser Sensors VII* **1169**, 226-232.
4. Menke P and Bosselmann T (1995) Temperature Compensation in Magnetooptic AC Current Sensors Using an Intelligent AC-DC Signal Evaluation. *IEEE J-LT* **13**(7), 1362-70.
5. Roger A, *et al* (1995) Vibration immunity for optical fiber current measurement. *IEEE J-LT* **13(7)**, 1371-1377.
6. Short S, *et al* (1998) Elimination of Birefringence Induced Scale Factor Errors in the In-Line Sagnac Interferometer Current Sensor. *IEEE J-LT* **16(10)**, 1844-1850.
7. Short S, Tantaswadi P, de Carvalho R, Russel B, and Blake J (1996) Environmental sensitivity comparison of in-line Sagnac and polarimetric type current sensor. *IEEE Trans. Power Delivery* **11(4)**, 1702-1706.
8. Born M and Wolf E (1980) In: *Principles of optics*, Oxford: Pergamon, 6th ed., 1980.
9. Carrara S (1988) State of Polarization In: *Drift reduction in optical fiber gyroscopes*, Ph.D. dissertation, Stanford U.
10. Tantaswadi P, Maheshwari S, and Tangtrongbenchasil C. (2001) Acoustic Vibration Sensitivity in Unidirectional Polarimetric Current Sensor (to be submitted to) Songklanakarin J. Sci. Tech.
11. Grattan K and Meggit B, ed. (1995) Optical Fiber Current Measurement In: Optical Fiber Sensor Technology, Vol. 1, Chapman & Hall, 432-438.

Appendix A.2

Manuscript of

A.2 P. Tantaswadi, S. Maheshwari, and C. Tangtrongbenchasil, "Vibration sensitivity in unidirectional polarimetric current sensor," *J. ScienceAsia,* submitted for publication.

Vibration Sensitivity in Unidirectional Optical Polarimetric Current Sensor

P. Tantaswadi, S. Maheshwari, and C. Tangtrongbenchasil

School of Electrical Engineering and Information Technology
Sirindhorn International Institute of Technology, Thammasat University, Thailand

ABSTRACT

The accuracy of current measurement in optical fiber current sensor is affected by the environment perturbations to the sensing fiber such as mechanical vibrations, acoustic perturbations, and temperature change. This paper proposed a novel mathematical model for vibration sensitivity in unidirectional polarimetric current sensors. We believe that it is the first time to model the effect of vibration to the single-mode-sensing fiber on the current measurement error in fiber optic polarimetric current sensor is formulated. Furthermore, this paper presents the experimental study of the effected of mechanical vibration on the current measurement error. The results from simulation and experimental show that the current measurement error varies linearly with the amplitude of vibration and slope of signal modulation depend on linear birefringence. The relation between slope of signal modulation and linear birefringence is sinusoidal. The simulation results agree well with the experimental results.

Keywords:linear birefringence, fiber-optic current sensors, magneto-optic current transformers, simulation and modeling, vibrations.

1. INTRODUCTION

Fiber-optic current sensors, which based on magneto-optic Faraday effect and Ampere's law, It have been received considerable attention for possible application in electric power industry as magneto-optic current transformers (MOCTs) in the past few decades [1]-[10]. These MOCTs inherently have several potential advantages over conventional ferromagnetic current transformers (CTs). These include flat bandwidth response (DC to several MHz), wide linear dynamic range (more than five orders of magnitude), no hysteresis, and by proper design insensitivity to electro-magnetic interference (EMI) and radio frequency interference (RFI) owing to their all-dielectric structure of fiber optics. Other advantages include smaller size, and consequently lighter weight, making installation easier. Finally, they are completely immune from catastrophic explosive failures, where as iron-core CTs are not [3].

MOCTs have reached a considerable technological standard and are planned to be installed in the power generating plants and substations. In practice, the current sensors are invariably exposed to highly stressful environments. Among these environmental perturbations in these environments are broad temperature ranges, humidity fluctuations, and acoustic vibrations [6]-[9]. However, the optical current sensor exhibits sensitivity to changes in the linear birefringence, δ, in their sensing coils. Changing stresses and temperature may change the total δ or its distribution along the sensing coil, which in turn changes the evolution of the state of polarization of the light through the sensing coil. For these applications the MOCT should not exceed the general accuracy limitations *i.e.* 0.3% for revenue metering applications.

The basic theory of birefringence and Faraday rotation in optical fiber is well known, but some interesting conclusions from this theory concerning the application to vibration sensitivity in fiber optic current sensors have not been drawn yet. Although there are a few literatures [6]-[8] related to the vibration sensitivity in polarimetric current sensor, a general mathematical model of vibration sensitivity due to birefringence effect at the sensing part in unidirectional polarimetric current sensor has not been shown. Corroborating experimental results are also presented.

2. PRINCIPLE

When light propagates in an optical fiber wound around a current carrying wire, the induced magnetic field causes a rotation of the linear polarization plane of lightwave by the magneto-optic Faraday effect. This angle of rotation, F, through which the plane of polarization rotates, is given by

$$F = V \oint_C \vec{H} \cdot d\vec{l} \tag{1}$$

where V is the Verdet constant of the optical fiber, $\vec{H}$ is the magnetic field intensity along the direction of light propagation, and l is the optical path along the fiber loop. From the Ampere's law, this closed loop integral of magnetic field around a wire is proportional the current, I, flowing through it, *i.e.*

$$I = \oint_C \vec{H} \cdot d\vec{l} \tag{2}$$

Therefore, the angle of rotation, F, in the fiber loop configuration is given by

$$F = VNI \tag{3}$$

where N is the integral number of turns of fiber wrapped around the current carrying wire. The stability of Faraday rotation based current sensors, through the Verdet constant, depends on source wavelength and temperature. For example, the operating wavelength λ is 633 nm and the Verdet constant V is 4.68 $\mu rad / A_{rms}$

To measure current I, with constant N and V, we can use polarimeter sensor to measure F Fig. 1 shows unidirectional polarimetric current sensor set-up. Linear polarized light from HeNe laser is coupled to the single-mode fiber. Polarization controller in front of the sensing fiber is to launch the linear polarized into the fast axis of fiber loop forming a sensing part. Light passes through a polarizer (we usually call an "analyzer") at the fiber output. θ is the angle between the analyzer and fast birefringence axis at the end of sensing fiber loop. A simplified configuration consists of input linear polarized electric field (E_{in}) entering the sensing fiber loop, an analyzer aligned θ degrees with respect to the birefringence fast axis of the fiber loop, and a detector. The analyzer angle θ of 45° provides maximum sensitivity and linear dynamic range.

The output electric field (E_{out}) of the sensor impinging on the detector can be described by Jones Calculus [1],[2]

$$E_{out} = P \cdot R(\theta) \cdot \vec{L} \cdot E_{in} \tag{4}$$

where $E_{in}, \vec{L}, R(\theta)$, and P represent input linearly polarized light in the x- axis, sensing fiber matrix, coordinate rotation matrix with the angle difference between the output analyzer and the birefringence fast axis at the fiber end (θ), and P is the analyzer matrix, ($=\begin{bmatrix} 1 & 0 \\ 0 & \varepsilon \end{bmatrix}$), respectively [1],[2]. Extinction ratio ε of a good quality polarizer is very small (ε is better than –50 dB or $\varepsilon \le 7\times10^{-3}$) and can be assumed negligible in our analysis.

$$\vec{L} = \begin{bmatrix} A & -B \\ B & A^* \end{bmatrix} \tag{5}$$

where

$$A = \cos\left(\frac{\alpha}{2}\right) + j\sin\left(\frac{\alpha}{2}\right)\cos(\chi) \tag{6}$$

$$B = \sin\left(\frac{\alpha}{2}\right)\sin(\chi) \tag{7}$$

$$\frac{\alpha}{2} = \sqrt{(F+T)^2 + \left(\frac{\delta}{2}\right)^2} \tag{8}$$

$$\tan\chi = \frac{2(F+T)}{\delta} \tag{9}$$

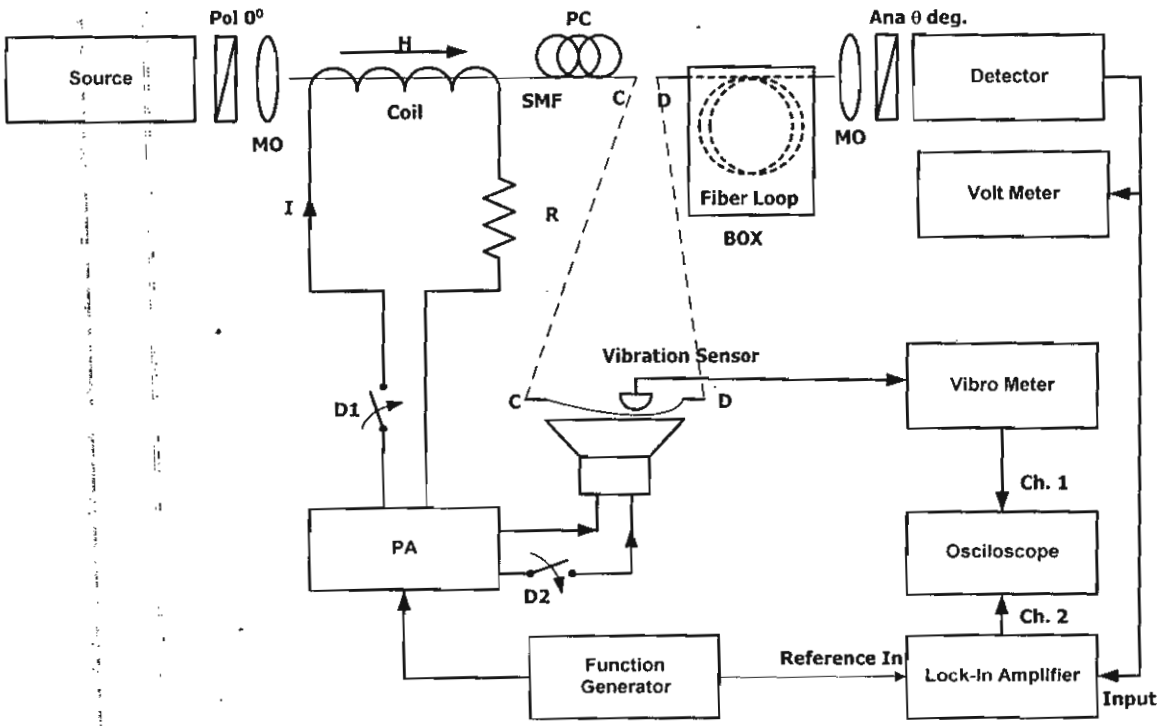

Figure 1: Unidirectional polarimetric current sensor and its experimental set-up, MO: microscope objective lens, SMF: single-mode fiber, PC: polarization controller, Ana: analyzer, PA: power amplifier

where δ, F, T and α are the linear birefringence, Faraday rotation, twisted (circular) birefringence, and total birefringence in radians. Coordination rotation matrix $R(\theta)$ is given by

$$R(\theta)=\begin{bmatrix}\cos\theta & \sin\theta\\ -\sin\theta & \cos\theta\end{bmatrix} \tag{10}$$

In our experiment, we align the analyzer with θ of 60°, where the output signal-to-noise ratio (SNR) is better than that of θ of 45°, where the sensitivity of the sensor is maximum. Using equation (4) to (10), normalized output intensity (Intensity $\propto |E_{out}|^2$) on the detector is given by

$$\frac{I_{60^o}}{I_0}=\frac{1}{4}+\frac{\sqrt{3}}{2}\frac{\sin(\alpha)}{\alpha}\cdot(F+T)+2\left[\frac{\sin(\alpha/2)}{\alpha}\cdot(F+T)\right]^2 \tag{11}$$

where I_0 is the maximum intensity at the detector. Substitute equation (8) into equation (11), we get

$$\frac{I_{60^o}}{I_0}=\frac{1}{4}+\frac{\sqrt{3}}{2}\frac{\sin\left(\sqrt{4(F+T)^2+\delta^2}\right)}{\sqrt{4(F+T)^2+\delta^2}}\cdot(F+T)+\left[1-\cos\left(\sqrt{4(F+T)^2+\delta^2}\right)\right]\cdot\frac{(F+T)^2}{4(F+T)^2+\delta^2} \tag{12}$$

2.1 CURRENT MEASUREMENT

Obviously, equation (12) shows that the normalized output intensity is a function of F, δ, and T. With the input light aligned to birefringence fast axis of the sensing fiber, in an ideal fiber ($\delta, T \approx 0$), we would expect only Faraday rotation ($F = VNI$) to occur. Equation (12) becomes

$$\frac{I_{60^o}}{I_0}=\frac{1}{2}\left[1+\sin\left(2F-30^o\right)\right] \tag{13}$$

Equation (13) indicates that the normalized output intensity is constant when there is no applied current ($F = 0$). When AC current ($I(t) = A\sin\omega t$) is applied (where A is zero-to-peak (0-p) amplitude in Ampere), F can be described by

$$F(t) = VNI(t) = (VNA)\sin\omega t = F_0\sin\omega t \tag{14}$$

where $\omega = 2\pi f$ and f is frequency of the applied current. V is the Verdet constant and a function of wavelength (4.68 $\mu rad / A_{rms}$ for wavelength of 633 nm). Then, $F_0 = VNA$ is constant and depends on the current amplitude, the number of turns, and wavelength of operation. Substitute equation (14) into (13), we obtain the phase modulation signal. Detector's output voltage (v_D) is proportional to the impinged output intensity ($v_D \propto I_{60^o}$) and is given by

$$v_D = \frac{K}{2}\left[1 + \sin\left(2F_0 \sin \omega t - 30^o\right)\right] \tag{15}$$

where K is the maximum output voltage at the detector.

When F_0 is small , the output voltage at the detector of equation (15) can be approximated by (see Appendix)

$$v_D(t) = v_{DC} + v_{AC}(t) \approx v_{DC} + v_{(0-p)} \sin \omega t \approx \frac{K}{2}\left[1 + 2\sqrt{3} \sin \omega t\right] \tag{16}$$

when F_0 is small and less than 0.04 radian, the output zero-to-peak (0-p) detector voltage $v_{(0-p)}$ is linear proportional to the applied current amplitude (A) as given by $v_{(0-p)} \propto 2\sqrt{3}F_0$.

2.2 SIGNAL MODULATION

Current measurement can be found by a ratio of $v_{(0-p)}$ and v_{DC}, which is known as "signal modulation." Thus, signal modulation using equation (16) is given by

$$\frac{v_{(0-p)}}{v_{DC}} = 2\sqrt{3}F_0 = 2\sqrt{3}VNA \tag{17}$$

The sensor output is linear up to .0.04 *rad* ($\sin x \approx x$) or about 8,500 A_{rms} (0.04 rad/V ; $V = 4.68\times10^{-6}$ for wavelength of 633 nm). If the applied current is 1,000 A_{rms} , the signal modulation using equation (17) will be $1.62\text{x}10^{-2}$. In practice, δ is not negligible but T is *i.e.* $\delta = 0.660$ and $T = 0.05$ radians. When the applied current is 1,000 A_{rms}, the signal modulation using equation (12) is 1.378×10^{-2}. Scale factor of the sensor is defined by

$$SF = \frac{\text{signal modulation (in practice)}}{\text{signal modulation of the ideal case}}$$

In this case, the scale factor SF is 0.85

3. MATHEMATICAL MODEL OF LINEAR BIREFRINGENCE CHANGE DUE TO VIBRATION

We model the linear birefringence in the sensing fiber being composed of bending-induced linear birefringence (δ_{DC}) and vibration-induced linear birefringence caused by transverse strain or vibration (δ_v), which can be described by [10]

$$\delta_v = \frac{2\pi}{\lambda}\Delta n l \tag{18}$$

where Δn is the refractive index change induced by stress in the medium (silica in this case), l is the effective length (under perturbation) of fiber, and λ is the center wavelength of the source. The refractive index change is given by [10]

$$\Delta n = -\frac{n^3}{2} p\sigma = 0.311\sigma \tag{19}$$

where n is the (unperturbed) refractive index of medium, σ is the strain and p is the photoelastic constant of fiber ($p = 0.2$ in silica). Value of the Faraday rotation (VNI) depends on the Verdet constant (V). Typical value of V is 4.68 $\mu rad/\mathrm{A}$ or 0.268°/kA. Because the vibration affects linear birefringence, to induce a π-radian birefringence change $\Delta n = \lambda/2 = 3.165\times10^{-7}$ for a fiber length of 1 m. We can find the strain of 1.019×10^{-6} using Equation (19).

The bending-induced birefringence (δ_{DC}) of a fiber loop with radius R under no tension can be described by

$$\delta_{DC} = K\left(\frac{r}{R}\right)^2 \quad °/\mathrm{m} \tag{20}$$

where $K = 7.7\times10^7$ °/m (for silica fiber) and r is the radius of fiber (= 62.5 5 μm). Thus, the (static) bending-induced linear birefringence per turn is

$$\delta_{DC} = \frac{2\pi K r^2}{R} \approx \frac{0.6\pi}{R} \quad °/\mathrm{turn} \tag{21}$$

In our case, R of 0.3 m results in δ_{DC} of 6.3 °/turn. Six turns of fiber loop result in δ_{DC} of 37.8°.

Assume that (total) linear birefringence (δ) in single-mode sensing part is the algebraic sum of the (static) bending-induced linear birefringence (δ_{DC} due to loop radius) and vibration-induced linear birefringence (δ_v). Then, the (total) linear birefringence can be expressed by

$$\delta = \delta_{DC} + \delta_v \sin(\omega_v t) \tag{22}$$

where $\omega_v = 2\pi f_v$ and f_v is the frequency of the vibration δ_v and T is much smaller than δ_{DC} in our configuration.

3.1 CURRENT MEASUREMENT ERROR DUE TO VIBRATIONS

In this section we formulate a mathematical model of the vibration sensitivity or measurement error due to vibration. In equation (12), even when no current and no vibration are applied ($F = 0$ and further assume that the δ_{DC} and T to be constant), the output will be constant. However, the presence of vibration perturbs the linear birefringence and modulates the angular rotation, which cannot be distinguishable from that of the Faraday rotation (F). This results in signal modulation even no applied current. It is named apparent current or false current. Substitute equation (22) into (12), we obtain a phase modulation signal. Assume the change of δ_{DC} and T (from vibrations) to be small and negligible. In this case, we

formulate a mathematical model for vibration sensitivity when only vibration on the sensing fiber ($F = 0$) is given by

$$\frac{I_{60^\circ}}{I_0} = \frac{1}{4} + \frac{\sqrt{3}}{2}\frac{\sin\left(\sqrt{4T^2 + (\delta_{DC} + \delta_v \sin\omega_v t)^2}\right)}{\sqrt{4T^2 + (\delta_{DC} + \delta_v \sin\omega_v t)^2}}.T + \left[1 - \cos\left(\sqrt{4T^2 + (\delta_{DC} + \delta_v \sin\omega_v t)^2}\right)\right]\frac{T^2}{4T^2 + (\delta_{DC} + \delta_v \sin\omega_v t)^2} \quad (23)$$

Using Lock-in amplifier or the spectrum analyzer, we can examine the frequency components of the DC, first-harmonic, second-harmonic, and higher harmonic components. Assume the values of the δ_{DC} and T to be 0.660 (37.8°) and 0.05 radians, respectively. The value of δ_v is assumed to vary linearly with the mechanical vibration to the sensing fiber and, thus, signal modulation varies with the same frequency. When δ_v is small and the applied vibration is of single-frequency, the signal modulation due to vibration can be approximated by (when $2T, \delta_v << \delta_{DC}$)

$$\frac{I_{60^\circ}}{I_0} = \frac{1}{4} + \frac{\sqrt{3}}{2}\frac{\sin(\delta_{DC} + \delta_v \sin\omega_v t)}{\delta_{DC} + \delta_v \sin\omega_v t}.T + \left[1 - \cos(\delta_{DC} + \delta_v \sin\omega_v t)\right]\frac{T^2}{(\delta_{DC} + \delta_v \sin\omega_v t)^2} \quad (24)$$

We can expand and approximate equation (24) using Bessel function (see Appendix) as follows:

$$\left.\frac{I_{60^\circ}}{I_0}\right|_{1f} = \frac{1}{4} + \frac{\sqrt{3}}{2}B_1\left[J_0(\delta_v)\sin(\delta_{DC}) + 2J_1(\delta_v)\cos(\delta_{DC})\sin(\omega_v t)\right] + B_2\left[1 - J_0(\delta_v)\cos(\delta_{DC}) + 2J_1(\delta_v)\sin(\delta_{DC})\sin(\omega_v t)\right] \quad (25)$$

where J_0 and J_1 are Bessel function of the first and second order term ,respectively.

$J_0(\delta_v) \approx 1$

$J_1(\delta_v) \approx 0.5\delta_v$

$$B_1 = \frac{T}{\sqrt{4T^2 + \delta^2}} = \frac{T}{\sqrt{4T^2 + (\delta_{DC} + \delta_v \sin(\omega_v t))^2}}$$

$$B_2 = \frac{T^2}{4T^2 + \delta^2} = \frac{T^2}{4T^2 + (\delta_{DC} + \delta_v \sin(\omega_v t))^2}$$

3.2 SIMULATED FALSE CURRENT DUE TO VIBRATIONS

Using equation (24) and (25), Figure 2 shows that when the vibration is small and is of single-frequency, the signal modulation varies linearly with δ_v and has the same frequency as that of the vibration. The other higher harmonics are negligible. Assume the values of the δ_{DC} and T to be 0.660 (37.8°) and 0.05 radians, respectively. Used the curve fitting for Figure 2 find slope of Signal modulation so that, the relation between vibration-induced linear birefringence δ_v and Signal modulation is

$$\text{Signal modulation} = 3.1652 \times \delta_v \tag{26}$$

When we vary the value of the bending-induced linear birefringence (δ_{DC}) with 1, 3, 6, 9 and 12 fiber turn coils were simulated. Figure 3 shows that the vibration is small and is of single-frequency, the signal modulation varies linearly with δ_v, slope of signal modulation change linearly with small δ_{DC} when increase in δ_{DC} the slope of signal modulation is not linearly with δ_{DC}. For figure 4 shows the relation between slope of signal modulation characteristic and the value of the bending-induced linear birefringence (δ_{DC}), we note that the slope of signal modulation change linearly with δ_{DC} less than 50°, the slope is maximum when $\delta_{DC} = 129^\circ$ and minimum when $\delta_{DC} = 0^\circ$ and 258°

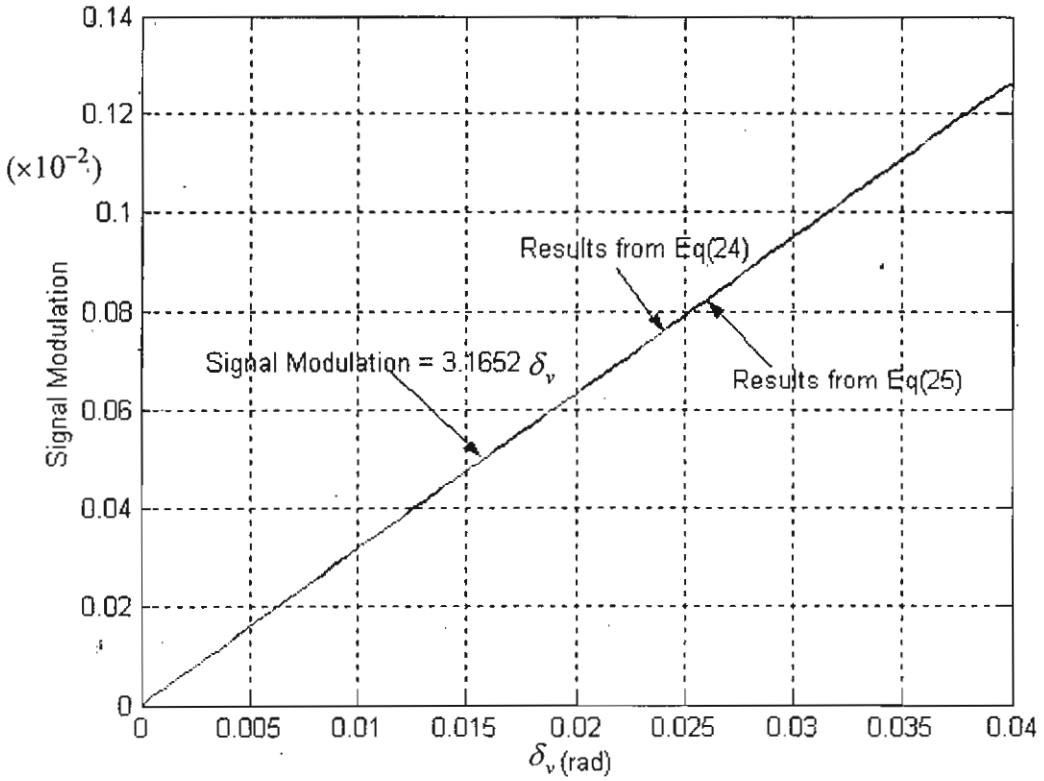

Figure 2: Signal modulation Vs vibration-induced linear birefringence δ_v

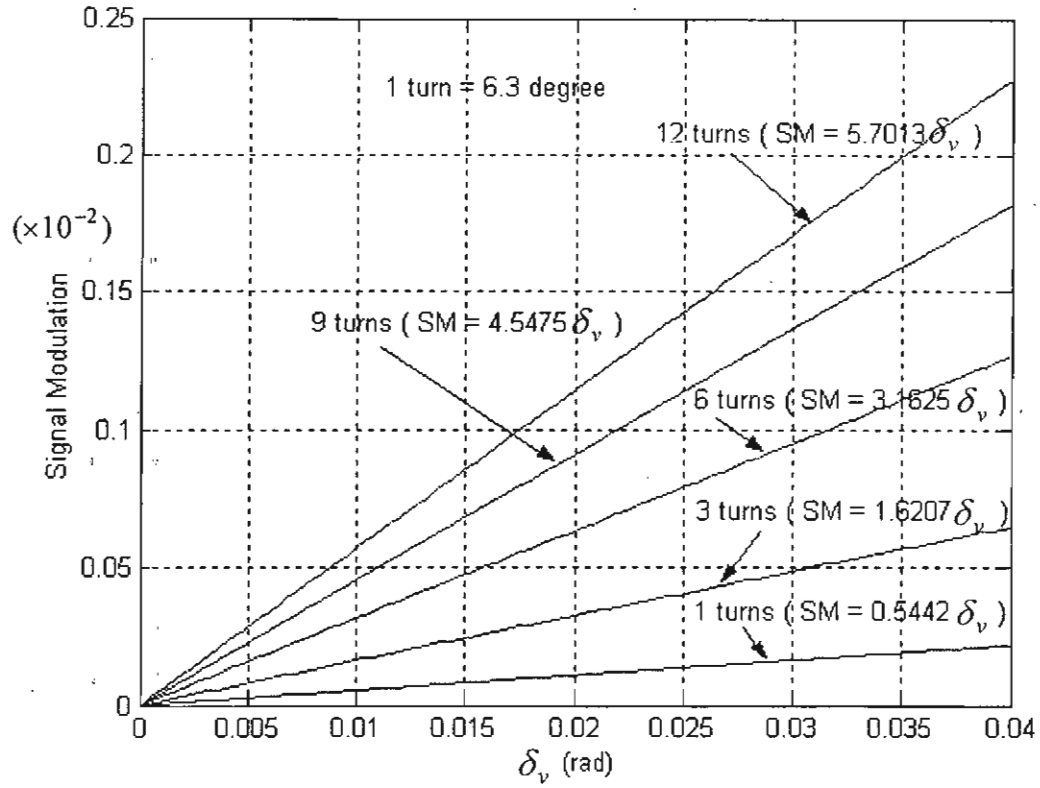

Figure 3: Signal modulation Vs δ_v of 1,3, 6, 9 and 12 turns

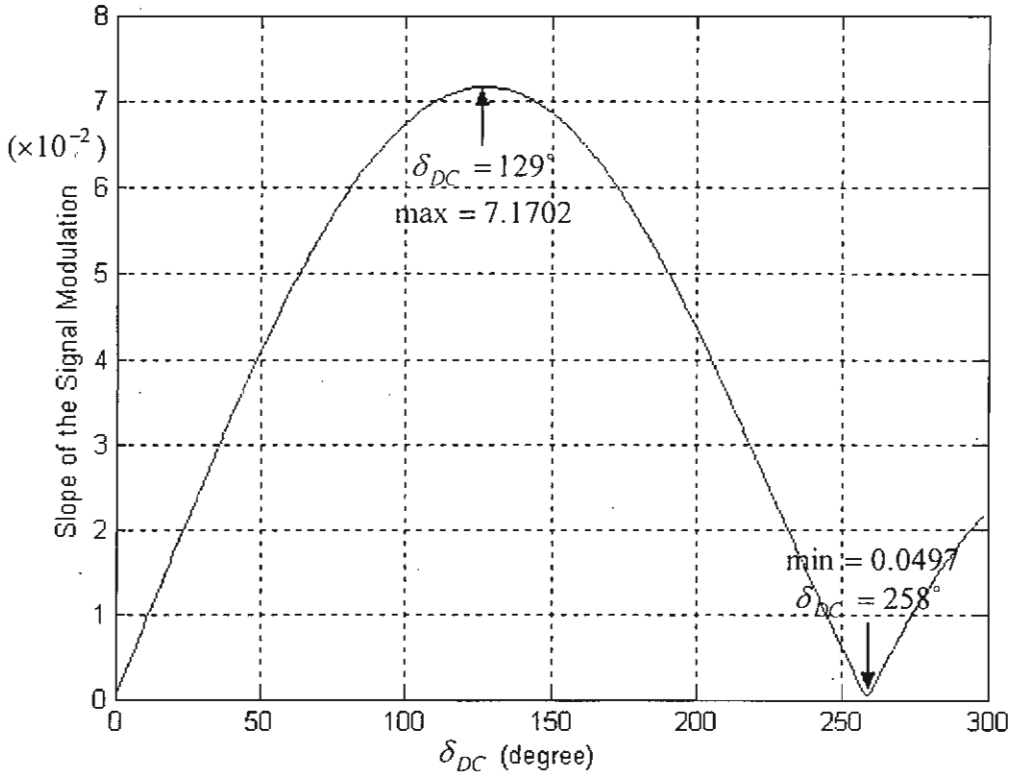

Figure 4: Slope of Signal modulation Vs δ_{DC}

1. EXPERIMENTAL SETUP AND RESULTS

The sensor depicted in Figure 1 was built. A wire coil was used as the current carrying conductor. It was wrapped around one turn of sensing fiber and had a 1,000 turns to simulate large value of current. The optical source was a HeNe laser with 20 mW of output optical power. The operating wavelength is 633 nm. 3M single-mode fiber was employed. Fiber polarization controller (PC) was used prior to the single-mode fiber loop (with a radius of 30 cm to simulate the sensing part) in order to launch the linearly polarization into the linear birefringence (fast) axis of the sensing fiber. The state of polarization of the output was linearly polarized. The analyzer was aligned 60° to the angle with maximum output intensity (fast axis of the fiber end).

4.1 ACTUAL CURRENT MEASUREMENT

We can find characteristics of the fiber sensor by applying current to the coil and then measuring signal modulation. The coil generates magnetic field and induces Faraday rotation in the sensor. Applied current of 1 A_{rms} to the coil of 1,000 turns is equivalent to the current of 1,000 A_{rms} to sensing fiber of 1 turn or 1,000 A_{rms}.turn. The power amplifier supplies the current to the sensing coil in Figure 1 (switch D1 is closed and D2 is opened). The sensor's output voltage consists of two parts: a DC part (v_{DC}) corresponding to the average output intensity at analyzer angle θ of 60°and an AC part (v_{AC}) corresponding to actual current measurement. A lock-in amplifier can measure its rms value. In an ideal case or annealed fiber being used (δ_{DC} is about 1 to 2 degrees/ turns), we get signal modulation of 1.62×10^{-2}. From our experiment, signal modulation is 1.29×10^{-2}. These agree well with our analysis that δ_{DC} and T are 0.660 and 0.05 radians, respectively.

4.2 CHARACTERIZATION OF RELATIONSHIPS BETWEEN VIBRATION AND FALSE CURRENT

In figure 1, mechanical vibration was applied just in front of the single-mode fiber loop. A speaker was kept in a closed box and about 7 cm of fiber was attached to the top of the box. This box was made from acoustic absorbing material in order to isolate acoustic perturbations from disturbing alignment of the photodetector and the other optic components in the system. Thus, only vibration sensitivity can be measured. A power amplifier supplies signal of 400 Hz to the speaker (switch D2 is closed and D1 is opened). This produces vibration of 400 Hz to the fiber. A piezo-electric accelerometer was attached to the top of the box closed to the fiber to quantify the magnitude and frequency contents of mechanical vibration. The vibration sensor is NP-3110s manufactured by Ono Sokki and its signal conditioner is IMV TrendVibro Z model VM 4105. The output voltage of the detector was given to a Stanford Research lock-in amplifier model SR 530 to read the rms value of the AC part ($v_{(0-p)}$). DC value (v_{DC}) is measured by a DC voltmeter. Figure 5 shows the effect of vibration on the sensor when no applied current to the sensing coil. The vibration amplitude is 6.63 (0-p) m/s^2 at the frequency of 400 Hz. Figure 6 shows signal modulation Vs amplitude of vibration from the accelerometer in $m_{(0-p)}/s^2$. The output of the IMV vibrometer and the lock-in amplifier were given to an oscilloscope (see Figure 5).

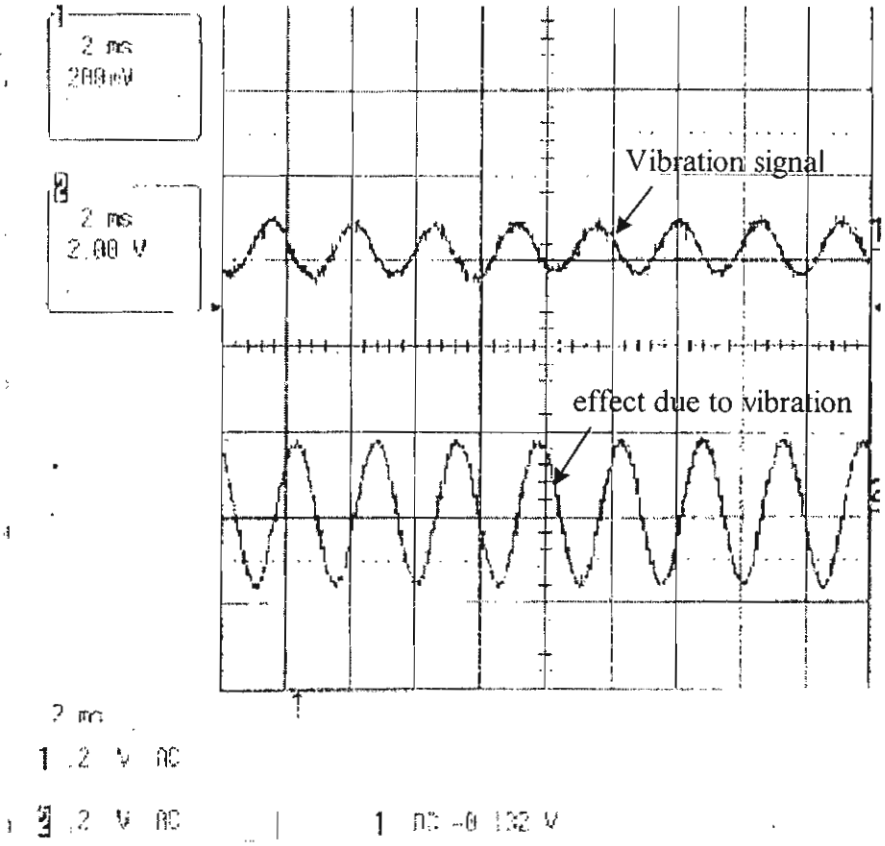

Figure 5: Vibration of 6.63 m/s^2 at the frequency of 400 Hz (top trace) and corresponding sensor's output (bottom trace)

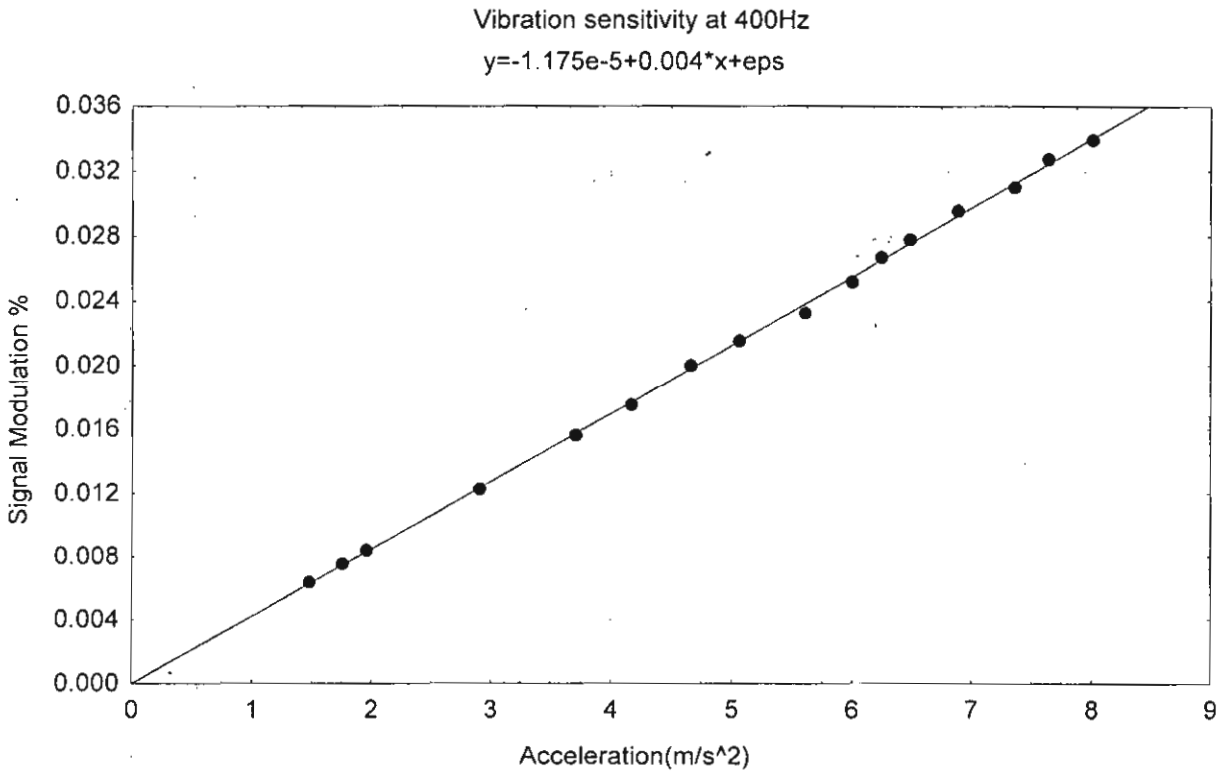

Figure 6: Signal modulation Vs vibration amplitude (0-p) m/s^2. The frequency of vibration is 400 Hz

2. DISCUSSIONS

In actual current measurement, under no vibration $\delta_v = 0$ only δ_{DC} and T are constant and the applied current of 1,000 A_{rms}.turn, the signal modulation is 1.378×10^{-2} (1.29×10^{-2} in our experiment) using Equation (12). This is due to the efficiency of magnetic producing coil is only 93.6%. The signal modulation (or false current) varies linearly with vibration amplitude (see Figure 7). Also, simulation of our model shows that signal modulation varies linearly with δ_v. Thus, δ_v varies linearly with vibration amplitude (see Figure 7). As a result, 1 g (9.8 m/s^2) of vibration produces around 46 A_{rms}.turns of the false current. With good packaging and the annealed sensing fiber (δ_{DC} is about 1 to 2 degrees/ turns) being used, the effect will be a few orders of magnitude smaller. In our system vibration lower than 0.6 m/s^2 (due to noise floor limit) does not result into false current. A damped packaging of the sensing fiber could do further reduction of the vibration sensitivity. It can be placed in a highly elastic silicone gel so no inert forces will be allowed and the fiber will be protected from deformation. Also, we can protect the fiber leads to the sensing fiber by using PM fiber leads which may be strewn virtually anywhere throughout the power systems with no concern of false signal detection due to vibrations. The noise equivalent current is about [CC1] 0.33 $A_{rms}.turn/\sqrt{H_z}$

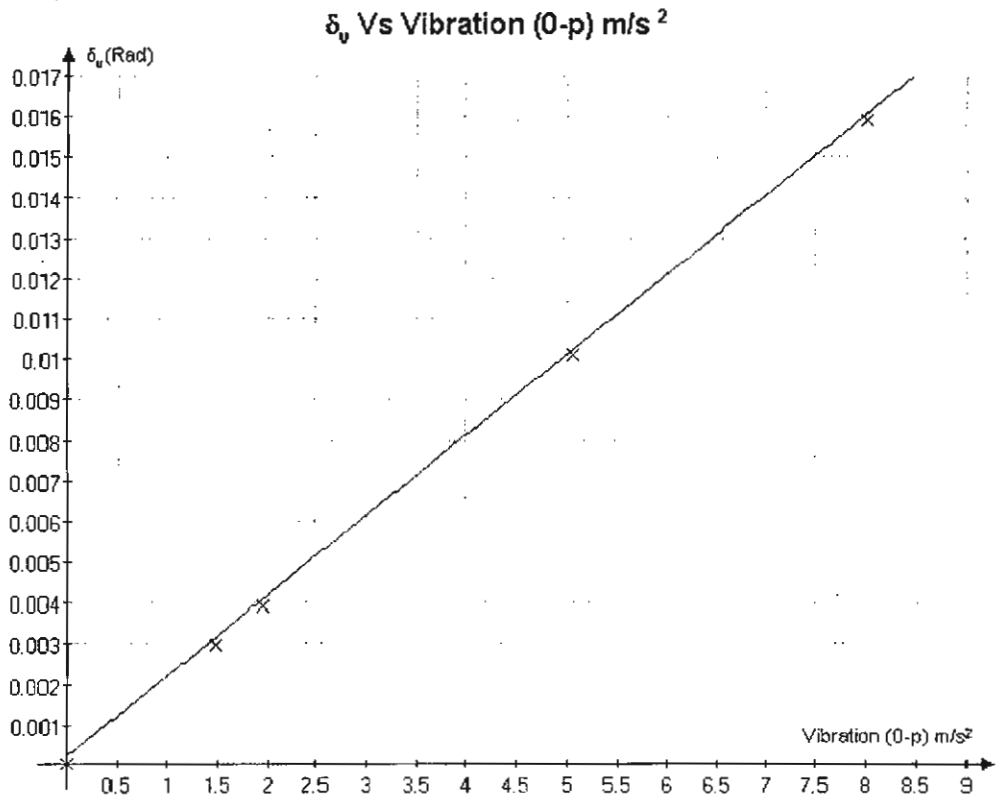

Figure 7: Linear birefringence change Vs Vibration amplitude (0-p) in m/s^2

3. CONCLUSION

We have demonstrated a novel mathematical model for vibration sensitivity in the unidirectional polarimetric current sensor (UDPS). Experimental study shows that the linear birefringence δ_V due to mechanical vibration (to our understanding, no experimental studies were reported for vibration sensitivity with a single frequency of vibration and no effect of

acoustic perturbations to the other optic components) changes linearly with vibration amplitude. This sensor's residual sensitivities to environmental disturbances can be further reduced by a damped packing such as putting sensing fiber part in a gel-filled tube together with employing two polarization scheme, where the two sensor's output at the +45° and –45° to the output fiber axes. Also, 'spun' low birefringence or annealed fiber can be used to reduce the value of (static) linear birefringence δ_{DC}. Further investigation of the magnitude of linear birefringence change under the influence of vibration should be done experimentally with the help of optical modulator.

4. ACKNOWLEDGEMENT

Funding was provided by The Thailand Research Fund (TRF) under Grant No. TRF:RSA/06/2541 and Thaikhadi Research Institute, Thammasat University. The authors would like to thank Dr. James N. Blake of Nxtphase, USA, Prof. Alan J. Rogers of University of Surrey, UK, and Assoc. Prof. Dr. Pichet Limsuwan of King Mongkut's University of Technology, Thonburi for help and fruitful discussions. Also, the authors would like to thank Mr. Karma Dorji for their assistance in this study.

REFERENCES

1. Tabor and Chen. 1969. Electromagnetic propagation through materials possessing both Faraday rotation and birefringence: experiments with Ytterrbium Orthoferrite. *J. Appl. Phys.* 40(7), 2760.
2. Smith A. 1978. Polarization and magnetooptic properties of single-mode optical fibre. *Appl. Opt:* 17(52).
3. Cease T, *et al* .1989. Optical voltage and current sensor used in revenue metering system. *IEEE Trans. Power Delivery,* 6(4), 1374-79.
4. Ren Z, *et al.* 1989. Discrimination between linear birefringence and Faraday rotation in optical fiber current sensors by polarization multiplexing. *Fiber Optic and Laser Sensors VII* 1169, 226-232.
5. Menke P and Bosselmann T. 1995. Temperature compensation in magnetooptic AC current sensors using an intelligent AC-DC signal evaluation. *IEEE J. Lightwave Technol.* 13(7), 1362-70.
6. Roger A, *et al.* 1995. Vibration immunity for optical fiber current measurement. *IEEE J. Lightwave Technol.* 13(7), 1371-1377.
7. Short S, *et al.* 1998. Elimination of birefringence induced scale factor errors in the in-Line Sagnac interferometer current sensor. *IEEE J. Lightwave Technol.* 16(10), 1844-1850.
8. Short S, Tantaswadi P, *et al* .1996. Environmental sensitivity comparison of in-line Sagnac and polarimetric type current sensor. *IEEE Trans. Power Delivery* 11(4), 1702-1706.
9. Tantaswadi P, *et al.* 2001. Study of current measurement error due to vibration in reciprocal fiber-optic polarimetric current sensor *IEEE PEDS'01*, Bali, Indonesia.
10. Rogers A. 1995. Optical Fiber Current Measurement In: *Optical Fiber Sensor Technology*, Grattan K and Meggit B, eds., Vol. I, Chapman & Hall, 432-438.
11. Born M and Wolf E .1980. In: *Principles of optics*, Oxford: Pergamon, 6th ed., 1980.
12. Carrara S .1988. State of Polarization In: *Drift reduction in optical fiber gyroscopes*, Ph.D. Dissertation, Stanford U, CA.

APPENDIX

Solve equation (13)

Assume $2F_0 << 1$, approximation of $\sin(2F_0 \sin\omega t - 30^\circ)$ is given by

$\sin(2F_0 \sin\omega t - 30^\circ) = \sin(2F_0 \sin\omega t)\cos(30^\circ) - \cos(2F_0 \sin\omega t)\sin(30^\circ)$,

where expansion of

$\sin(2F_0 \sin\omega t) = 2[J_1(2F_0)\sin\omega t + J_3(2F_0)\sin 3\omega t + ..]$,

$\cos(2F_0 \sin\omega t) = J_0(2F_0) + 2[J_2(2F_0)\sin 2\omega t + J_4(2F_0)\sin 4\omega t + ..]$,

when $x << 1$, the approximation of

$J_0(x) \approx 1$,

$J_1(x) \approx 0.5x$. Therefore, $J_1(2F_0) \approx F_0$,

$J_2(x), J_3(x), J_4(x) << 1$

Thus,

$$1 + \sin(2F_0 \sin\omega t - 30^\circ) \approx \frac{1}{2} + \sqrt{3}[J_1(2F_0)\sin\omega t + J_3(2F_0)\sin 3\omega t + ..] - [J_2(2F_0)\sin 2\omega t + J_4(2F_0)\sin 4\omega t + ..]$$

$$\approx \frac{1}{2} + \sqrt{3}J_1(2F_0)\sin\omega t$$

$$\approx \frac{1}{2} + \sqrt{3}F_0 \sin\omega t$$

we can expand and approximated equation (24) using Bessel function.

In equation (24), First we define that

$$B_1 = \frac{T}{\sqrt{4T^2 + \delta^2}} = \frac{T}{\sqrt{4T^2 + (\delta_{DC} + \delta_v \sin(\omega_v t))^2}}$$

$$B_2 = \frac{T^2}{4T^2 + \delta^2} = \frac{T^2}{4T^2 + (\delta_{DC} + \delta_v \sin(\omega_v t))^2}$$

where

$$\sin(\delta_v \sin(\omega_v t)) = 2\sum_{k=0}^{\infty} J_{2k+1}(\delta_v)\sin((2k+1)\omega_v t)$$

$$\cos(\delta_v \sin(\omega_v t)) = J_0(\delta_v) + 2\sum_{k=1}^{\infty} J_{2k}(\delta_v)\cos(2k\omega_v t)$$

$$\left.\frac{I_{60^\circ}}{I_0}\right|_{1f} = \frac{1}{4} + \frac{\sqrt{3}}{2} B_1[J_0(\delta_v)\sin(\delta_{DC}) + 2J_1(\delta_v)\cos(\delta_{DC})\sin(\omega_v t)]$$

$$+ B_2[1 - J_0(\delta_v)\cos(\delta_{DC}) + 2J_1(\delta_v)\sin(\delta_{DC})\sin(\omega_v t)]$$

When $\delta_v << 1$ the approximated of

$J_0(\delta_v) \approx 1$ and $J_1(\delta_v) \approx 0.5\delta_v$

Appendix A.3

Letters of acceptance of the manuscripts A.1 and A.2

Science Asia
Journal of the Science Society of Thailand
วารสารของสมาคมวิทยาศาสตร์แห่งประเทศไทย
http://scienceasia.tiac.or.th ISSN 1513-1874

May 28, 2001

Dr. Prinya Tantaswadi,
Sirindhorn Institute of Technology,
Thammasat University,
P.O.Box 22, Thammasat-Rangsit Post Office,
Klong Luang, Pathumthani 12121.

Dear Dr. Prinya,

Thank you very much for submitting the manuscript entitled: Numerical Investigation of Vibration Sensitive in a Reciprocal Fibre-optic Polarimetric Current Sensor (Code 0105-195, received 24 May 2001) for consideration for publication in *ScienceAsia*.

The manuscript has been sent to independent referees for review. We will inform you as soon as possible after receiving comments from the referees.

Thank you again for your interest in contributing to our journal.

Yours sincerely,

Prof. Dr. MR. Jisnuson Svasti
Editor
ScienceAsia

EDITORIAL OFFICE: c/o Department of Biochemistry, Faculty of Science, Mahidol University
Rama VI Road, Bangkok 10400
Tel:+66-2-2461360-69 ext.6619 Fax:2480375 E-mail: scjss@mahidol.ac.th

ScienceAsia
Journal of the Science Society of Thailand
วารสารของสมาคมวิทยาศาสตร์แห่งประเทศไทย
http://sciencoasia.tioc.or.th ISSN 1513-1874

September 20, 2001

Dr. Prinya Tantaswadi,
Sirindhorn Institute of Technology,
Thammasat University,
P.O.Box 22, Thammasat-Rangsit Post Office,
Klong Luang, Pathumthani 12121.
E-mail: prinya@siit.tu.ac.th

Dear Dr. Prinya,

Thank you very much for submitting the manuscript entitled: Vibration Sensitivity in Unidirectional Optical Polarimetric Current Sensor (Code 0109-234, received 19 September 2001) for consideration for publication in *ScienceAsia.*

The manuscript has been sent to independent referees for review. We will inform you as soon as possible after receiving comments from the referees.

Thank you again for your interest in contributing to our journal.

Yours sincerely,

Prof. Dr. MR. Jisnuson Svasti
Editor
ScienceAsia

EDITORIAL OFFICE: c/o Department of Biochemistry, Faculty of Science, Mahidol University
Rama VI Road, Bangkok 10400
Tel:+66-2-2461360-69 ext.5843 Fax:2480375 E-mail: scjss@mahidol.ac.th

Appendix B

The following sections contain reprints of

B.1 P. Tantaswadi, " Simulation of birefringence effects in reciprocal fiber-optic polarimetric current sensor," *Int. Conf. on Meas. of Light, LIGHTMETRY 2000*, Proc. SPIE, Pultusk, Poland, June 2000, pp. 158-164.

B.2 A. Andreev and P. Tantaswadi, " Mathematical model for calculation of the optical rotation and the contrast of the image," *Int. Conf. on Meas. of Light, LIGHTMETRY 2000*, Proc. SPIE, Pultusk, Poland, June 2000, pp. 206-210.

B.3 P. Tantaswadi, S. Maheshwari, and C. Tangtrongbenchasil "Study of current measurement error due to vibration in reciprocal fiber-optic polarimetric current sensor," *IEEE-PEDS 2001*, Oct. 2001, Bali, Indonesia, pp. 699-704.

B.4 P. Tantaswadi, S. Maheshwari, and C. Tangtrongbenchasil "Experimental study of vibration sensitivity in unidirectional polarimetric current sensors," *Int. Symp. on Opt. and Quantum Tech.* (ISOQT), Dec. 2001, KMITL, Bangkok, pp. 94-99.

B.5 S. Pothiya, P. Tantaswadi, and S. Maheshwari "Mathematical modeling of vibration sensitivity in unidirectional polarimetric current sensors," *Int. Symp. on Opt. and Quantum Tech.* (ISOQT), Dec. 2001, KMITL, Bangkok, pp. 113-118.

B.6 P. Tantaswadi and C. Tangtrongbenchasil "Simulation of uniformly distributed vibration effects on a reciprocal fiber-optic

polarimetric current sensor," *Int. Symp. on Opt. and Quantum Tech.* (ISOQT), Dec. 2001, KMITL, Bangkok, pp. 119-122.

Appendix B.1

Reprint of

P. Tantaswadi, " Simulation of birefringence effects in reciprocal fiber-optic polarimetric current sensor," *Int. Conf. on Meas. of Light, LIGHTMETRY 2000*, Proc. SPIE, Pultusk, Poland, June 2000, pp. 158-164.

Simulation of birefringence effects in reciprocal fiber-optic polarimetric current sensor

P. Tantaswadi
Sirindhorn International Institute of Technology, Thammasat University,
Department of Electrical Engineering, PO Box 22,
Thammasat Rangsit Post Office, Pathumthani 12121, Thailand
E-mail: prinya@siit.tu.tac.th

ABSTRACT

We present a mathematical model for calculating the effect of birefringence in reciprocal fiber-optic polarimetric current sensor. The model will aid in designing a configuration with immunity to environmental perturbations, which affect birefringence properties of single-mode fiber used in the sensing part and cause fault current readings, such as acoustic vibrations.

Keywords: optical current sensor, environmental perturbations, polarimetric current sensor, birefringence, and state of polarization

1. INTRODUCTION

There have been several ongoing researches in the area of fiber optic current sensors in the past few decades [1-5]. Several potential advantages over conventional ferromagnetic current transformers include immunity to electromagnetic interference (EMI), no hysteresis, broad linear dynamic range, and broad bandwidth, which is very useful for false current detection. However, the performance of fiber optic current sensor is limited by the susceptibility to the environmental perturbations, i.e. temperature and acoustic perturbations, in the sensing part. The perturbations affect the birefringence property of the fiber in the sensing part. Unidirectional polarimetric current sensor suffers from environmental perturbations due to varying birefringence in the sensing part [6]. This results in false current reading from environmental perturbations.

In this paper, we analyze the performance of reciprocal fiber optic current sensor including the output state of polarization, normalized contrast ratio, and effects of birefringence on the sensor. The accuracy of the sensor is within 0.3% of the actual value and satisfies application in revenue metering.

2. PRINCIPLES

When light propagates in an optical fiber wound around a current carrying wire, the induced magnetic field causes a rotation of the linear polarization plane of lightwave by the magneto-optic Faraday effect. This angle of rotation, $\Delta\phi$, through which the plane of polarization rotates, is given by

$$\Delta\phi = V \oint_C \vec{H} \cdot d\vec{l}\,, \tag{1}$$

where V is the Verdet constant of the optical fiber, is the magnetic filed intensity along the direction of light propagation, and l is the optical path along the fiber loop. From the Ampere's law, this closed loop integral of magnetic field around a wire is proportional the current, I, flowing through it, *i.e.*

$$I = \oint_C \vec{H} \cdot d\vec{l}\,. \tag{2}$$

Therefore, the angle of rotation, $\Delta\phi$, in the fiber loop configuration is given by

$$\Delta\phi = VNI\,, \tag{3}$$

where N is the integral number of turns of fiber wrapped around the current carrying wire. The stability of Faraday rotation based current sensors, through the Verdet constant, depends on source wavelength and temperature. For example, the operating wavelength λ is 633 nm and the Verdet constant V is 4.68 $\mu rad/$ A.

Lightmetry: Metrology, Spectroscopy, and Testing Techniques Using Light, Maksymilian Pluta, Editor,
Proceedings of SPIE Vol. 4517 (2001) © 2001 SPIE · 0277-786X/01/$15.00

To measure current I, with constant N and V, we can use polarimeter sensor to measure $\Delta\phi$. In conventional unidirectional polarimetric current sensor, a linearly polarized light is launched into single-mode sensing fiber and the output polarization is analyzed by a Wollaston prism for evaluation of current and static linear birefringence [3]. In practice, the propagation of light through the fiber loop exhibiting additional linear birefringence due to bending and twist-induced circular birefringence can be described by Jones calculus (see next section). These birefringences affect the accuracy and stability of the sensor. Reciprocal fiber-optic current sensor (see Fig. 1) interrogates the light in both directions. Since linear and twist-induced birefringences exhibit reciprocal characteristics, the reciprocal rotation of these birefringences cancels when light propagation along and back-reflected down a fiber. The Faraday magneto-optic effect exhibits nonreciprocal characteristics, the Faraday rotation doubles when light propagation along and back-reflected down a fiber. Thus, this optical circuit has the advantage of minimizing the birefringence induced offset problems associated with the unidirectional polarimetric current sensor.

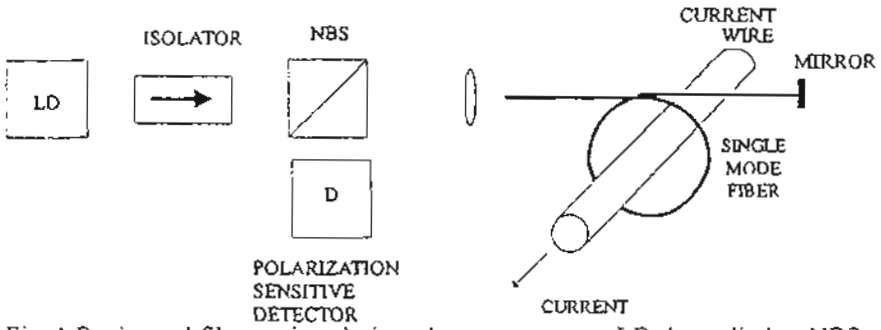

Fig. 1 Reciprocal fiber optic polarimetric current sensor, LD: laser diodes, NBS: non-polarizing beam splitter

3. STATE OF POLARIZATION

To analyze the performance of the sensor, we first look at the output state of polarization. The output electric field (E_{out}) of the sensor can be described by Jones matrix

$$E_{out} = \frac{1}{2}\vec{L}\cdot M\cdot\overleftarrow{L}\cdot E_{in}, \tag{4}$$

where E_{in}, $\vec{L}$, M, and $\overleftarrow{L}$ represent input linearly polarized light in the x axis, sensing fiber matrix when light propagating in the forward direction, Jones matrix of the mirror, and sensing fiber matrix when light propagating in the backward direction, respectively [1-2].

$$\vec{L} = \begin{bmatrix} A & -B \\ B^{*} & A^{*} \end{bmatrix}, \tag{5}$$

where

$$A = \cos\frac{\alpha}{2} + j\sin\frac{\alpha}{2}\cos(\chi)$$
$$B = \sin\frac{\alpha}{2}\sin(\chi) \tag{6}$$

$$\frac{\alpha}{2} = \sqrt{(VNI+T)^2 + (\frac{\delta}{2})^2} \tag{7}$$

$$\tan\chi = 2(VNI+T)/\delta. \tag{8}$$

The *VNI* is the Faraday rotation induced by current, and T is the circular birefringence. δ represents total linear birefringence. α represents the resulting elliptical birefringence. Assume both the total linear and circular birefringence to be uniformly distributed along the single-mode fiber optic sensing part.

$$\bar{L} = \begin{bmatrix} C & -D \\ D & C^* \end{bmatrix}, \tag{9}$$

where

$$C = \cos\frac{\beta}{2} + j\sin\frac{\beta}{2}\cos(\zeta)$$
$$D = \sin\frac{\beta}{2}\sin(\zeta) \tag{10}$$

$$\frac{\beta}{2} = \sqrt{(VNI - T)^2 + (\frac{\delta}{2})^2} \tag{11}$$

$$\tan\zeta = 2(VNI - T)/\delta, \tag{12}$$

$$M = \begin{bmatrix} 1 & 0 \\ 0 & 1 \end{bmatrix}$$

With linearly polarized input at the birefringence axis of sensing fiber, the output electric field can be described by

$$E_x = \frac{1}{2}(AC - BD) = a_1 \exp(j\delta_x), \tag{13}$$

$$E_y = \frac{1}{2}(AD + BC^*) = a_2 \exp(j\delta_y), \tag{14}$$

where a_1, δ_x, a_2, and δ_y are the amplitude and phase of the electric field in the x and y- axis, respectively.

The output state of polarization can be expressed on the Poincaré sphere (S_1, S_2, S_3) [7,8]

$$S_1 = a_1^2 - a_2^2,\ S_2 = 2a_1 a_2 \cos(\delta_x - \delta_y), \text{ and } S_3 = 2a_1 a_2 \sin(\delta_x - \delta_y) \tag{15}$$

In this Poincaré sphere, the state of polarization can be plotted on the surface of a sphere. Right circular polarization is on the north pole, left circular on the south pole, linear polarization on the equator, and elliptical polarization in between [8]. With input light aligned to birefringence axis of the sensing fiber, in ideal fiber ($\delta, T \approx 0$), we would expect only Faraday rotation occurs. In this sensor, the rotation angle is $2VNI$. This is due to the fact that Faraday rotation of *VNI* in the forward direction down the fiber and, by nonreciprocal effect of Faraday effect, additional Faraday rotation of *VNI* in the backward direction down the same fiber. Thus, the total Faraday rotation of $2VNI$ occurs in the sensor. Assume that the input light is linearly polarized in the x-axis or horizontal direction. It is (1,0,0) on Poincaré sphere or a dot shown in Fig. 2. In Fig. 2 (a), the Faraday rotation angle of $2VNI$ will be equivalent to $4VNI$ along the equator (angle on the sphere is twice as much as the angular rotation and output is still linearly polarized). For example, the *VNI* of 0.01 π radians produces 0.04 π radians of rotation along the equator. The characteristic curve of a practical case (δ = 1 π and T = 100 π radians or δ/T = 1%) is shown in Fig. 2 (b). It is similar to the ideal case but a very small deviation from the equator. The deviation from the ideal case produces some small susceptibility to varying birefringence and will be demonstrated in the next section. Fig. 2 (c) with thin line for $\delta = \pi/6$ and $T = 0$ and thick line: $\delta = \pi/2$ and $T = \pi$ (δ/T = 50%) shows that the sensor is not practical for current sensing when T does not dominate δ or δ/T is not small.

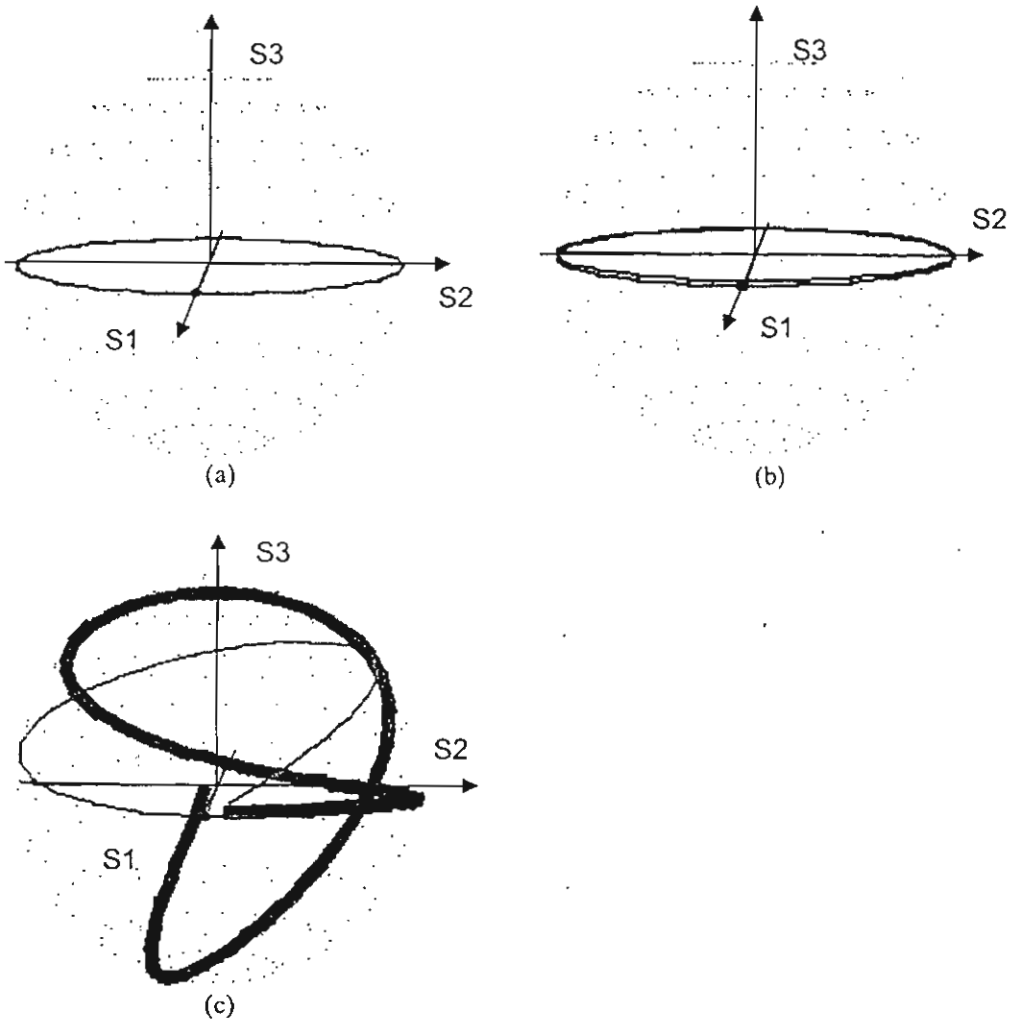

Fig.2 Characteristic curves of the output polarization on the Poincare sphere for F=0 to π radians when (a) ideal case: $\delta = 0$ and $T = 0$ (b) $\delta = 1\ \pi$ and $T = 100\ \pi$ radians (c) the thin line: $\delta = \pi/6$ and $T = 0$ and the thick line: $\delta = \pi/2$ and $T = \pi$ radians.

4. ANALYTICAL DESCRIPTIONS OF THE NORMALIZED CONTRAST RATIO

The Wollaston prism is aligned 45° and –45 ° to birefringence axis of the output end of the sensing fiber. The contrast ratio (K) is defined by

$$K = \left| \frac{I_{xo} - I_{yo}}{I_{xo} + I_{yo}} \right|, \qquad (16)$$

where I_{xo}, I_{yo} are the intensity in the 45° and –45 ° to birefringence axis of the output end of the sensing fiber, respectively. We can simplify the expression in eq. (16) using eq. (4) to (12). Then, the contrast ratio (K) is given by

$$K = Sin(\alpha)Cos(\beta)Sin(\chi) + \frac{Sin\beta}{2}[Sin(2\chi - \zeta)(Cos\alpha - 1) + Sin\zeta(Cos\alpha + 1)]. \qquad (17)$$

Ideal case, T and δ are very small and negligible (such that $T, \delta \approx 0$) Eq. (17) becomes

$$K = Sin(4VNI) \tag{18}$$

K provides the measurement of current and is linear ($K = Sin(4VNI) \approx 4VNI$) up to few tenths of a radians, or about 10^5 Amperes for a one-turn sensing coil. K is independent of the circular and linear birefringence in the sensing fiber. However, in practice, the use of high circular birefringence T or "spun" fiber ($F, \delta << T$) can overcome the intrinsic linear birefringence. To understand the performance of the sensor, we show the characteristic plot of K (see Fig. 3) as a function of linear birefringence (δ) and twist-induced circular birefringence (T). The VNI is assumed to be 0.01π and the expected value of K from eq. (18) is 0.125333.

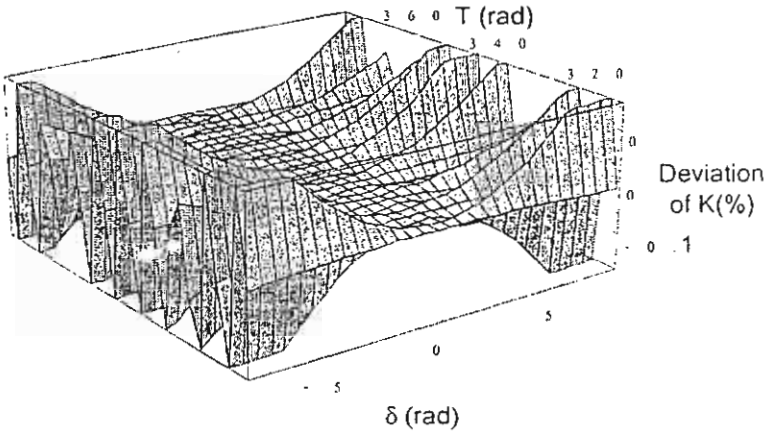

Fig. 3 The contrast ratio (K) as a function of linear birefringence (δ) and twisted circular birefringence (T)

The required intrinsic circular birefringence may be obtained by spun high birefringence fiber, twisted low birefringence fiber or winding low birefringence fiber in a toroidal geometry [5]. In the toroidal configuration, T is about 120 π and δ is about a few π radians. In this sensor, Fig. 3 shows that the deviation of K in percent is within 0.15% of the ideal case ($T, \delta \approx 0$) when the range of the linear birefringence and circular birefringence are (-2.5 π, 2.5 π) and (100 π, 120 π) radians, respectively.

4.1 Deviation of K Vs linear birefringence

This sensor exhibits small dependence on linear birefringence. Fig. 4 shows that deviation of K in percent is below 0.002% when δ is less than 1 π radians when $VNI = 0.05\pi$ and T = 100 π radians. In this case, the approximation of K is $Sin(4VNI)[1-2.228656\text{x}10^{-6}\delta^2] = 0.58779[1-2.228656\text{x}10^{-6}\delta^2]$.

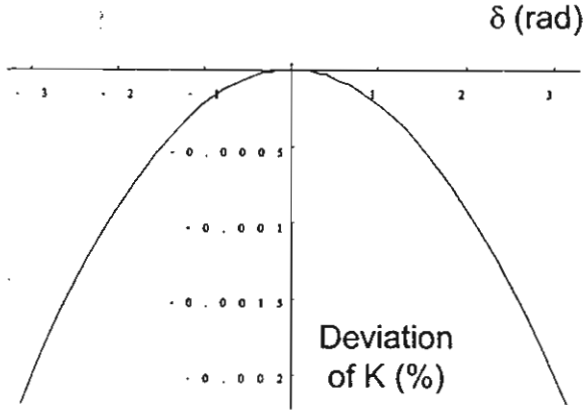

Fig.4 Simulated deviation of K in percent varies with linear birefringence (VNI= 0.05π, T= 100π)

4.2 Apparent current Vs linear birefringence

Environmental perturbations on the sensing fiber can cause angular rotation of lightwave polarization and may affect birefringence property of the sensing fiber. The result could be mislead as actual current. Ref. 6 shows that mechanical vibrations with a magnitude of 3.0 $g_{p\text{-}p}$ ($9.8 m/s^2$) applied to sensing fiber of unidirectional polarimetric sensor can cause apparent current of 400 $A_{p\text{-}p}$. Simulated apparent current (T= 100 π and $\delta = \pi \cos(100\pi t)$) for this sensor is shown in Fig. 5. Very small apparent current of less than 6.47×10^{-7} Amperes for 633 nm wavelength when δ is $(-\pi,\pi)$ radians as shown in Fig. 5(a). The frequency of varying birefringence is chosen to be 50 Hz, which is common to electric power systems [6].

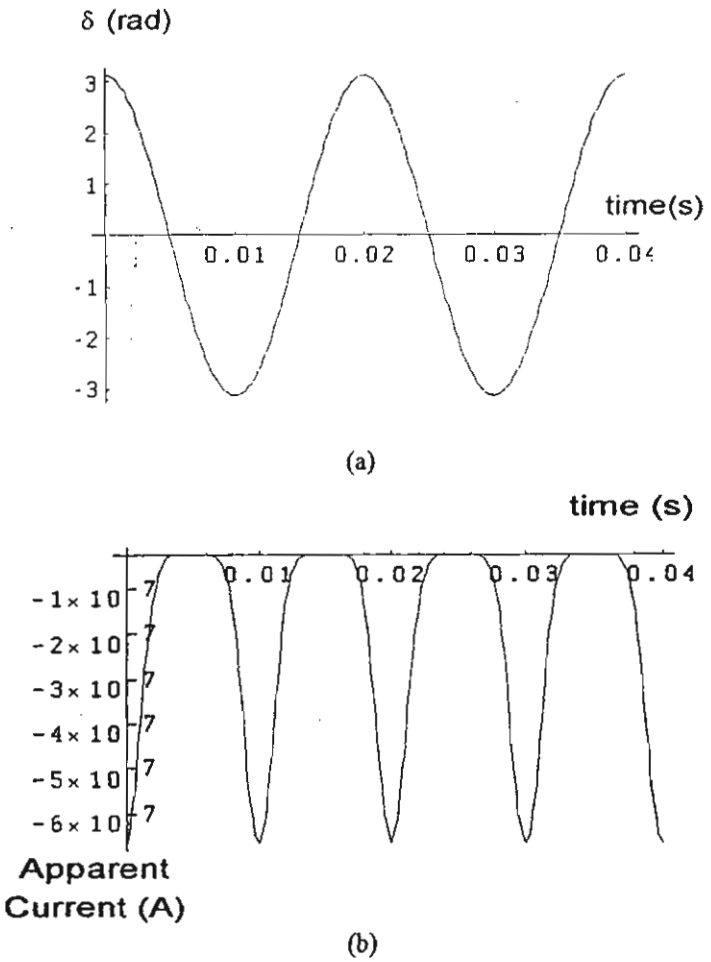

Fig.5 Simulated apparent current (b) in Amperes Vs birefringence (a) (VNI= 0 and T= 100π)

5.CONCLUSIONS

The mathematical model of reciprocal fiber-optic current sensor is demonstrated. The state of polarization of the sensor output is similar to that of ideal case when δT is small (T dominates δ and VNI). Stability of the K value as a function of δ and T are shown. For large T, deviation of K (%) is a quadratic function of δ. The apparent current shows that the susceptibility of sensor to varying linear birefringence is small and negligible.

6. ACKNOWLEDGEMENT

Funding was provided by Thai Research Foundation (TRF). The authors would like to thank Dr. James N. Blake for helps and fruitful discussions.

7. REFERENCES

1. Tabor, *et. al.*, "Electromagnetic propagation through materials possesing both Faraday rotation and birefringence: experiments with Ytterrbium Orthoferrite," J. Appl. Phys., vol.40, no.7, pp. 2760, 1969.
2. A. Smith, "Polarization and magnetooptic properties of single-mode optical fibre," Appl. Opt. , vol. 17, no. 52, 1978.
3. Z. Ren, *et. al.*, "Discrimination between linear birefringence and Faraday rotation in optical fiber current sensors by polarization multiplexing," SPIE vol. 1169, Fiber Optic and Laser Sensors VII, 1989, pp. 226-232
4. T. Bosselmann, *et. al.*, "Intrinsic temperature compensation of magnetooptic AC current transformers with glass ring sensor head," OFS 1994, pp. 20-23.
5. A. Roger, *et. al.*, "Vibration immunity for optical fiber current measurement," IEEE J-LT, Vol. 13, no. 7, Jul. 1995, pp. 1371-1377.
6. S. Short, P. Tantaswadi, R. de Carvalho, B. Russel, and J. Blake, "Environmental sensitivity comparison of in-line Sagnac and poalrimetric type current sensor,"
7. M. Born and E Wolf, *Principles of optics*, Oxford: Pergamon, 6th ed., 1980.
8. S. Carrara, *Drift reduction in optical fiber gyroscopes*, Ph.D. dissertation, Stanford U., Nov. 1988.

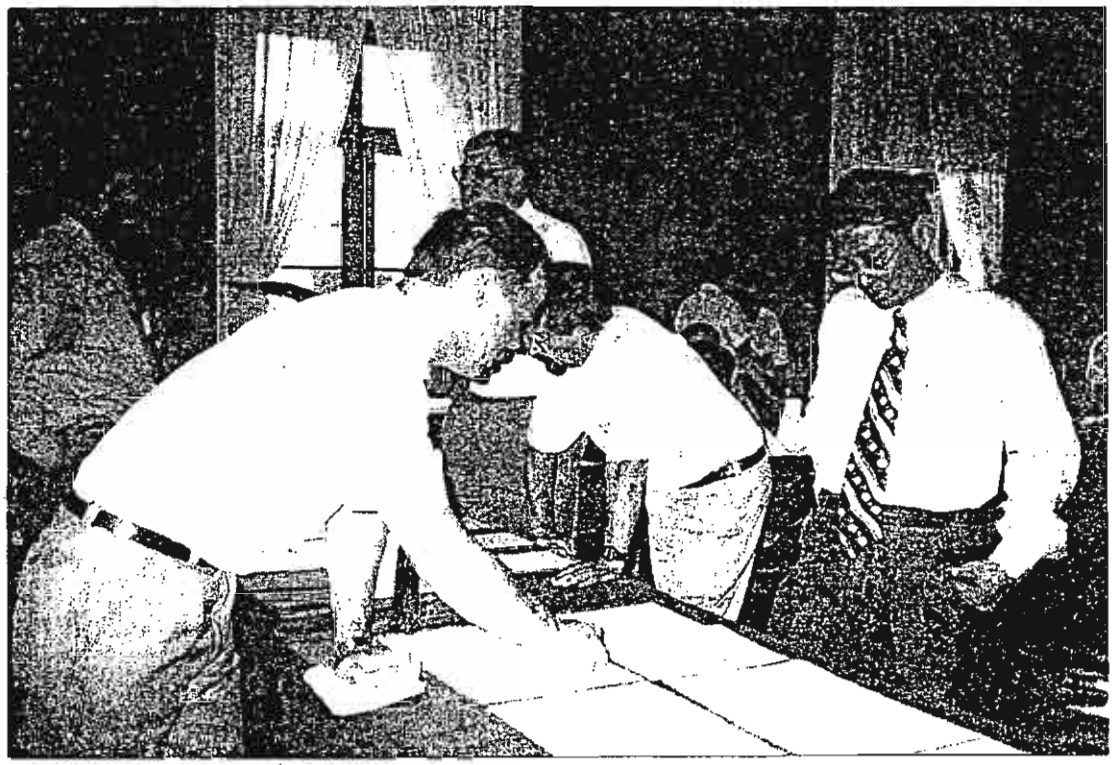

Prinya Tantaswadi (right) is discussing a poster paper on time-domain and spectral-domain two-beam interferometry authored by Petr Hlubina (left) and Pavel Stejskal (see paper No.41).

Appendix B.2

Reprint of

A. Andreev and P. Tantaswadi, " Mathematical model for calculation of the optical rotation and the contrast of the image," *Int. Conf. on Meas. of Light, LIGHTMETRY 2000*, Proc. SPIE, Pultusk, Poland, June 2000, pp. 206-210.

Mathematical model for calculation of the optical rotation and the contrast of the image

A. Andreev and P. Tantaswadi
Sirindhorn International Institute of Technology, Thammasat University,
Department of Electrical Engineering, PO Box 22,
Thammasat Rangsit Post Office, Pathumthani 12121, Thailand
E-mail: prinya@siit.tu.tac.th

ABSTRACT

We present a simple mathematical model for calculating the contrast of image and the parameters of the half-shade analyzer. Practical application of the model and accuracy of the measurements are discussed. Effect of the sensitivity of the angle of rotation on accuracy of the measurements and optical loss are also calculated. Method of the direct measurements of the magnetic domain contrast will also be described.

Keywords: optical rotation, contrast of image, and half-shade analyzer

1. INTRODUCTION

There are a number of the scientific paper deals with calculation and measurement of the half-shade analyzer parameters and contrast of the image of the optical active specimen in the polarized light [1-3]. This paper describes simple universal mathematical model with application to optical rotation and contrast measurements. Theory has been applied in experiments with Faraday effect studying of the domain structure of the thin magneto-optic iron garnet films. It is difficult to adjust the analyzer for a maximum contrast of the domain structure visually and the optimal angle of the analyzer rotation must be calculated when optical rotation is known.

2. PRINCIPLES

Arrangement of the optical components is shown in Fig.1.

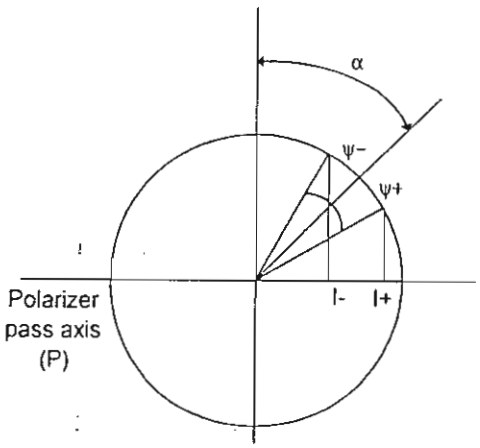

Fig. 1 Configuration of the polarizing components.

With application to contrast calculation ψ_- and ψ_+ are angles of the Faraday rotation of the plane of polarization of a linearly polarized light passed through two domains with opposite direction of the magnetization. α is an angle of analyzer

Lightmetry: Metrology, Spectroscopy, and Testing Techniques Using Light, Maksymilian Pluta, Editor,
Proceedings of SPIE Vol. 4517 (2001) © 2001 SPIE · 0277-786X/01/$15.00

pass axis orientation with respect to crossed axis of the polarizer. In measurements of the optical rotation with the half-shade analyzer $-\psi$ and $+\psi$ are angles between the passed axis of two parts of the analyzer and the cutting plane. α is an angle of the cutting plane of orientation of the half-shade analyzer with respect to the crossed orientation of the true direction of the polarization needed to be measured. The true properties of the half-shade analyzer can be calculated without specimen. and in this case α is angle of the analyzer cutting plane orientation with respect to crossed axis of the polarizer. In contrast measurement, the arrangement of optical system is polarizer, specimen, and then analyzer. The arrangement of optical rotation measurement is polarizer, specimen, and then the half-shade analyzer.

3. MATHEMATICAL MODEL AND RESULTS

To simplify the mathematical formulas we do not take into account the optical losses in the optical components and in the specimen. Because in precision measurements high quality polarizers are used and in practical measurements the angles α and ψ are small. in our model we use Malus' law with permanent residual light flux I_{ex} in extinction orientation of the polarizing components.

We illustrate our model by the example of the calculation the contrast of the magnetic domain structure. Intensity of the light passed through two domains with opposite direction of the magnetization I_- and I_+ are

$$I_- = I_{tr} \cdot \sin^2(\alpha - \psi) + I_{ex} \cdot \tag{1}$$

$$I_+ = I_{tr} \cdot \sin^2(\alpha + \psi) + I_{ex} \cdot \tag{2}$$

I_{tr} is the optical flux through the pass axis orientation of the polarizing components.

We defined contrast of the domains to be

$$K = \left| \frac{I_+ - I_-}{I_+ + I_-} \right| \tag{3}$$

Substituting (1) and (2) into (3) we get

$$K = \left| \frac{\sin 2\alpha \cdot \sin 2\psi}{\Delta - \cos 2\alpha \cdot \cos 2\psi} \right|, \tag{4}$$

where $\Delta = 1 + 2\varepsilon$ and $\varepsilon = I_{ex}/I_{tx}$ is the extinction ratio of the analyzer. To obtain the maximum contrast (K_m), we apply $\frac{\partial}{\partial \alpha} K = 0$, $\frac{\partial^2}{\partial \alpha^2} K > 0$. We get

$$K_m = \frac{|\sin 2\psi|}{\sqrt{\Delta^2 - \cos^2 2\psi}}. \tag{5}$$

This can be achieved with optimal angle α_{opt}

$$\alpha_{opt} = \frac{1}{2} \arccos \frac{\cos 2\psi}{\Delta}. \tag{6}$$

If $\alpha, \psi, \varepsilon << 1$, we obtain simple formulas:

$$K_m = \frac{\psi}{\sqrt{\psi^2 + \varepsilon}} \tag{7}$$

$$\alpha_{opt} = \sqrt{\psi^2 + \varepsilon} \tag{8}$$

Results of the contrast calculation according to equation (4) with rotation angle $\psi = 0.25°$ are shown in Fig. 2.

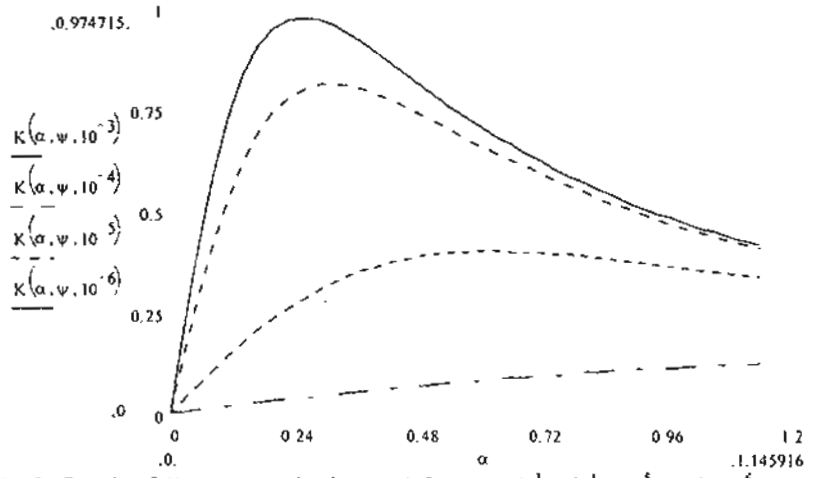

Fig. 2 Graph of K versus α (in degrees) for $\varepsilon = 10^{-3}$, 10^{-4}, 10^{-5}, and 10^{-6}, $\psi = 0.25°$

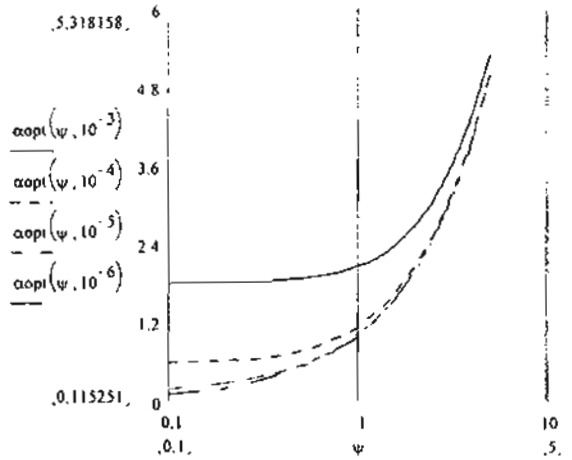

Fig. 3 Graph of α_{opt} (in degrees) versus ψ (in degrees) for $\varepsilon = 10^{-3}$, 10^{-4}, 10^{-5}, and 10^{-6}

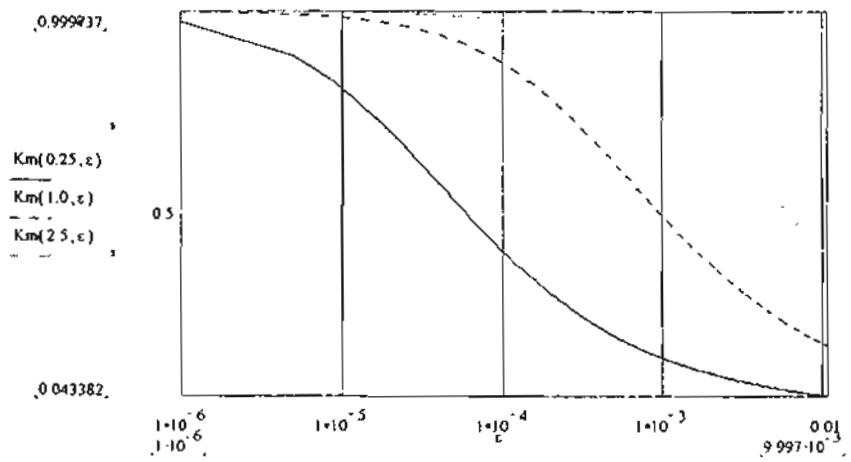

Fig. 4 Graph of K_m versus ε for $\psi = 0.25°$, 1°, and 2.5°

Fig. 2 shows that the high contrast of the image can be achieved only with high quality polarizing components when $\varepsilon < 10^{-4}$. The contrast K_m and the angle α_{opt} (see Fig. 3) decrease with the decreasing of the optical rotation ψ. Relative error of the contrast K_m and the optimal angle α_{opt} calculation using formulas (7) and (8) do not exceed 0.01 % up to the angle ψ of 30° compared to the calculation of equations (5) and (6). Note that the angles α and ψ appear in the equation (4) symmetrically.

Fig. 4 shows that the maximum contrast ratio of the image K_m decreases as ε increases for ψ = 0.25°, 1°, and 2.5°. This fact we use for investigation of the half-shade analyzer when K is the contrast on the comparison field, ψ is the cutting angle and α is angle of the half-shade analyzer orientation with respect to polarizer. Accuracy of measurements with half-shade analyzer depends on the cutting angle ψ, sensitivity of the reading system with angle α (30" in our experiment), and contrast sensitivity of the human eyes of 4%. Intensity at the detector is important with a low extinction ratio ε of 10^{-5} for α_{opt} = 0.31° and ψ = 0.25°, we get K_m = 81%, $I_-/I_{tr} = 1.109*10^{-5}$, and $I_+/I_{tr} = 1.055*10^{-4}$. In this case, loss of light is extremely large. For this reason, in practice, the half-shade analyzer has angle of ψ = 2.5° when α = 0.31°, we get $I_-/I_{tr} = 1.470264*10^{-3}$, $I_+/I_{tr} = 2.413362*10^{-3}$, and K = 24.3% (when K_m = 99.7%). The intensities will be at least 20 times more than the compared to the first case. When photodetectors are used sensitivity and accuracy of the polarimeter will be increased. Also, proposed model allows calculation of the optical losses in polarization arrangement using equations (1) and (2).

3.1 Optical loss

The practical experiment set up consists of polarized light source, a piece specimen i.e. thin magneto-optic film (see Fig. 3), analyzer, and a photodetector. Transmittance of a thin magneto-optic film exposed to magnetic fields with opposite magnetization direction is given by

$$T = [P I_+ + (1 - P) I_-]/I_0, \tag{9}$$

where P and $1-P$ are the areas with different intensities of the light transmitted by the oppositely magnetized domain. The total area is normalized to 1. The parameters I_- and I_+ are defined earlier in eq. (1) and (2). I_0 is the input light intensity (will be used in eqs. (1) and (2) instead of I_{tr}). For example, P = 0.5, ψ = 0.25°, α = 0.31°, and $\varepsilon = 10^{-5}$, we get $T = 2.054*10^{-5}$. Then, the optical loss can be calculated.

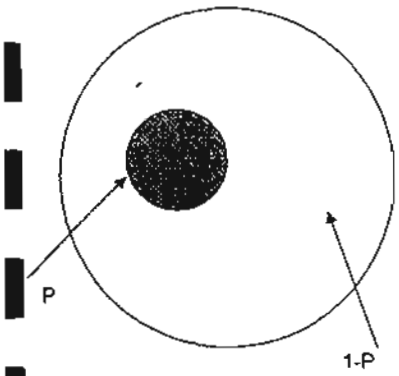

Fig.3 Configuration of the specimen: P and 1-P areas with different intensities of the light transmitted by the oppositely magnetized domain

To observe the contrast of the magnetic domain structure in magneto-optic thin film, applying magnetic field with opposite directions on the top and bottom of the film induces opposite magnetization directions on the film. The position of the domain wall changes with respect to the applied magnetic field. "Bright" and "dark" domains can be observed. We first measure

optical rotation with half-shade analyzer on specimen under saturation in the opposite magnetization directions. After we get the maximal contrast of the image, optimal orientation of the analyzer angle α_{opt} can be calculated using equations (6) or (8). In this case, ψ is the angle of Faraday rotation and the value of extinction ratio ε of the analyzer is required. Maximal contrast of the two domains can be measured directly by equation (3), if differential, summing, and divider circuits are used.

4. CONCLUSIONS

The mathematical model can be used with routine measurements with temperate accuracy. Equations (7) and (8) are useful for fast calculation of the contrast of the domain structure and optimal angle of the analyzer orientation. Parameters of the half-shade analyzer also can be calculated on the base of this mathematical model. In our experiments we first measure optical rotation with half-shade analyzer on specimen under saturation in the opposite directions. After we get the maximal contrast of the image, optimal orientation of the analyzer angle α can be calculated using equations (6) or (8). Maximal contrast of the two domains can be measured directly by equation (3), if differential, summing, and divider circuits are used.

5. ACKNOWLEDGEMENT

Funding was provided by Thai Research Foundation (TRF).

6. REFERENCES

1. A. Yariv, *Optoelectronics*, 4th ed., Saunder College Pub., 1991.
2. R. Azzam, "Division-of wave-front polarizing beam splitter and half-shade device using dielectric thin film on dielectric substrate,"in Appl. Opt., vol. 23, 1984.
3. Y. Didosyan, *et. al.*, "Magneto-Optical Current Sensor by Domain Wall Motion in Orthoferrites," IEEE Trans. instrum. & meas, Vol. 49, no. 1, Apr. 2000, pp. 14-18.

On behalf of the principal author (A.Andreev), Prinya Tantaswadi is delivering an oral introduction to their poster paper. Close to him, Andrei Lavrinenko (left) and V.V. Shkurko are sitting.

Appendix B.3

Reprint of

P. Tantaswadi, S. Maheshwari, and C. Tangtrongbenchasil "Study of current measurement error due to vibration in reciprocal fiber-optic polarimetric current sensor," *IEEE-PEDS 2001*, Oct. 2001, Bali, Indonesia, pp. 699-704.

Study of Current Measurement Error due to Vibration in Reciprocal Fiber-Optic Polarimetric Current Sensor

Prinya Tantaswadi, *Member, IEEE*, Charoen Tangtrongbenchasil, and Somna Maheshwari

***Abstract*-- We present a mathematical model for investigating vibration effects on reciprocal fiber-optic polarimetric current sensor. The model will aid in designing a configuration with immunity to environmental (acoustic) perturbations. The perturbations affect birefringence properties of single-mode sensing fiber and cause current measurement error.**

***Index Terms*--Current measurement, fiber-optic current sensors, simulation and modeling, vibrations.**

I. INTRODUCTION

FIBER-OPTIC current sensors, which rely on magneto-optic Faraday effect and Ampere's law, have been received considerable attention for possible application in electric power industry as magneto-optic current transformers (MOCT) in the past few decades [1]-[9]. These MOCTs inherently have several potential advantages over conventional ferromagnetic current transformers (CTs). These include flat bandwidth response (DC to several MHz), wide linear dynamic range (more than five orders of magnitude), no hysteresis, and by proper design insensitivity to electro-magnetic interference (EMI) and radio frequency interference (RFI) owing to their all-dielectric structure of fiber optics. Other advantages include smaller size, and consequently lighter weight; making installation easier. Finally, they are completely immune from catastrophic explosive failures, where as iron-core CTs are not [3].

Several approaches of Faraday-based current sensors have been demonstrated. Although fiber-optic current sensors have several advantages over conventional CTs, they have yet to overcome undesirable susceptibility to environmental perturbations, *i.e.* temperature and acoustic perturbations, in the sensing part [7]-[8]. One approach uses unidirectional polarimetric technique. This method of current sensing detects the intensity change due to polarization rotation from the induced magnetic field generated by current. The accuracy of this sensing method suffers from both linear and circular birefringence in the sensing fiber. To counter the birefringence errors, a reciprocal polarimetric type current sensor has been developed. The perturbations affect the birefringence property of the fiber in the sensing part. Unidirectional polarimetric current sensors suffer from environmental perturbations due to varying birefringence in the sensing part [8],[9]. This results in false current readings from environmental perturbations.

In this paper, we analyze the performance of a reciprocal fiber optic current sensor including the output state of polarization, normalized contrast ratio, and effects of vibration on the sensor. The accuracy of the sensor is within 0.3% of the actual value and satisfies application in revenue metering.

II. PRINCIPLES

When light propagates in an optical fiber wound around a current carrying wire (see Fig. 1), the induced magnetic field causes a rotation of the linear polarization plane of lightwave by the magneto-optic Faraday effect. This angle of rotation, $\Delta\phi$, through which the plane of polarization rotates, is given by

$$\Delta\phi = V\oint_C \vec{H}\cdot d\vec{l}\ , \tag{1}$$

where V is the Verdet constant of the optical fiber, $\vec{H}$ is the magnetic field intensity along the direction of light propagation, and l is the optical path along the fiber loop. From Ampere's law, this closed loop integral of magnetic field around a wire is proportional the current, I, flowing through it, *i.e.*

$$I = \oint_C \vec{H}\cdot d\vec{l}\ . \tag{2}$$

Therefore, the angle of rotation, $\Delta\phi$, in the fiber loop configuration is given by

$$\Delta\phi = VNI\ , \tag{3}$$

where N is the integral number of turns of fiber wrapped around the current carrying wire. The stability of Faraday rotation based current sensors, through the Verdet constant, depends on source wavelength and temperature. For example, the operating wavelength λ is 633 nm and the Verdet constant V is 4.68 $\mu rad/$ A.

To measure current I, with constant N and V, we can use a polarimetric sensor to measure $\Delta\phi$. In conventional

This work was supported by Thailand Research Funds under Grant No. TRF: RSA/06/2541.

Dr. Prinya Tantaswadi, Mr. Charoen Tangtrongbenchasil, and Mrs. Somna Maheshwari are with Sirindhorn International Institute of Technology, Thammasat University, School of Electrical Engineering and Information Technology, PO Box 22, Thammasat Rangsit Post Office, Pathumthani 12121,THAILAND (telephone: 662-986-9009 ext. 1805, fax: 662-986-9113, e-mail: prinya@siit.tu.ac.th)

0-7803-7233-6/01/$10.00 ©2001 IEEE.

unidirectional polarimetric current sensors, a linearly polarized light is launched into a single-mode sensing fiber and the output polarization is analyzed by a Wollaston prism for evaluation of the current and static linear birefringence [4],[5]. In practice, the propagation of light through the fiber loop exhibiting additional linear birefringence due to bending and twist-induced circular birefringence can be described by Jones calculus (see next section). These birefringences affect the accuracy and sensitivity to environmental perturbations *i.e.* temperature and vibrations of the sensor. Reciprocal fiber-optic current sensors (see Fig. 1) interrogate the light in both directions. Since linear and twist-induced birefringences exhibit reciprocal characteristics, the reciprocal rotation of these birefringences cancels when light propagates along and is back-reflected down a fiber. The Faraday magneto-optic effect exhibits nonreciprocal characteristics, the Faraday rotation doubles when light propagates along and is back-reflected down a fiber. Thus, this optical circuit has the advantage of minimizing the birefringence induced offset problems associated with the unidirectional polarimetric current sensor.

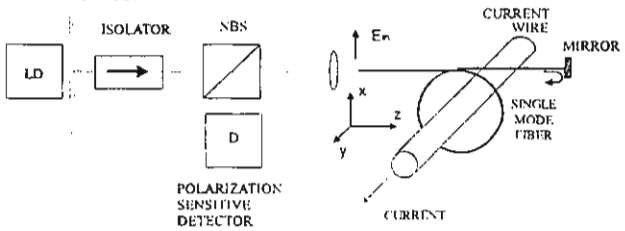

Fig. 1. Reciprocal fiber-optic polarimetric current sensor, LD: laser diodes, NBS: non-polarizing beam splitter.

III. State of Polarizations (SOP)

To analyze the performance of the sensor, we first look at the sensor's output state of polarization. The output electric field (E_{out}) of the sensor can be described by the Jones matrix [1],[2]:

$$E_{out} = \frac{1}{2}\tilde{L}\cdot M\cdot \vec{L}\cdot E_{in}. \tag{4}$$

where E_{in} represent input linearly polarized light in the x axis

$$(i.e.\ E_{in} = \begin{bmatrix} E_x = 1 \\ E_y = 0 \end{bmatrix} = \begin{bmatrix} 1 \\ 0 \end{bmatrix}).$$

$\vec{L}$ represents a sensing fiber matrix when light propagating forward (from left-to-right in Fig. 1).

$\tilde{L}$ represents a sensing fiber matrix when light propagating backward (from right-to-left), and M is the Jones matrix of the mirror.

$$\vec{L} = \begin{bmatrix} A & -B \\ B & A^* \end{bmatrix}, \tag{5}$$

where

$$A = \cos\frac{\alpha}{2} + j\sin\frac{\alpha}{2}\cos(\chi), \tag{6}$$

$$B = \sin\frac{\alpha}{2}\sin(\chi), \tag{7}$$

$$\frac{\alpha}{2} = \sqrt{(VNI+T)^2 + (\frac{\delta}{2})^2} \tag{8}$$

and $\tan\chi = 2(VNI+T)/\delta$. . (9)

The VNI is the Faraday rotation induced by current and T is the circular birefringence. δ represents total linear birefringence. α represents the total birefringence. Assume both the total linear and circular birefringence to be uniformly distributed along the single-mode fiber optic sensing part.

$$\tilde{L} = \begin{bmatrix} C & -D \\ D & C^* \end{bmatrix}, \tag{10}$$

where

$$C = \cos\frac{\beta}{2} + j\sin\frac{\beta}{2}\cos(\zeta), \tag{11}$$

$$D = \sin\frac{\beta}{2}\sin(\zeta). \tag{12}$$

$$\frac{\beta}{2} = \sqrt{(VNI-T)^2 + (\frac{\delta}{2})^2}. \tag{13}$$

and $\tan\zeta = 2(VNI-T)/\delta$. (14)

$$M = \begin{bmatrix} 1 & 0 \\ 0 & 1 \end{bmatrix}. \tag{15}$$

With linearly polarized input at the birefringence axis of sensing fiber, the normalized output electric field using (4), (5), (10), and (15) can be described by

$$E_x = AC - BD = a_1\exp(j\delta_x). \tag{16}$$

$$E_y = AD + BC^* = a_2\exp(j\delta_y). \tag{17}$$

where a_1, δ_x, a_2, and δ_y are the amplitude and phase of the electric field in the x- and y- axis, respectively.

The output state of polarization can be expressed on the Poincaré sphere (S_1, S_2, S_3) [10],[11]

$$S_1 = a_1^2 - a_2^2, \tag{18.1}$$

$$S_2 = 2a_1 a_2\cos(\delta_x - \delta_y). \tag{18.2}$$

and $S_3 = 2a_1 a_2\sin(\delta_x - \delta_y)$. (18.3)

In this Poincaré sphere, the state of polarization can be plotted on the surface of a sphere. Right circular polarization is on the North Pole, left circular on the South Pole, linear polarization on the equator, and elliptical polarization in between [10],[11]. With input light aligned to birefringence axis of the sensing fiber, in an ideal fiber ($\delta, T \approx 0$), we would expect only Faraday rotation to occur. In this sensor, the rotation angle is $2VNI$. This is due to the fact that Faraday rotation is VNI in the forward direction down the fiber and, by nonreciprocal effect of Faraday effect, additional Faraday rotation is VNI in the backward direction down the same fiber.

Thus, the total Faraday rotation of $2VNI$ occurs in the sensor. Assume that the input light is linearly polarized in the x-axis or vertical direction. It is (1,0,0) on Poincaré sphere or a dot shown in Fig. 2. In Fig. 2 (a), the Faraday rotation angle of $2VNI$ will be equivalent to $4VNI$ along the equator (angle on the sphere is twice as much as the angular rotation and output is still linearly polarized). For example, the VNI of 0.01 π radians produces 0.04 π radians of rotation along the equator [see Fig. 8(a)]. The characteristic curve of a practical case (δ = 2 π and T = 120 π radians or $\delta/2T = 0.83\%$) is shown in Fig. 2 (b). It is similar to the ideal case but with a very small deviation from the equator. The deviation from the ideal case produces some small susceptibility to varying birefringence and will be demonstrated in the next section. Fig. 2 (c) with thin line for δ = π/6 and T = 0 and thick line: δ = π/2 and T = π ($\delta/2T = 25\%$) shows that the sensor is not practical for current sensing when T does not dominate δ or $\delta/2T$ is not small. Fig. 2 (b) shows that the desired response, which is close to that of the ideal one in Fig. 2(a), can be obtained by large T or $\delta/2T \ll 1$. The characteristic curve evolves around the equator (see Fig. 2 (a) and (b)).

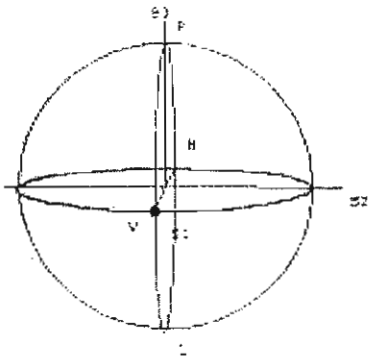

(a)

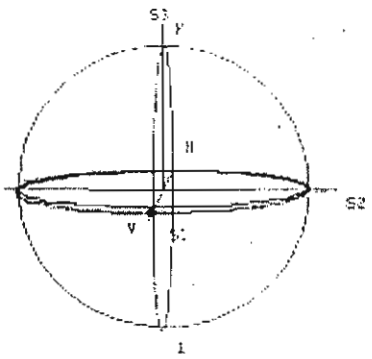

(b)

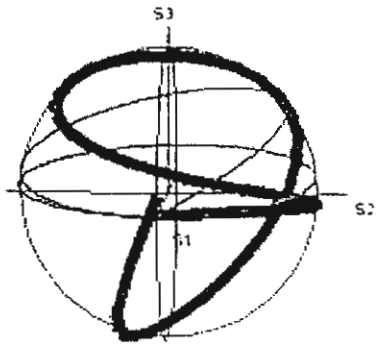

(c)

Fig. 2. Characteristic curves of the output polarization on the Poincaré sphere for VNI = 0 to π radians for (a) ideal case: δ = 0 and T = 0 (b) δ = 2 π and T = 120 π radians (c) the thin line: δ = π/6 and T = 0 and the thick line: δ = π/2 and T = π radians

IV. Analytical Descriptions of The Normalized Contrast Ratio (K)

The Wollaston prism is aligned 45° and –45 ° to the birefringence axis of the output end of the sensing fiber. The contrast ratio (K) is defined by

$$K = \frac{I_{xo} - I_{yo}}{I_{xo} + I_{yo}}. \tag{19}$$

where I_{xO} and I_{yO} are the intensity at 45° and –45 ° with respect to the birefringence fast axis of the output end of the sensing fiber, respectively. We can derive (19) using (4) to (15). Then, the contrast ratio (K) is given by

$$K = Sin(\alpha)Cos(\beta)Sin(\chi) + \frac{Sin\beta}{2}[Sin(2\chi - \zeta)(Cos\alpha - 1) + Sin\zeta\,(Cos\alpha + 1)] \tag{20}$$

Ideal case, T and δ are very small and negligible (such that $T, \delta \approx 0$). Equation (20) becomes

$$K = K_{ideal} = Sin(4VNI) \tag{21}$$

K provides the measurement of current and is linear ($K = Sin(4VNI) \approx 4VNI$) up to few tenths of a radian, or about 10^5 Amperes for a one-turn sensing coil. K is independent of the circular and linear birefringence in the sensing fiber. However, in practice, the use of high circular birefringence T or "spun" fiber ($VNI, \delta << T$) can overcome the intrinsic linear birefringence. To understand the performance of the sensor, we show the characteristic plot of the deviation of K, which is defined by,

$$\Delta K(\%) = \frac{(K - K_{ideal})}{K_{ideal}} \times 100\% \tag{22}$$

as a function of linear birefringence (δ) and twist-induced circular birefringence (T) (see Fig. 3). The VNI is assumed to be 0.01π and the expected value of K_{ideal} from (21) is 0.125333. Fig. 3 shows the case when T is large and

$\delta/2T \ll 1$. The sensor shows reduced sensitivity to vibration significantly compared to that of the one-way "unidirectional" polarimetric sensor [8],[9].

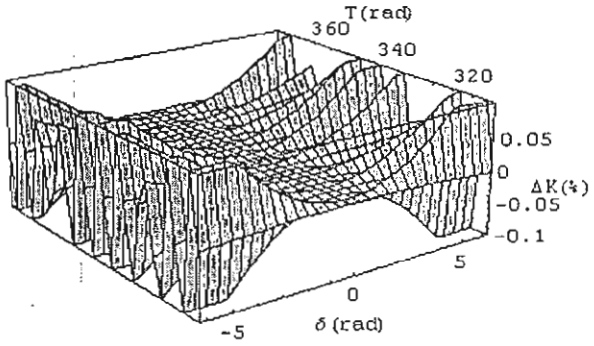

Fig. 3 The deviation of K (ΔK) as a function of linear birefringence (δ) and twisted circular birefringence (T)

The required intrinsic circular birefringence may be obtained by spun high birefringence fiber, twisted low birefringence fiber or winding low birefringence fiber in a toroidal geometry (see Fig. 4) [6],[7]. In the toroidal configuration, which we use in our simulation, T is about 120 π and δ is about a few π radians.

A. Mathematical Descriptions of Linear Birefringence Vs Vibration

There are two sources of linear birefringence in the sensing fiber: bending-induced linear birefringence (δ) and vibration-induced linear birefringence caused by transverse strain or vibration (δ_v), which can be described by [12]

$$\delta_v = 2\pi/\lambda \, \Delta n \, l, \tag{23}$$

where Δn is the refractive index change induced by stress in the medium (silica in this case), l is the effective length (under perturbation) of fiber, and λ is the center wavelength of the source. The refractive index change is given by

$$\Delta n = -n^3/2 \, p\sigma = 0.311\sigma, \tag{24}$$

where n is the (unperturbed) refractive index of medium, σ is the strain, and p is the photoelastic constant of fiber (p = 0.2 in silica). Value of the Faraday rotation (VNI) depends on the Verdet constant (V). Typical value of V is 4.68 *μrad/* A or 0.268°/(kA). In our case, we wrap the sensing fiber around an acrylic torus (see Fig. 4) so that the bend-induced linear birefringence is about a few π radians and a large twist-induced birefringence is about 120 π radians. As a result, the conditions of $\delta/2T \ll 1$ and $VNI \ll \delta \ll T$ are satisfied [6],[7]. Because the vibration affects linear birefringence, to induce a π-radian birefringence change

$\Delta n = \lambda/2 = 3.165\times10^{-7}$ for a fiber length of 1 m. We can find the strain of 1.019×10^{-6} using (24). Reference [9] shows that δ_v in unidirectional polarimetric current sensor of 0.2 *rad* results in an apparent current of several hundred Amperes. In the following sections we will assume that δ_v changes by 0.2 π *rad* (a few times larger than 0.2 *rad*) between – 0.1 π and 0.1 π from the static bend-induced linear birefringence δ (assumed to be 1.9 π radians).

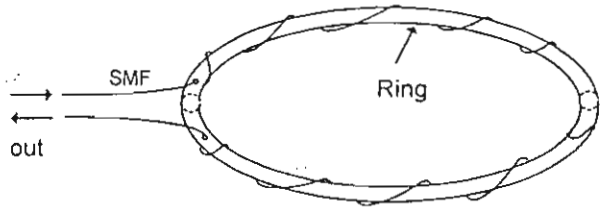

Fig. 4 The schematic of winding sensing fiber around a torus (with outside diameter of 45 cm) in order to add a large amount of circular birefringence, SMF: single-mode fiber. The torus has a cross section diameter of about 2 cm

In this sensor, Fig. 5 shows that the deviation of K in percent is within 0.10% of the ideal case ($T, \delta \approx 0$) when the range of the linear birefringence and circular birefringence are (1.8 π, 2.0 π) and (119.5 π, 120.5 π) radians, respectively.

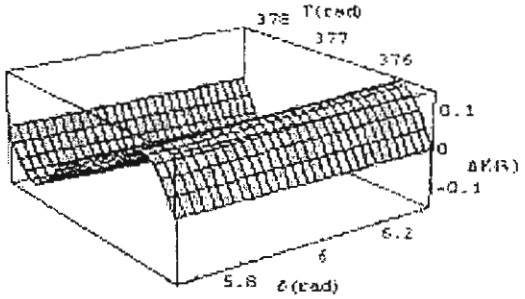

Fig. 5 In case of birefringence changes due to vibration, the deviation of K (ΔK) when VNI = 0.01 π radians as a function of linear birefringence (δ is between 1.8 π and 2.0 π radians) and circular birefringence (T is between 119.5 π and 120.5 π radians).

B. Deviation of K (ΔK) Vs Linear Birefringence

This sensor exhibits small dependence on linear birefringence. Fig. 6 shows that the absolute value of the deviation of K in percent is below 0.007% when δ is less than 2 π radians when $VNI = 0.01\pi$ and T = 120 π radians. In this case, the approximation of K is

$Sin(4VNI)[1-1.750\times10^{-4}\delta^2] = 0.125333[1-1.750\times10^{-4}\delta^2]$.

Using (22), $\Delta K(\%)$ is given by

$$|\Delta K(\%)| = 1.750\times10^{-4}\delta^2. \tag{25}$$

Maximum δ to achieve the accuracy of 0.3% for revenue metering application from (25) is 13.18 π *rad*.

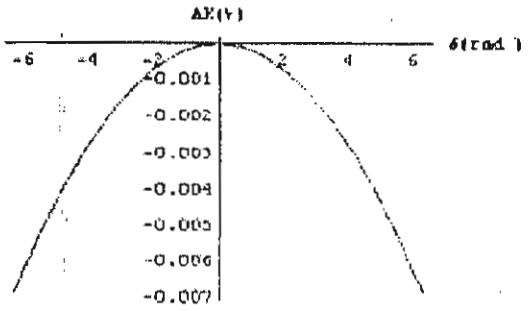

Fig.6 Simulated deviation of K in percent varies with linear birefringence ($VNI = 0.01\pi$, $T = 120\pi$)

C. *Apparent current Vs Linear Birefringence*

Environmental acoustic perturbations and mechanical vibration on the sensing fiber can cause angular rotation of lightwave polarization and may affect birefringence property of the sensing fiber [6]-[9],[12]. The result could be misread as actual current. Reference [8] shows that mechanical vibrations with a magnitude of 3.0 g_{p-p} ($1g = 9.8m/s^2$) applied to a sensing fiber of unidirectional polarimetric sensor can cause an apparent current of 400 A_{p-p}. Simulated apparent current ($T = 120\ \pi, \delta_v = 0.1\pi \sin(2\pi f_v t)$, and the total linear birefringence is assumed to vary between 1.8π and 2.0π radians) for this sensor is shown in Fig. 7. The frequency of vibration or varying linear birefringence (f_v) is chosen to be 50 Hz, which is common to electric power systems [8]. Very small apparent currents of less than 2.0×10^{-5} Amperes for 633 nm wavelength when the total linear birefringence δ is (1.8π, 2.0π) radians and theδ_v is shown in Fig. 7(a).

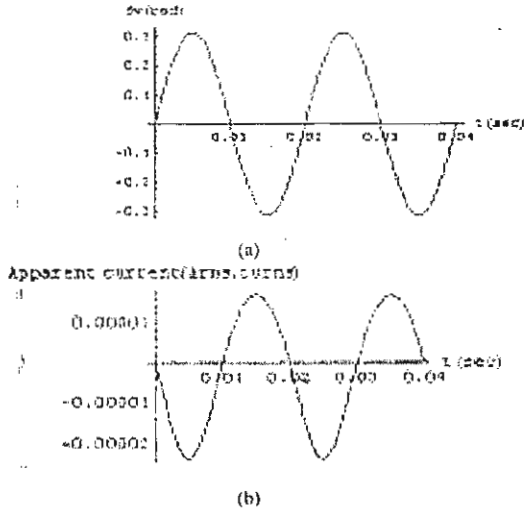

(a)

(b)

Fig.7 Simulated apparent current (b) in Amperes.turns Vs birefringence (a) ($VNI = 0$ and $T = 120\pi$)

V. Mathematical Model and State of Polarization

Reference [9] shows that the linear birefringence change due to vibration of 0.2 radians can induce a large apparent current (equivalent to several hundred A_{p-p}) in unidirectional polarimetric current sensor. However, Fig. 5 indicates that when both δ and T change as much as 0.2 π (many times larger than 0.2 radians) and 1 π radians, respectively, the ΔK or accuracy of the sensor is within 0.1% (0.3% is required for revenue metering). Fig. 8 shows the two cases when δ and T change due to vibration and the current is applied ($VNI = 0.01\ \pi$) to the sensor. The dot and small line in Fig. 8 represent the SOP under vibration when δ and T change, respectively.

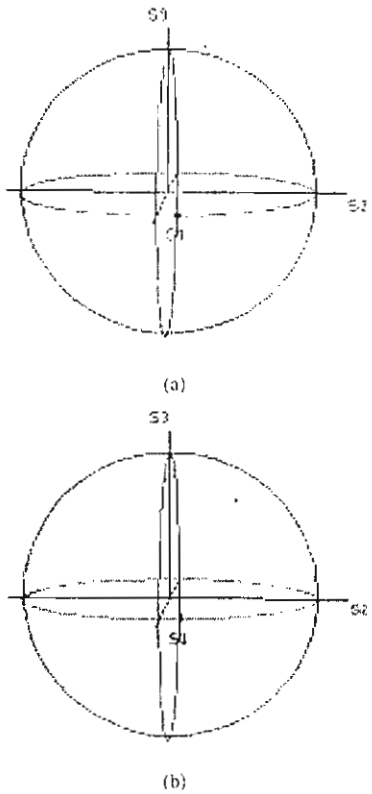

(a)

(b)

Fig. 8 State of polarization of the output of sensor with vibration on the Poincaré sphere $VNI = 0.01\ \pi$ (a) linear birefringence (δ is between 1.8 π and 2.0 π radians) $T = 120\ \pi$ (b) twisted circular birefringence (T is between 119.5 π and 120.5 π radians) $\delta = 2\ \pi$ radians.

VI. Discussion and Conclusion

The mathematical model of reciprocal fiber-optic current sensor is demonstrated. The performance of the current sensor is similar to that of the ideal case ($\delta, T \approx 0$). This can be shown by the state of polarization of the sensor output when $\delta/_{2T}$ is small (T dominates δ and VNI). To satisfy the conditions of $\delta/_{2T} \ll 1$ and $VNI \ll \delta \ll T$ helical winding on a acrylic torus is used. We can find the normalized contrast ratio K being affected by unwanted changes in linear birefringence δ caused by acoustic perturbations and mechanical vibrations and circular birefringence T. For large T, deviation of K (%) is a quadratic function of δ but the contribution of perturbations and vibrations is small and within 0.1% (0.3% of the actual value required for applications in

revenue metering). The apparent current shows that the susceptibility of sensor to varying linear birefringence is small and negligible.

ACKNOWLEDGMENT

The authors would like to thank Dr. James N. Blake of Nxtphase, USA, Prof. Alan J. Rogers of University of Surrey, UK, and Assoc. Prof. Dr. Pichet Limsuwan of King Mongkut's University of Technology, Thonburi for help and fruitful discussions. Also, the authors would like to thank Mr. Parvich Tokakuna, Ms. Phanraphee Bunphalamlert, and Mr. Yodtao Yodying for their assistance in "Mathematica" programming.

REFERENCES

[1] Tabor and Chen, "Electromagnetic propagation through materials possessing both Faraday rotation and birefringence: experiments with Ytterrbium Orthoferrite," *J. Appl. Phys.*, vol. 40, no. 7, pp. 2760, 1969.

[2] A. Smith, "Polarization and magnetooptic properties of single-mode optical fibre," *Appl. Opt.*, vol. 17, no 52, 1978.

[3] T. Cease, S. Weikel, and J. Driggans, "Optical voltage and current sensor used in revenue metering system," *IEEE Trans. On Power Delivery*, vol. 6, no. 4, pp. 1374-79, Oct. 1991.

[4] Z. Ren, *et al.*, "Discrimination between linear birefringence and Faraday rotation in optical fiber current sensors by polarization multiplexing," *SPIE Proc.*, vol. 1169, Fiber Optic and Laser Sensors VII, pp. 226-232, 1989.

[5] P. Menke and T. Bosselmann "Temperature Compensation in Magnetooptic AC Current Sensors Using an Intelligent AC-DC Signal Evaluation," *IEEE J. Lightwave Technol.*, vol. 13, no. 7, pp. 1362-70, 1995.

[6] A. Roger, *et al.*, "Vibration immunity for optical fiber current measurement," *IEEE J. Lightwave Technol.*, vol. 13, no. 7, pp. 1371-77, 1995.

[7] S. Short, *et al.*, "Elimination of Birefringence Induced Scale Factor Errors in the In-Line Sagnac Interferometer Current Sensor," *IEEE J. Lightwave Technol.*, vol. 16, no. 10, pp. 1844-50, 1998.

[8] S. Short, P. Tantaswadi, R. de Carvalho, B. Russel, and J. Blake, " Environmental sensitivity comparison of in-line Sagnac and polarimetric type current sensor," *IEEE Trans. Power Delivery*, vol. 11, no. 4, pp. 1702-06, 1996.

[9] P. Tantaswadi and S. Maheshwari, "Vibration sensitivity in unidirectional polarimetric current sensor," *J. Sci. Asia*, submitted for publication.

[10] M. Born and E. Wolf, *Principles of Optic*, 6th ed., Oxford: Pergamon, 1980.

[11] S. Carrara, "Drift reduction in optical fiber gyroscopes," Ph.D. dissertation, Stanford University, CA, 1988.

[12] A. Rogers, "Optical Fiber Current Measurement," in *Optical Fiber Sensor Technology*, vol. I, K. Grattan and B. Meggit, Eds., Chapman & Hall, 1995, pp. 432-38.

Appendix B.4

Reprint of

P. Tantaswadi, S. Maheshwari, and C. Tangtrongbenchasil "Experimental study of vibration sensitivity in unidirectional polarimetric current sensors," *Int. Symp. on Opt. and Quantum Tech.* (ISOQT), Dec. 2001, KMITL, Bangkok, pp. 94-99.

1st ISOQT

1st INTERNATIONAL SYMPOSIUM ON
OPTICAL AND QUANTUM TECHNOLOGY

7-8 December, 2001
Department of Applied Physics
Faculty of Science, KMITL, Bangkok.

Sponsored by

King Mongkut's Institute of Technology Ladkrabang
Bangkok,Thailand.

Ministry of University Affairs
Thailand.

and

The Abdus Salam International Centre For Theoretical Physics
Trieste, Italy

Organized by

Faculty of Science, KMITL, Bangkok, Thailand

Experimental Study of Vibration Sensitivity in Unidirectional Polarimetric Current Sensors

P. Tantaswadi, S. Maheshwari, and C. Tangtrongbenchasil
Sirindhorn International Institute of Technology, Thammasat University,
School of Electrical Engineering and Information Technology,
PO Box 22,Thammasat Rangsit Post Office, Pathumthani 12121

Abstract

Accuracy of current measurement in optical fiber current sensor is affected by the environment perturbations to the sensing fiber such as mechanical vibrations, acoustic perturbations, and temperature changes. This paper presents the experimental study of the effect of mechanical vibrations on the current measurement error. Results show that current measurement error varies linearly with the amplitude of vibration. We also develop a novel mathematical model for vibration sensitivity in unidirectional polarimetric current sensors. In this paper, we believe that it is the first time that the effect of vibration to the single-mode-sensing fiber on the current measurement error in fiber optic polarimetric current sensor is formulated. Simulation results agree well with the experimental results.

Keywords: current sensor, polarimetry

1. INTRODUCTION

Fiber-optic current sensors have received considerable attention for possible application in electric power industry as magneto-optic current transformers (MOCTs) [1]-[5]. These MOCTs inherently have several potential advantages over conventional ferromagnetic current transformers (CTs) like flat bandwidth response (DC to several MHz), wide linear dynamic range (more than five orders of magnitude), no hysteresis, insensitive to EMI and RFI owing to their all-dielectric structure. smaller size, lighter weight, easy installation, immune to catastrophic explosive failures [1].

In practice the current sensors are invariably exposed to acoustic vibrations [2]-[4]. Vibration change the linear birefringence (δ) in the sensing coil of fiber which in turn changes the evolution of the state of polarization of the light through the sensing coil.

In this paper a general mathematical model of vibration sensitivity due to birefringence effect in sensing part in unidirectional polarimetric is presented. Corroborating experimental results are also presented.

2. PRINCIPLES

When plane polarized light propagates in an optical fiber wound around a current carrying wire, the induced magnetic field causes a rotation of the linear polarization plane of lightwave by the magneto-optic Faraday effect. This angle of Faraday rotation, F, is given by $F = VNI$, (1)
where V is the Verdet constant of the optical fiber, N is the integral number of turns of fiber , I is the current through the wire. The Verdet constant depends on source wavelength and temperature. For example, the operating wavelength λ is 633 nm and the Verdet constant V is 4.68 $\mu rad/ A_{rms}$.

In Eq (1) to measure current I, with constants N and V, we need to measure Faraday rotation, F, for which we can use a unidirectional polarimeter sensor shown in Figure 1. It consists of input linear polarized electric field (E_{in}) entering the sensing fiber loop, an analyzer aligned θ degrees with respect to the birefringence fast axis of the fiber loop, and a detector.

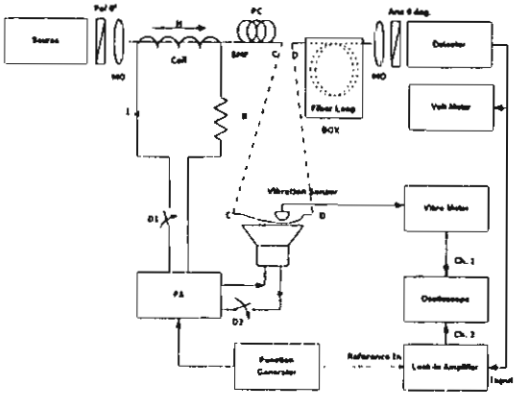

Figure 1 Unidirectional polarimetric current sensor and its experimental set-up, MO: microscope objective lens, SMF: single-mode fiber, PC: polarization controller, Ana: analyzer, PA: power amplifier

In our experiment, we align the analyzer with θ of 60°, where the output signal-to-noise ratio (SNR) is better than that at θ of 45°, where the sensitivity of the sensor is maximum. A normalized intensity at output ($Intensity \propto |E_{out}|^2$) of the detector is given by [2]

$$\frac{I_{60^\circ}}{I_0} = \frac{1}{4} + \frac{\sqrt{3}}{2}\frac{\sin\left(\sqrt{4(F+T)^2+\delta^2}\right)}{\sqrt{4(F+T)^2+\delta^2}}\cdot(F+T) + \left[1-\cos\left(\sqrt{4(F+T)^2+\delta^2}\right)\right]\cdot\frac{(F+T)^2}{4(F+T)^2+\delta^2}, \quad (2)$$

where E_{out} is the output electric field and I_0 is the maximum intensity at the detector. δ, F, T, and α are the linear birefringence, Faraday rotation, twist-induced (circular) birefringence, and total birefringence in radians.

2.1 Current measurement

For an ideal fiber (δ, T=0) Eq (2) becomes

$$\frac{I_{60^\circ}}{I_0} = \frac{1}{2}\left[1+\sin(2F-30^\circ)\right] \quad (3)$$

In Eq (3) when no current is applied (F=0) the output is constant. When AC current ($I(t) = A\sin\omega t$) is applied (where A is zero-to-peak amplitude in Ampere), F can be described by

$$F(t) = V\,N\,I(t) = (VNA)\sin\omega t = F_0\sin\omega t \quad (4)$$

$F_0 = VNA$ is a constant. Substituting Eq (4) into (3), we obtain the phase modulation signal at detector's output.

$$v_D = \frac{K}{2}\left[1+\sin(2F_0\sin\omega t - 30^\circ)\right], \quad (5)$$

where K is the maximum output voltage at the detector. For very small value of F_0 Eq (3) can be approximated by [2]

$$v_D(t) = v_{DC} + v_{AC}(t) \approx v_{DC} + v_{(0-p)}\sin(\omega t) = \frac{K}{2}\left[1+2\sqrt{3}F_0\sin(\omega t)\right] \quad (6)$$

When F_0 is small and less than 0.04 radian, detector voltage $v_{(0-p)}$ is linear proportional to the applied current amplitude (A) as given by $V_{(0-p)} \propto 2\sqrt{3}F_0$.

2.2 Signal Modulation

Current measurement can be found by a ratio of $v_{(0-p)}$ to v_{DC}, which is known as "signal modulation." Thus signal modulation using Eq (6) is given by

$$\frac{v_{(0-p)}}{v_{DC}} = 2\sqrt{3}F_0 = 2\sqrt{3}VNA \quad (7)$$

The sensor output is linear up to 0.04 rad ($\sin(x) \approx x$, when $x < 0.04\,rad$) or about 8,500A_{rms} ($.04rad/\ V = 4.68\times10^{-6}\,rad$ for wavelength of 633 nm). If the applied current is 1000 A_{rms} the signal modulation using Eq (7) will be $1.62\text{x}10^{-2}$. In practice, δ is not negligible but T is e.g. δ = 0.660 and T = 0.05 radians. When the applied current is 1,000 A_{rms}, the signal modulation using Eq (2) and (6) is $1.378\text{x}10^{-2}$. Scale factor of the sensor is defined by $SF = \frac{\text{signal modulation (in experiment)}}{\text{signal modulation of the ideal case}}$.

In this case, the scale factor SF is 0.85.

3. MATHEMATICAL MODELING OF LINEAR BIREFRINGENCE CHANGE Vs VIBRATION (11)

We consider the linear birefringence in the sensing fiber being composed of bending-induced linear birefringence (δ_{DC}) and vibration-induced linear birefringence(δ_v). Vibration induced linear birefringence is caused by transverse strain or vibration [3]

$$\delta_v = {}^{2\pi}/_{\lambda}\,\Delta n\, l, \quad (8)$$

where Δn is the refractive index change induced by stress in the medium (silica in this case), l is the effective length (under perturbation) of fiber, and λ is the center

wavelength of the source. The refractive index change is given by $\Delta n = -n^3/2\, p\sigma = 0.311\sigma$, where n is the (unperturbed) refractive index of medium, σ is the strain and p is the photoelastic constant of fiber (p = 0.2 in silica). The (static) bending-induced birefringence (δ_{DC}) per turn of a fiber loop with radius R under no tension can be described by [3]

$$\delta_{DC} \approx \frac{0.6\pi}{R} \ ^{o}/\text{turn}. \qquad (10)$$

In our case, R of 0.3 m results in δ_{DC} of 6.3 °/turn. Six turns of fiber loop result in δ_{DC} of 37.8°.In our case, R of 0.3 m results in δ_{DC} of 6.3 °/turn. Six turns of fiber loop result in δ_{DC} of 37.8°.

We assume that (total) linear birefringence (δ) in single-mode sensing part is the algebraic sum of the (static) bending-induced linear birefringence and vibration-induced linear birefringence.

$$\delta = \delta_{DC} + \delta_v \sin(\omega_v t), \qquad (11)$$

where $\omega_v = 2\pi f_v$ and f_v is the frequency of the vibration δ_v and T is much smaller than δ_{DC} in our configuration.

3.1 Current measurement error due to vibrations

In this section we formulate a mathematical model of the vibration sensitivity. In Eq (2), if no current (F = 0) and no vibration are applied (and assume that the δ_{DC} and T are constant), the output should be constant. However when the vibration is present it perturbs the linear birefringence and modulates the angular rotation, which is not distinguishable from that of the Faraday rotation (F). Substituting Eq (11) into (2), we obtain a phase modulation signal even at no applied current. It is named apparent current or false current and is given by

$$\frac{I_{ac}}{I_o} = \frac{1}{4} + \frac{\sqrt{3}}{2}\frac{\sin\left(\sqrt{4T^2 + (\delta_{DC} + \delta_v \sin\omega_v t)^2}\right)}{\sqrt{4T^2 + (\delta_{DC} + \delta_v \sin\omega_v t)^2}} \cdot T + \left[1 - \cos\left(\sqrt{4T^2 + (\delta_{DC} + \delta_v \sin\omega_v t)^2}\right)\right] \cdot \frac{T^2}{4T^2 + (\delta_{DC} + \delta_v \sin\omega_v t)^2} \qquad (12)$$

The value of δ_V is assumed to vary linearly with the mechanical vibration and thus signal modulation varies with the same frequency When $2T, \delta_v \ll \delta_{DC}$, Eq (12) becomes (9)

$$\frac{I_{ac}}{I_o} = \frac{1}{4} + \frac{\sqrt{3}}{2}\frac{\sin(\delta_{DC} + \delta_v \sin\omega_v t)}{\delta_{DC} + \delta_v \sin\omega_v t} \cdot T + [1 - \cos(\delta_{DC} + \delta_v \sin\omega_v t)] \cdot \frac{T^2}{(\delta_{DC} + \delta_v \sin\omega_v t)^2} \qquad (13)$$

3.2 Simulated false current due to vibrations

Using Eq (13), it is shown in Figure 2 that for small vibration of single-frequency, the signal modulation varies linearly with δ_v and has the same frequency as that of the vibration.

4. EXPERIMENTAL SETUP AND RESULTS

The sensor depicted in Figure 1 was built. A wire coil with 1000 turns to simulate large value of current was used as the current carrying conductor. It was wrapped around one turn of sensing fiber The optical source was a HeNe laser with 20 mW of output optical power at operating wavelength of 633 nm. A single-mode fiber manufactured by 3M was employed. Fiber polarization controller (PC) was used prior to the single-mode fiber loop (with a radius of 30 cm to simulate the sensing part) in order to launch the linearly polarization into the linear birefringence (fast) axis of the sensing fiber. The analyzer was aligned 60° to the angle with maximum output intensity (fast axis of the fiber end).

4.1 Actual current measurement

We can find characteristics of the fiber sensor by applying current to the coil and then measuring signal modulation. The coil generates magnetic field and induces Faraday rotation in the sensor. Applied current of 1 A_{rms} to the coil of 1,000 turns is equivalent to the current of 1,000 A_{rms}. The power amplifier supplies the current to the sensing coil in Figure 1 (switch D1 is closed and D2 is opened). The sensor's output voltage consists of two parts: a DC part (v_{DC}) corresponding to the average output intensity at analyzer angle θ of 60°and an AC part (v_{AC}) corresponding to actual current measurement. Its rms value can be measured by a lock-in amplifier. In an ideal (23)

case (δ_{DC} is about 1 to 2 degrees/ turns), we get signal modulation of 1.62×10^{-2}. From our experiment, signal modulation is 1.29×10^{-2}. This agrees well with our analysis that δ_{DC} and T are 0.660 and 0.05 radians, respectively.

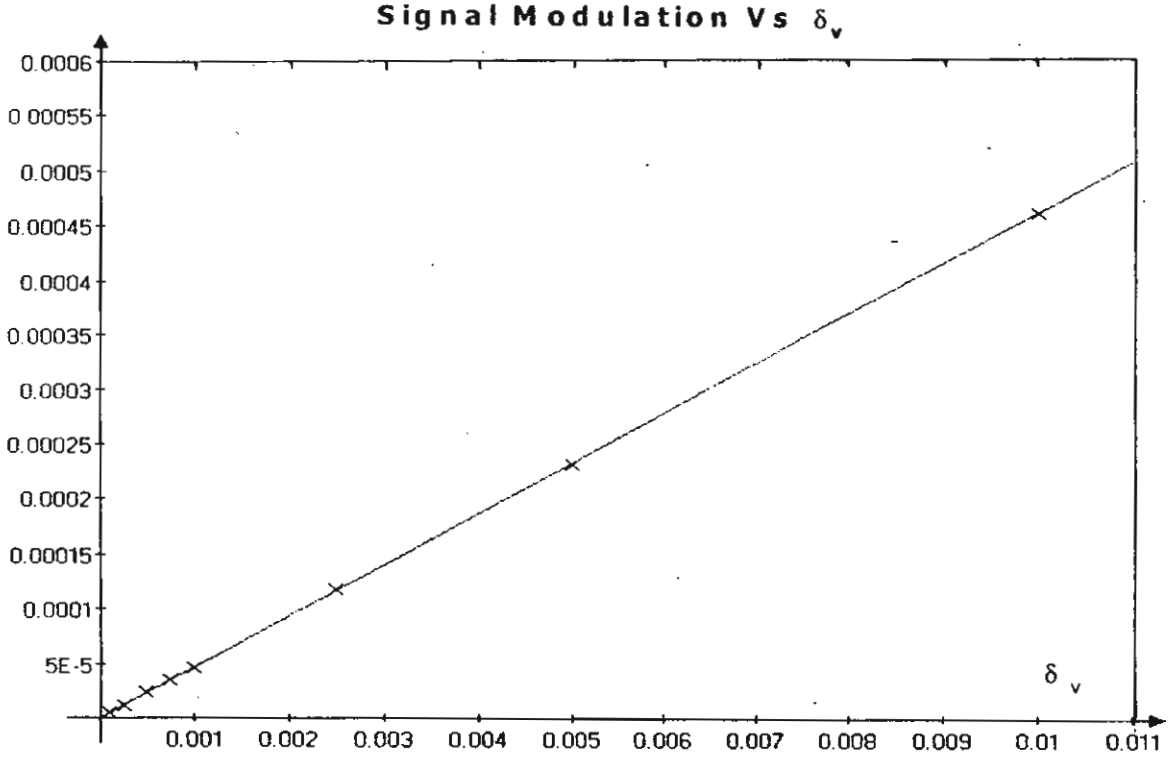

Figure 2 Signal modulation Vs vibration-induced linear birefringence δ_v.

4.2 Relationship between vibration and false current

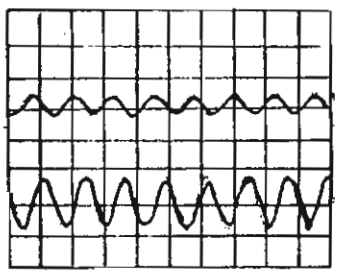

Figure 3 Vibration of 6.63 m/s^2 at the frequency of 400 Hz (top trace) and corresponding sensor's output (bottom trace).

In Figure 1, mechanical vibration was applied just in front of the single-mode fiber loop. A speaker was kept in a closed box and about 7 cm of fiber was attached to the top of the box. This box was made from acoustic absorbing material in order to isolate acoustic perturbations from disturbing alignment of the photodetector and the other optic components in the system. A power amplifier supplies signal of 400 Hz to the speaker (switch D2 is closed and D1 is opened). This produces vibration of 400 Hz. A piezo-electric accelerometer was attached to the top of the box closed to the fiber to quantify the magnitude and frequency contents of mechanical vibration. The vibration sensor is

NP-3110s manufactured by Ono Sokki and its signal conditioner is IMV TrendVibro Z model VM 4105. The output voltage of the detector was given to a Stanford Research lock-in amplifier model SR 530 to read the rms value of the AC part ($v_{(0\text{-}p)}$). DC value (v_{DC}) is measured by a DC voltmeter.

Figure 3 shows the effect of vibration on the sensor when no applied current to the sensing coil. The vibration amplitude is 6.63 (0-p) m/s^2 at the frequency of 400 Hz. Figure 4 shows signal modulation Vs amplitude of vibration from the accelerometer in $m_{(0\text{-}p)}$ /s^2. The output of the IMV vibrometer and the lock-in amplifier were given to an oscilloscope (see Figure 3).

5. DISCUSSIONS

In actual current measurement, under no vibration (δ_V = 0), δ_{DC} and T are constant, the applied current is 1.000 A_{rms}.turn, the signal modulation is 1.378x10^{-2} using Eq (2). In our experiment it was 1.29x10^{-2} this is due to the efficiency of magnetic producing coil being only 93.6%. The signal modulation (or false current) varies linearly with vibration amplitude (see Figure 5). Also, simulation of our model shows that signal modulation varies linearly with δ_V. Thus, δ_V varies linearly with vibration amplitude (see Figure 5).

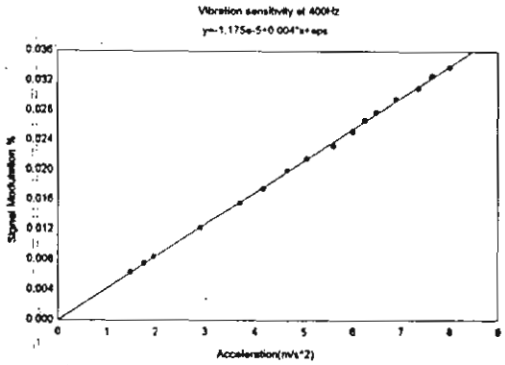

Figure 4 Vibration amplitude (0-p) m/s^2 Vs Signal modulation. The Vibration frequency is 400 Hz.

As a result, 1 g (9.8 m/s^2) of vibration produces around 46 A_{rms}.turns of the false current. With good packaging and the annealed sensing fiber (δ_{DC} is about 1 to 2 degrees/ turns) , the effect will be smaller by a few orders of magnitude. In our system vibration lower than 0.6 m/s^2 (due to noise floor limit) does not result into false current. Also, we can protect the fiber leads to the sensing fiber by using PM fiber leads which may be strewn virtually anywhere throughout the power systems with no concern of false signal detection due to vibrations. The noise equivalent current is about $0.33A_{rms}/\sqrt{Hz}$.

6. CONCLUSION

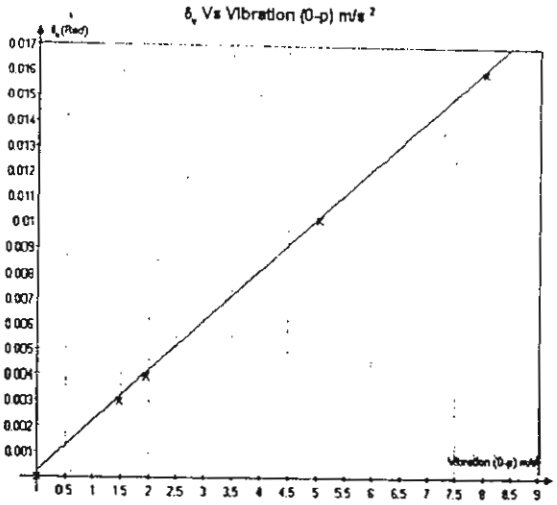

Figure 5 Linear birefringence change Vs Vibration amplitude (0-p) in m/s^2.

We have demonstrated a novel mathematical model for vibration sensitivity in the unidirectional polarimetric current sensor (UDPS). Experimental study shows that the linear birefringence δ_V due to mechanical vibration (to our understanding, no experimental studies were reported for vibration sensitivity with a single frequency of vibration and no effect of acoustic perturbations to the other optic components) changes linearly with vibration amplitude. This sensor's residual sensitivities to environmental disturbances can be further reduced by a damped packing such as putting sensing fiber part in a gel-filled tube together with employing two polarization scheme, where the two sensor's output at the +45° and –

45^0 to the output fiber axes. Also, 'spun' low birefringence or annealed fiber can be used to reduce the value of (static) linear birefringence δ_{DC}. Further investigation of the magnitude of linear birefringence change under the influence of vibration should be done experimentally with the help of optical modulator.

7. ACKNOWLEDGEMENT

Funding was provided by Thai Research Funds (TRF) under . Grant No. TRF:RSA/06/2541 and Thaikhadi Research Institute, Thammasat University.

REFERENCES

[1] T. Cease, *et al.*, Optical Voltage and Current Sensor used in Revenue Metering System. *IEEE Trans. Power Delivery*, **6** (4): 1374-79, 1989.

[2] S. Pothiya, *et al.*, Mathematical Modeling of Vibration Sensitivity in Unidirectional Polarimetric Current Sensor, Submission, *1st ISOQT*, 2001.

[3] A. Rogers, Optical Fiber Current Measurement In: *Optical Fiber Sensor Technology*, Grattan K and Meggit B, eds., **Vol. I**: 432-438, Chapman & Hall, 1995.

[4] A. Roger, *et al.*, Vibration Immunity for Optical Fiber Current Measurement. *IEEE J. Lightwave Technol.*, **13**(7): 1371-1377, 1995..

[5] A. Smith, Polarization and Magnetooptic Properties of Single-mode Optical Fibre. *Appl. Opt.*, **17**(52), 1978.

Appendix B.5

Reprint of

S. Pothiya, P. Tantaswadi, and S. Maheshwari "Mathematical modeling of vibration sensitivity in unidirectional polarimetric current sensors," *Int. Symp. on Opt. and Quantum Tech.* (ISOQT), Dec. 2001, KMITL, Bangkok, pp. 113-118.

Mathematical Modeling of Vibration Sensitivity in Unidirectional Polarimetric Current Sensors

S. Pothiya, P. Tantaswadi, and S. Maheshwari
Sirindhorn International Institute of Technology, Thammasat University
School of Electrical Engineering and Information Technology
PO Box 22,Thammasat Rangsit Post Office, Pathumthani 12121

Abstract

This paper proposed a novel mathematical modeling for vibration sensitivity in unidirectional polarimetric current sensors. We believe that it is the first time to model the effect of vibration to the single-mode sensing fiber on the current measurement error in unidirectional polarimetric current sensors. In this paper, simulation results agree well with experimental results done by Tantaswadi [1].

Keywords:linear birefringence, fiber-optic current sensors, magneto-optic current transformers, simulation and modeling, vibrations.

1. INTRODUCTION

Fiber-optic current sensors, which based on magneto-optic Faraday effect and Ampere's law, It have been received considerable attention for possible application in electric power industry as magneto-optic current transformers (MOCTs) in the past few decades [1]-[5].

However, the optical current sensor exhibits sensitivity to changes in the linear birefringence, δ, in their sensing coils. Changing stresses and temperature may change the total δ or its distribution along the sensing coil, which in turn changes the evolution of the state of polarization of the light through the sensing coil.

The basic theory of birefringence and Faraday rotation in optical fiber is well known, but some interesting conclusions from this theory concerning the application to vibration sensitivity in fiber optic current sensors have not been drawn yet. Although there are a few literatures [1]-[4] related to the vibration sensitivity in polarimetric current sensor, a general mathematical model of vibration sensitivity due to birefringence effect at the sensing part in unidirectional polarimetric current sensor has not been shown. Reference [1] shows experimental study of this system. Simulation results agree well with experimental results.

2. PRINCIPLES

When light propagates in an optical fiber wound around a current carrying wire, the induced magnetic field causes a rotation of the linear polarization plane of lightwave by the magneto-optic Faraday effect. This angle of Faraday rotation, F, through which the plane of polarization rotates, is given by

$$F = V\oint_C \vec{H}\cdot d\vec{l}\,, \qquad (1)$$

where V is the Verdet constant of the optical fiber, $\vec{H}$ is the magnetic field intensity along the direction of light propagation, and l is the optical path along the fiber loop. From the Ampere's law, this closed loop integral of magnetic field around a wire is proportional the current, I, flowing through it, *i.e.* $I = \oint_C \vec{H}\cdot d\vec{l}$. (2)

Therefore, the angle of rotation, F, in the fiber loop configuration is given by

$$F = VNI \qquad (3)$$

where N is the integral number of turns of fiber wrapped around the current carrying wire. The stability of Faraday rotation based current sensors, through the Verdet

constant, depends on source wavelength and temperature.

To measure current I, with constants N and V, we can use polarimeter sensor to measure Faraday rotation F. Figure 1 shows unidirectional polarimetric current sensor set-up. Linear polarized light from HeNe laser is coupled to the single-mode fiber. Polarization controller in front of the sensing fiber is to launch the linear polarized into the fast axis of fiber loop forming a sensing part. Light passes through a polarizer (we usually call an "analyzer") at the fiber output. θ is the angle between the analyzer and fast birefringence axis at the end of sensing fiber loop. A simplified configuration consists of input linear polarized electric field (E_{in}) entering the sensing fiber loop, an analyzer aligned θ degrees with respect to the birefringence fast axis of the fiber loop, and a detector. The analyzer angle θ of 45° provides maximum sensitivity and linear dynamic range.

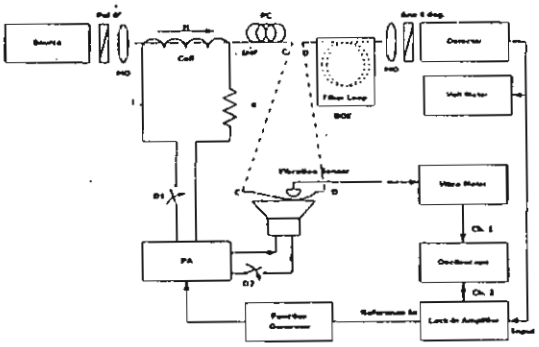

Figure 1 Unidirectional polarimetric current sensor and its experimental set-up, MO: microscope objective lens, SMF: single-mode fiber, PC: polarization controller, Ana: analyzer, PA: power amplifier

The output electric field (E_{out}) of the sensor impinging on the detector can be described by Jones Calculus [2]

$$E_{out} = P \cdot R(\theta) \cdot \bar{L} \cdot E_{in} \tag{4}$$

where $E_{in}, \bar{L}, R(\theta)$, and P represent input linearly polarized light in the x-axis, sensing fiber matrix, coordinate rotation matrix with the angle difference between the output analyzer and the birefringence fast axis at the fiber end (θ), and P is the analyzer matrix, respectively.

$$\bar{L} = \begin{bmatrix} A & -B \\ B & A^{*} \end{bmatrix} \tag{5}$$

where

$$A = \cos\left(\frac{\alpha}{2}\right) + j\sin\left(\frac{\alpha}{2}\right)\cos(\chi) \tag{6}$$

$$B = \sin\left(\frac{\alpha}{2}\right)\sin(\chi) \tag{7}$$

$$\frac{\alpha}{2} = \sqrt{(F+T)^2 + \left(\frac{\delta}{2}\right)^2} \tag{8}$$

$$\tan\chi = \frac{2(F+T)}{\delta} \tag{9}$$

where δ, F, T, and α are the linear birefringence, Faraday rotation, twisted (circular) birefringence, and total birefringence in radians. Coordination rotation matrix $R(\theta)$ is given by

$$R(\theta) = \begin{bmatrix} \cos\theta & \sin\theta \\ -\sin\theta & \cos\theta \end{bmatrix} \tag{10}$$

In our experiment, we align the analyzer with θ of 60°, where the output signal-to-noise ratio (SNR) is better than that at θ of 45°, where the sensitivity of the sensor is maximum. Using equation (4) to (10), normalized output intensity (Intensity $\propto |E_{out}|^2$) on the detector is given by

$$\frac{I_{60^\circ}}{I_0} = \frac{1}{4} + \frac{\sqrt{3}}{2}\frac{\sin(\alpha)}{\alpha}\cdot(F+T) + 2\left[\frac{\sin(\alpha/2)}{\alpha}\cdot(F+T)\right]^2 \tag{11}$$

where I_0 is the maximum intensity at the detector. Substituting equation (8) into equation (11), we get

$$\frac{I_{60^\circ}}{I_0} = \frac{1}{4} + \frac{\sqrt{3}}{2}\frac{\sin\left(\sqrt{4(F+T)^2+\delta^2}\right)}{\sqrt{4(F+T)^2+\delta^2}}\cdot(F+T) + \left[1-\cos\left(\sqrt{4(F+T)^2+\delta^2}\right)\right]\cdot\frac{(F+T)^2}{4(F+T)^2+\delta^2} \tag{12}$$

2.1 Current measurement

Obviously, equation (12) shows that the normalized output intensity is a function

of F, δ, and T. With the input light aligned to birefringence fast axis of the sensing fiber, in an ideal fiber ($\delta, T \approx 0$), we would expect only Faraday rotation ($F=VNI$) to occur. Equation (12) becomes

$$\frac{I_{60^\circ}}{I_0} = \frac{1}{2}\left[1+\sin\left(2F-30^\circ\right)\right] \quad (13)$$

Equation (13) indicates that the normalized output intensity is a constant when there is no applied cur-rent ($F=0$). When AC current ($I(t)=A\sin\omega t$) is applied (where A is zero-to-peak *(0-p)* amplitude in Ampere), F can be described by

$$F(t) = VNI(t) = (VNA)\sin\omega t = F_0 \sin\omega t \quad (14)$$

where $\omega = 2\pi f$ and f is frequency of the applied current. V is the Verdet constant and a function of wavelength (4.68 μ *rad*/A_{rms} for wavelength of 633 nm). Then, $F_0 = VNA$ is a constant and depends on the current amplitude, the number of turns, and wavelength of operation. Substituting equation (14) into (13), we obtain the phase modulation signal. Detector's output voltage (v_D) is proportional to the impinged output intensity ($v_D \propto I_{60^\circ}$) and is given by

$$v_D = \frac{K}{2}\left[1+\sin\left(2F_0\sin\omega t-30^\circ\right)\right] \quad (15)$$

where K is the maximum output voltage at the detector. When F_0 is small, the output voltage at the detector of equation (15) can be approximated by

$$v_D(t) = v_{DC} + v_{AC}(t) \approx v_{DC} + v_{(0-p)}\sin\omega t \approx \frac{K}{2}\left[1+2\sqrt{3}\sin\omega t\right] \quad (16)$$

when F_0 is small and less than 0.04 radian, the output zero-to-peak *(0-p)* detector voltage $v_{(0-p)}$ is linear proportional to the applied current amplitude (A) as given by $v_{(0-p)} \propto 2\sqrt{3}F_0$.

2.2 Signal Modulation

Current measurement can be found by a ratio of $v_{(0-p)}$ to v_{DC}, which is known as "signal modulation." Thus, signal modulation using equation (16) is given by

$$v_{(0-p)}/v_{DC} = 2\sqrt{3}F_0 = 2\sqrt{3}VNA \quad (17)$$

The sensor output is linear up to 0.04 *rad* ($\sin(x) \approx x$, when $x < 0.04\,rad$) or about 8,500 A_{rms} (0.04 *rad*/*V* ; $V = 4.68\times10^{-6}$ for wavelength of 633 nm). If the applied current is 1,000 A_{rms}, the signal modulation using equation (17) will be 1.62×10^{-2}. In practice, δ is not negligible but T is *e.g.* $\delta = 0.660$ and $T = 0.05$ radians. When the applied current is 1,000 A_{rms}, the signal modulation using equation (12) is 1.378×10^{-2}. Scale factor of the sensor is defined by

$$SF = \frac{\text{signal modulation (in experiment)}}{\text{signal modulation of the ideal case}}.$$

In this case, the scale factor SF is 0.85.

3. MATHEMATICAL MODELING OF LINEAR BIREFRINGENCE CHANGE DUE TO VIBRATIONS

We model the linear birefringence in the sensing fiber being composed of bending-induced linear birefringence (δ_{DC}) and vibration-induced linear birefringence caused by transverse strain or vibration (δ_v), which can be described by [3]

$$\delta_v = \frac{2\pi}{\lambda}\Delta n l, \quad (18)$$

where Δn is the refractive index change induced by stress in the medium (silica in this case), l is the effective length (under perturbation) of fiber, and λ is the center wavelength of the source. The refractive index change is given by

$$\Delta n = -\frac{n^3}{2}p\sigma = 0.311\sigma, \quad (19)$$

where n is the (unperturbed) refractive index of medium, σ is the strain and p is the photoelastic constant of fiber ($p=0.2$ in silica). Value of the Faraday rotation (VNI) depends on the Verdet constant (V). Typical value of V is 4.68 $\mu rad/A$ or $0.268^\circ/(kA)$. Because the vibration affects linear birefringence, to induce a π-radian birefringence change $\Delta n = \lambda/2 = 3.165\times10^{-7}$ for a fiber length of 1 m. We can find the strain of 1.019×10^{-6} using Equation (19).

The (static) bending-induced birefringence (δ_{DC}) per turn of a fiber loop with radius R under no tension can be described by [3]

$$\delta_{IX} \approx \frac{0.6\pi}{R} \ ^{\circ}/\text{turn}. \qquad (20)$$

In our case, R of 0.3 m results in δ_{IXC} of 6.3 °/turn. Six turns of fiber loop result in δ_{IXC} of 37.8°.

Assume that (total) linear birefringence (δ) in single-mode sensing part is the algebraic sum of the (static) bending-induced linear birefringence (δ_{IXC} due to loop radius) and vibration-induced linear birefringence (δ_V). Then, the (total) linear birefringence can be expressed by

$$\delta = \delta_{IX} + \delta_v \sin(\omega_v t) \qquad (21)$$

where $\omega_v = 2\pi f_v$ and f_v is the frequency of the vibration δ_v and T is much smaller than δ_{DC} in our configuration.

4. CURRENT MEASUREMENT ERROR DUE TO VIBRATIONS

In this section we formulate a mathematical model of the vibration sensitivity or current measurement error due to vibration. In equation (12), even when no current and no vibration are applied ($F = 0$ and further assume that the δ_{DC} and T to be constant), the output will be constant. However, the presence of vibration perturbs the linear birefringence and modulates the angular rotation, which cannot be distinguishable from that of the Faraday rotation (F). This results in signal modulation even there is no applied current. It is named apparent current or false current. Substituting equation (21) into (12), we obtain a phase modulation signal. Assume the change of δ_{DC} and T (from vibrations) to be small and negligible. In this case, we formulate a mathematical model for vibration sensitivity when only vibration on the sensing fiber ($F = 0$) to be given by

$$\frac{I_{\omega}}{I_0} = \frac{1}{4} + \frac{\sqrt{3}}{2}\frac{\sin\left(\sqrt{4T^2 + (\delta_{DC} + \delta_v \sin\omega_v t)^2}\right)}{\sqrt{4T^2 + (\delta_{DC} + \delta_v \sin\omega_v t)^2}} \cdot T + \left[1 - \cos\left(\sqrt{4T^2 + (\delta_{DC} + \delta_v \sin\omega_v t)^2}\right)\right] \cdot \frac{T^2}{4T^2 + (\delta_{DC} + \delta_v \sin\omega_v t)^2} \qquad (22)$$

Using Lock-in amplifier or the spectrum analyzer, we can examine the frequency components of the DC, first-harmonic, second-harmonic, and higher harmonic components. Assume the values of the δ_{DC} and T to be 0.660 (37.8°) and 0.05 radians, respectively. The value of δ_V is assumed to vary linearly with the mechanical vibration to the sensing fiber and, thus, signal modulation varies with the same frequency. When δ_V is small and the applied vibration is of single-frequency, the signal modulation due to vibration can be approximated by (when $2T, \delta_v << \delta_{IX}$)

$$I_{\omega}/I_0 = \frac{1}{4} + \frac{\sqrt{3}}{2}\frac{\sin(\delta_{IX} + \delta_v \sin\omega_v t)}{\delta_{IX} + \delta_v \sin\omega_v t} \cdot T + [1 - \cos(\delta_{IX} + \delta_v \sin\omega_v t)] \cdot \frac{T^2}{(\delta_{IX} + \delta_v \sin\omega_v t)^2} \qquad (23)$$

Expanding equation (23) using Bessel function(see Appendix), we obtain

$$\left.\frac{I_{\omega}}{I_0}\right|_{Approx} = \frac{1}{4} + \frac{\sqrt{3}}{2} B_1\left[\begin{matrix} J_0(\delta_v)\sin(\delta_{IX}) + \\ 2J_1(\delta_v)\cos(\delta_{IX})\sin(\omega_v t)\end{matrix}\right] + B_3\left[\begin{matrix} 1 - J_0(\delta_v)\cos(\delta_{IX}) + \\ 2J_1(\delta_v)\sin(\delta_{IX})\sin(\omega_v t)\end{matrix}\right] \cdot \qquad (24)$$

where J_k is the Bessel function of the first kind of order k.

5. SIMULATED FALSE CURRENT DUE TO VIBRATIONS

In Figure2, I and IIf represent exact and approximated signal modulation calculation using equation (23) and (24), respectively. It shows that when the vibration is small and is of single-frequency, the signal modulation varies linearly with δ_v and has the same frequency as that of the vibration. The other higher harmonics are negligible. The relation between vibration-induced linear birefringence δ_v and signal modulation is

Signal modulation = $3.1715\times10^{-2}\delta_v$ (25)

For example, δ_v of 10^{-2} *rad* will result in signal modulation of 3.1715×10^{-2}% or false current of 23.02 *Arms. turn* using signal modulation of 1.378×10^{-2} for 1,000 *Arms. turn* (see section 2.2). Similarly, we find

the relationship between false current and δ_v *(rad) i.e.*

False current $[A_{rms}.\ turn] = 2.302\times10^{-3}\delta_v$ (26)

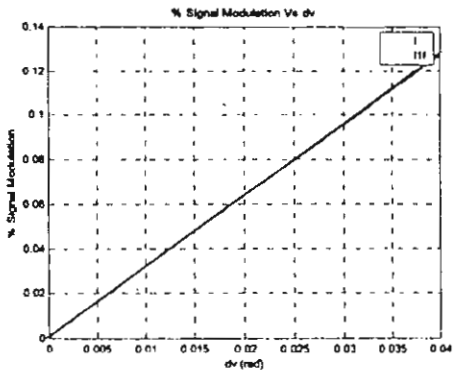

Figure 2 Signal modulation Vs vibration-induced linear birefringence δ_v

6. CONCLUSION

We have demonstrated a novel mathematical modeling for vibration sensitivity in the unidirectional polarimetric current sensor (UDPS). The experimental study shows that the linear birefringence δ_V due to mechanical vibration changes linearly with vibration amplitude. This sensor's residual sensitivities to environmental disturbances can be further reduced by a damped packing such as putting sensing fiber part in a gel-filled tube together with employing two polarization scheme, where the two sensor's output at the +45° and –45° to the output fiber axes. Also, 'spun' low birefringence or annealed fiber can be used to reduce the value of (static) linear birefringence δ_{DC}. Further investigation of the magnitude of linear birefringence change under the influence of vibration should be done experimentally with the help of optical modulator.

7. ACKNOWLEDGEMENT

Funding was provided by The Thailand Research Fund (TRF) under Grant No. TRF:RSA/06/2541 and Thaikhadi Research Institute, Thammasat University. The authors would like to thank Dr. James N. Blake of Nxtphase, USA, Prof. Alan J. Rogers of University of Surrey, UK, and Assoc. Prof. Dr. Pichet Limsuwan of King Mongkut's University of Technology at Thonburi, Thailand for help and fruitful discussions.

8. APPENDIX

We can expand equation (23) using Bessel function. In equation (23), first we define

$$B_1 = \frac{T}{\sqrt{4T^2+\delta^2}} = \frac{T}{\sqrt{4T^2+\left(\delta_{DC}+\delta_v\sin(\omega_v t)\right)^2}}$$

$$B_2 = \frac{T^2}{4T^2+\delta^2} = \frac{T^2}{4T^2+\left(\delta_{DC}+\delta_v\sin(\omega_v t)\right)^2},$$

where

$$\sin\left(\delta_v\sin(\omega_v t)\right) = 2\sum_{k=0}^{\infty} J_{2k+1}(\delta_v)\sin\left((2k+1)\omega_v t\right)$$

$$\cos\left(\delta_v\sin(\omega_v t)\right) = J_0(\delta_v) + 2\sum_{k=1}^{\infty} J_{2k}(\delta_v)\cos(2k\omega_v t)$$

$$\left.\frac{I_{\omega}}{I_0}\right|_{Approx.} = \frac{1}{4} + \frac{\sqrt{3}}{2}B_1\left[J_0(\delta_v)\sin(\delta_{DC}) + 2J_1(\delta_v)\cos(\delta_{DC})\sin(\omega_v t)\right]$$
$$+ B_2\left[1 - J_0(\delta_v)\cos(\delta_{DC}) + 2J_1(\delta_v)\sin(\delta_{DC})\sin(\omega_v t)\right]$$
$$+ \text{higher harmonic terms}$$

When $\delta_v << 1$, the contribution of higher harmonic terms is negligible and the approximation of

$J_0(\delta_v) \approx 1$ and $J_1(\delta_v) \approx 0.5\delta_v$.

REFERENCES

[1] P. Tantaswadi, *et al.* Experimental Study of Vibration Sensitivity in Unidirectional Polarimetric Current Sensors, Submissions, *1st ISOQT*, 2001.

[2] A. Smith. Polarization and Magnetooptic properties of single-mode optical fibre. *Appl. Opt.*, **17**(52), 1978.

[3] A. Rogers. Optical Fiber Current Measurement In: *Optical Fiber Sensor Technology*, Grattan K and Meggit B, eds., Vol. I: 432-438, Chapman & Hall, 1995.

[4] A. Rogers, *et al.* Vibration immunity for optical fiber current measurement. IEEE *J. Lightwave Technol.*, **13**(7): 1371-1377, 1995.

[5] T. Cease, *et al.* (1989) Optical Voltage and Current Sensor used in Revenue

Metering System. *IEEE Trans. Power Delivery*, 6(4): 1374-79, 1989.

Appendix B.6

Reprint of

P. Tantaswadi and C. Tangtrongbenchasil "Simulation of uniformly distributed vibration effects on a reciprocal fiber-optic polarimetric current sensor," *Int. Symp. on Opt. and Quantum Tech.* (ISOQT), Dec. 2001, KMITL, Bangkok, pp. 119-122.

Simulation of Uniformly Distributed Vibration Effects on a Reciprocal Fiber-optic Polarimetric Current Sensors

P. Tantaswadi and C. Tangtrongbenchasil
Sirindhorn International Institute of Technology, Electrical Engineering Program, Thammasat University
PO Box 22, Thammasat Rangsit, Post Office, Pathumthani 12121

Abstract

Mechanical vibration affects the accuracy of optical fiber current sensor causing error in optical current measurement. In practice, the sensing part of the optical sensor is susceptible to environmental perturbations such as mechanical vibration to the sensing fiber. Reciprocal polari-metric sensor configuration can reduce current measurement error due to the vibration. The accuracy of our model is within 0.01% of the actual value and satisfies application in metering.

Keywords – fiber optic current sensor, uniformly distributed vibration effect, polarimetric current sensor.

1. INTRODUCTION

Fiber optic current sensors rely on Ampere's law and Faraday effects. These are used in the electric power industry for revenue metering, relay, protec-tion and control. The advantages over conven-tional current transformers (CTs) include broad linear dynamic range (more than five orders of magnitude), broad bandwidth (DC to many MHz), no hysteresis, and by proper design, insensitivity to electro-magnetic interference (EMI) and radio-frequency interference (RFI).

Several approaches of fiber optic current sensor based on Faraday effect has been demonstrated [1]. Fiber-optic current sensors have several advantages over conventional CTs, but they have yet to overcome undesirable susceptibility to environ-mental perturbations, *e.g.* temperature, and acoustic vibrations in the sensing part [1]–[2]. One ap-proach is unidirectional polarimetric technique but it suffers from both linear and circular birefrin-gences in the sensing fiber. A reciprocal polarimetric current sensor configuration has been presented to counter the birefringences error. The vibrations affect the birefringence property of the fiber in the sensing part. Unidirectional polari-metric current sensors suffer from environmental perturbations due to varying birefringence in the sensing part [2]. The results are shown in false current readings from environmental perturbations.

In this paper, we show a reciprocal fiber optic current sensor configuration including normalized contrast ratio, and effects of uniformly distributed vibration on the sensor. The accuracy of this sensor is within 0.01% of the actual value and satisfies application in metering (accuracy of 0.3%).

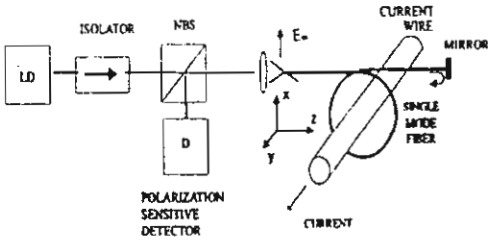

Figure 1 Reciprocal fiber optic polarimetric current sensor configuration, LD: laser diodes, NBS: non-polarizing beam splitter

2. SENSOR PRINCIPLES

Based on magneto-optic Faraday effect, when light propagates in an optical fiber wound around a current carrying wire (see Figure 1), the induced magnetic field causes a rotation of the linear polarization plane of light wave. This angle of Faraday rotation, ΔF, through which the plane of polarization rotates, is given by

$$\Delta F = V \oint_C \vec{H} \cdot d\vec{l} \,, \qquad (1)$$

where V is the Verdet constant of the optical fiber, $\vec{H}$ is the magnetic field intensity along the direction of light propagation, and l is the optical path along the fiber loop. Relying on Ampere's law, this closed loop integral of magnetic field around a wire is proportional the current, I, flowing through it, *i.e.*

$$I = \oint_C \vec{H} \cdot d\vec{l} \,. \qquad (2)$$

Therefore, the angle of rotation, ΔF in the fiber loop configuration is given by

$$\Delta F = VNI, \tag{3}$$

where N is the number of turns of optical fiber wrapped around the current carrying wire. The stability of Faraday rotation based current sensors, through the Verdet constant, depends on source wavelength and temperature.

To measure current I, with constants N and V, we can use a polarimetric sensor to measure ΔF. For the conventional unidirectional polarimetric current sensors, linearly polarized light is launched into a single-mode sensing fiber and a Wollaston prism for evaluation of the current and static linear birefringence [3]-[4] analyzes the output polarization. In practice, light travels through the fiber loop exhibiting additional linear birefringence due to bending and twist-induced circular birefringence can be described by Jones calculus (see next section). These birefringences affect the accuracy and sensitivity to environmental perturbations *i.e.* vibrations of the sensor. Reciprocal fiber-optic current sensors (see Figure 1) interrogate the light in both directions. Since linear and twist-induced birefringences exhibit reciprocal characteristics, the reciprocal rotation of these birefringences cancel when light propagates along and is back-reflected down a fiber. The Faraday magneto-optic effect exhibits nonreciprocal characteristics but the Faraday rotation doubles when light propagates along and is back-reflected down a fiber. Thus, this optical configuration has the advantage to minimize the birefringence induced offset problems associated with the unidirectional polarimetric current sensor.

3. MATHEMATICAL DESCRIPTIONS OF A RECIPROCAL FIBER-OPTIC POLARIMETRIC CURRENT SENSOR

We assume that vibration on the sensing part of optical fiber is uniformly distributed. Then, we analyze for uniformly distributed vibration on reciprocal fiber-optic polarimetric current sensor.

Firstly we launched input light to non-polarizing beam splitter and passes though single-mode fiber with input angle (η) of 45°. Then it continues to forward path of fiber loop to mirror. After that it travels back to the backward path of fiber loop and go to the same path. The following composite Jones Matrix [5]-[6] describing the system is given by

$$E_{out} = \begin{bmatrix} E_x \\ E_y \end{bmatrix} = \frac{1}{2}\tilde{L}\cdot M\cdot\tilde{L}\cdot R(\eta)\cdot E_{in}, \tag{4}$$

$$E_{in} = \begin{bmatrix} E_x = 1 \\ E_y = 0 \end{bmatrix} = \begin{bmatrix} 1 \\ 0 \end{bmatrix}, \tag{5}$$

$$R(\eta) = \begin{bmatrix} \sin\eta & \cos\eta \\ -\cos\eta & \sin\eta \end{bmatrix}, \tag{6}$$

$$\tilde{L} = \begin{bmatrix} A & -B \\ B & A^* \end{bmatrix}, \tag{7}$$

$$\tilde{L} = \begin{bmatrix} C & -D \\ D & C^* \end{bmatrix}, \tag{8}$$

$$A = \cos\frac{\alpha}{2} + j\sin\frac{\alpha}{2}\cos(\chi), \tag{9}$$

$$B = \sin\frac{\alpha}{2}\sin(\chi), \tag{10}$$

$$C = \cos\frac{\beta}{2} + j\sin\frac{\beta}{2}\cos(\zeta), \tag{11}$$

$$D = \sin\frac{\beta}{2}\sin(\zeta), \tag{12}$$

$$\alpha = \sqrt{4(VNI+T)^2+\delta^2}, \tag{13}$$

$$\beta = \sqrt{4(VNI-T)^2+\delta^2}, \tag{14}$$

$$\tan\chi = \frac{2(VNI+T)}{\delta}, \tag{15}$$

$$\tan\zeta = \frac{2(VNI-T)}{\delta}. \tag{16}$$

4. ANALYSIS OF THE NORMALIZED CONTRAST RATIO (K)

The Wollaston prism is aligned at 45° and -45° to the birefringence axis of the output end of the sensing fiber. The contrast ratio (K) is defined as

$$K = \frac{I_{45^\circ} - I_{-45^\circ}}{I_{45^\circ} + I_{-45^\circ}} \tag{17}$$

Then, we can derive Eq (4) by using Eq (5) to (12) as:

$$K = -\cos(\alpha)\cos(\beta) + \cos(\zeta-\chi)\sin(\alpha)\sin(\beta) \tag{18}$$

For ideal case, T and $\delta \approx 0$ are negligible, so Eq (18) becomes

$$K_{ideal} = -\cos(4VNI) \tag{19}$$

However, in practice, the use of high circular birefringence T or "spun" fiber ($VNI, \delta << T$, e.g. $\delta = 1.9\pi, T = 120\pi$) can overcome the intrinsic linear birefringence. This K is called K_{dc}, which is (see Appendix)

$$K_{dc} = -\cos(4VNI) + \frac{\delta^2}{\alpha\beta}\sin(\alpha)\sin(\beta) \tag{20}$$

To understand the performance of this sensor, we show the characteristic plot of the deviation of K (ΔK), which is

$$\Delta K(\%) = \frac{K - K_{dc}}{K_{dc}} \times 100\% \qquad (21)$$

In this sensor, Figure 2 shows that the deviation of K in percentage is within 0.01 % of ideal case (T, $\delta \approx 0$) when the range of the linear and circular birefringences are (1.8π, 2.0π) and (119.5π, 120.5π) radians, respectively.

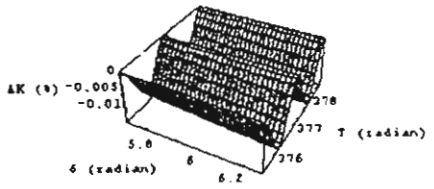

Figure 2 The deviation of K (ΔK) when $VNI = 0.01\ \pi$ radians as a function of δ is between $1.8\ \pi$ and $2.0\ \pi$ radians T is between $119.5\ \pi$ and$120.5\ \pi$ radians.

5. DEVIATION OF K (ΔK) Vs LINEAR BIREFRINGENCE

This sensor exhibits small dependence on linear birefringence. Figure 3 shows that the absolute value of the deviation of K in percentage is below 1×10^{-4}% when δ is between $-2\ \pi$ and $2\ \pi$ radians when $VNI = 0.01\ \pi$ and $T = 120\ \pi$ radians. Using Eq (18), (20), and (21), $\Delta K(\%)$ is given by

$$\Delta K(\%) = 2.59616\times10^{-6}\delta^2 - 9.24994\times10^{-5}. \qquad (22)$$

In Figure 3 gives maximum δ to achieve the accuracy of 9.24994×10^{-5}% for revenue metering application from Eq (22) is 0 *rad.*

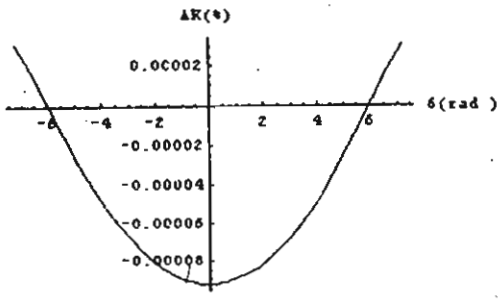

Figure3 Simulated deviation of K in percent varies with linear birefringence ($VNI = 0.01\pi$, $T = 120\pi$).

6. APPENRENT CURRENT VS LINEAR BIREFRINGENCE

Acoustic vibration on the sensing fiber can cause angular rotation of light wave polarization and may affect birefringence property of the sensing fiber [8]. The result could be misread as an actual current. Mechanical vibrations with a magnitude of 3.0 $g_{p\text{-}p}$ ($1g = 9.8m/s^2$) applied to a sensing fiber of unidirectional polarimetric sensor can cause an apparent current of 400 $A_{p\text{-}p}$. Simulated apparent current ($T = 120\ \pi$, $\delta_v = 0.3$ sin ($2\pi\ f_v\ t$), and the total linear birefringence is assumed to vary between 1.8π and 2.0π radians) for this sensor is shown in Figure 4. The frequency of vibration or varying linear birefringence (f_v) is chosen to be 50 Hz, which is common to electric power systems [1]. Very small apparent currents of less than 2.5×10^{-8} Amperes for 633 nm wavelength when the total linear birefringence δ is (1.8π, 2.0π) radians and theδ_v is shown in Figure 4(a).

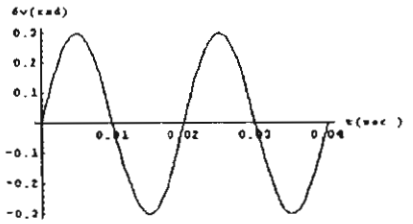

(a)

(b)

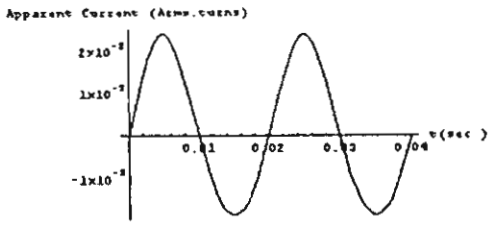

Figure4 Simulated apparent current (b) in Amperes. turns Vs birefringence (a) (VNI= 0 and T= 120π)

7. DISCUSSION AND CONCLUSION

The mathematical modeling of reciprocal fiber-optic current sensor configuration is demonstrated. The performance of the current sensor is similar to that of the ideal case (δ, $T \approx 0$). To satisfy the conditions of $\frac{\delta}{2T} \square 1$ and $VNI \square\ \delta \square\ T$ helical winding on an acrylic torus is presented. We can find the normalized contrast

ratio K being affected by undesired changes in linear birefringence δ caused by acoustic vibrations and circular birefringence T. For large T, deviation of K (%) is a quadratic function of δ but the contribution of vibrations is small and within 0.01 % (0.01 % of the actual value required for applications in metering). The apparent current shows that the susceptibility of sensor to varying linear birefringence is small and negligible.

8. REFERENCES

[1] S. Short, et al. Elimination of Bbirefringence Induced Scale Factor Errors in the in-line Sagnac Interferometer Current Sensor. *IEEE J-LT*, 16(10): 1844-1850, October 1998.

[2] S. Short, P. Tantaswadi, et al. Environmental Sensitivity Comparison of in-line Sagnac and Polarimetric Type Current Sensor. *IEEE Trans. Power Delivery*, 11(4): 1702-1706, 1996.

[3] Z. Ren, et al. Discrimination Between Linear Birefringence and Faraday Rotation in Optical Fiber Current Sensors by Polarization Multiplexing *Fiber Optic and Laser Sensors VII*, 1169: 226-232, 1989.

[4] P. Menke and T. Bosselmann. Temperature Compensation in magnetooptic AC Current Sensors using an Intelligent AC-DC Signal Evaluation. *IEEE J-LT*, 13(7): 1362-70, (1995).

[5] Tabor, et. al Electromagnetic Propagation Through Materials Possesing Both Faraday Rotation and Birefringence: Experiments with Ytterbium Orthoferrite. *J. Appl. Phys.*, 40(7): 2760.

[6] A. Smith. Polarization and Magnetooptic Properties of Single-mode Optical Fibre. *Appl. Opt.*: 17(52), (1978).

[7] S. Short, P. Tantaswadi, et al. (1996) Environmental Sensitivity Comparison of in-line Sagnac and Polarimetric Type Current Sensor. *IEEE Trans. Power Delivery*, 11(4): 1702-1706 (1996).

[8] K. Grattan and B. Meggit, ed. Optical Fiber Current Measurement. *Optical Fibers Sensor Technology*, **Vol. 1**, Chapman & Hall: 432-438, (1995).

9. ACKNOWLEDGEMENTS

Funding was provided by Thai Research Foundation (TRF) and partially by Thaikhadi Research Institute, Thammasat University. The authors would like to thank Dr. James N. Blake of Nxtphase, USA, Prof. Alan J. Rogers of University of Surrey, UK, and Assoc. Prof. Dr. Pichet Limsuwan of King Mongkut's University of Technology, Thonburi for help and fruitful discussions.

10. APPENDIX

To verify K_{dc}, From Eq (18)

$K = -\cos(\alpha)\cos(\beta) + \cos(\zeta - \chi)\sin(\alpha)\sin(\beta)$

K_{dc} is occurred in practical when $\delta = 1.9\pi$ and $T = 120\pi$, $T \gg VNI$ and

$$\left(\frac{\delta}{2(T+VNI)}\right)^2 \approx \left(\frac{\delta}{2(T-VNI)}\right)^2 \ll 1.$$

$$\text{So } \alpha \approx 2(T+VNI)\sqrt{1+\left(\frac{\delta}{2\cdot(T+VNI)}\right)^2}$$

$$\approx 2(T+VNI)\left(1+\frac{1}{2}\left(\frac{\delta}{2(T+VNI)}\right)^2\right)$$

$$\approx 2(T+VNI)$$

where $\sqrt{1+x} \approx 1+\frac{x}{2}$, $x \ll 1$,

$$\beta \approx 2(T-VNI)\sqrt{1+\left(\frac{\delta}{2\cdot(T-VNI)}\right)^2}$$

$$\approx 2(T-VNI)\left(1+\frac{1}{2}\left(\frac{\delta}{2(T-VNI)}\right)^2\right),$$

$$\approx 2(T-VNI)$$

where $\sqrt{1-x} \approx 1-\frac{x}{2}$, $x \ll 1$

then, $\alpha - \beta = 4VNI$, the first term on the right-hand side of Eq (18) becomes

$$-\cos(\alpha)\cos(\beta) = -\cos(\alpha-\beta)$$
$$= -\cos(4VNI)$$

and $\cos(\zeta-\chi) = \cos(\zeta)\cos(\chi) + \sin(\zeta)\sin(\chi)$, using Eq (15) and (16) to obtain

$$\cos(\zeta-\chi) = \frac{\delta^2}{\alpha\beta} + \frac{4}{\alpha\beta}(T^2 - VNI^2)$$

when VNI is very small and $2T \approx \alpha \approx \beta$, then $\cos(\zeta-\chi)$ become

$$\cos(\zeta-\chi) = \frac{\delta^2}{\alpha\beta} - 1$$

Substitute into Eq (18), to get

$$K_{dc} = -\cos(\alpha)\cos(\beta) - \sin(\alpha)\sin(\beta) + \frac{\delta^2}{\alpha\beta}\sin(\alpha)\sin(\beta)$$

$$= -\cos(\alpha-\beta) + \frac{\delta^2}{\alpha\beta}\sin(\alpha)\sin(\beta)$$

$$= -\cos(4VNI) + \frac{\delta^2}{\alpha\beta}\sin(\alpha)\sin(\beta)$$